LOAN DOCUMENT

DTIC ACCESSION NUMBER

LEVEL

INVENTORY

0

AFRL-ML-TY-TR-1999-4550

DOCUMENT IDENTIFICATION

25 Jul 1996

DISTRIBUTION STATEMENT A
Approved for Public Release
Distribution Unlimited

DISTRIBUTION STATEMENT

H
A
N
D
L
E

W
I
T
H

C
A
R
E

ACCESSION FOR

NTIS	GRA&I	
DTIC	TRAC	
UNANNOUNCED		☐
JUSTIFICATION		

BY

DISTRIBUTION/

AVAILABILITY CODES

DISTRIBUTION	AVAILABILITY AND/OR SPECIAL

A-1

DISTRIBUTION STAMP

DATE ACCESSIONED

DATE RETURNED

20000211 039

DATE RECEIVED IN DTIC

REGISTERED OR CERTIFIED NUMBER

DTIC FORM 70A
JUN 90

DOCUMENT PROCESSING SHEET

PREVIOUS EDITIONS MAY BE USED UNTIL
STOCK IS EXHAUSTED.

LOAN DOCUMENT

AFRL-ML-TY-TR-1999-4550

THE REMOVAL OF NO$_X$ USING A PULSED STREAMER CORONA DISCHARGE IN THE PRESENCE OF ETHYLENE

SWAMINATHAN KALYANA

FLORIDA STATE UNIVERSITY
2525 POTTSDAMER STREET
TALLAHASSEE FL 32310-6046

Approved for Public Release: Distribution Unlimited

AIR FORCE RESEARCH LABORATORY
MATERIALS & MANUFACTURING DIRECTORATE
AIRBASE & ENVIRONMENTAL TECHNOLOGY DIVISION
TYNDALL AFB FL 32403-5323

NOTICES

USING GOVERNMENT DRAWINGS, SPECIFICATIONS, OR OTHER DATA INCLUDED IN THIS DOCUMENT FOR ANY PURPOSE OTHER THAN GOVERNMENT PROCUREMENT DOES NOT IN ANY WAY OBLIGATE THE US GOVERNMENT. THE FACT THAT THE GOVERNMENT FORMULATED OR SUPPLIED THE DRAWINGS, SPECIFICATIONS, OR OTHER DATA DOES NOT LICENSE THE HOLDER OR ANY OTHER PERSON OR CORPORATION; OR CONVEY ANY RIGHTS OR PERMISSION TO MANUFACTURE, USE, OR SELL ANY PATENTED INVENTION THAT MAY RELATE TO THEM.

THIS REPORT IS RELEASABLE TO THE NATIONAL TECHNICAL INFORMATION SERVICE (NTIS). AT NTIS, IT WILL BE AVAILABLE TO THE GENERAL PUBLIC, INCLUDING FOREIGN NATIONS.

THIS TECHNICAL REPORT HAS BEEN REVIEWED AND IS APPROVED FOR PUBLICATION.

JOSEPH D. WANDER, PhD   CHRISTINE WAGENER-HULME, Lt Col, USAF, BSC
Program Manager   Chief, Environmental Technology Development Branch

RANDY L. GROSS, Col, USAF, BSC
Chief, Airbase & Environmental Technology Division

REPORT DOCUMENTATION PAGE		Form Approved OMB No. 0704-0188

1. AGENCY USE ONLY *(Leave blank)*	2. REPORT DATE 25 July 1996	3. REPORT TYPE AND DATES COVERED Master's Thesis: May 1994 - May 1996

4. TITLE AND SUBTITLE The Removal of NOx Using a Pulsed Streamer Corona Discharge in the Presence of Ethylene	5. FUNDING NUMBERS F08637-93-C-0020 PE: 6022F Project Number: 1900-A35B
6. AUTHOR(S) Kalyana, Swaminathan	

7. PERFORMING ORGANIZATION NAME(S) AND ADDRESS(ES) Florida State University 2525 Pottsdamer Street Tallahassee FL 32310-6046	8. PERFORMING ORGANIZATION REPORT NUMBER

9. SPONSORING/MONITORING AGENCY NAME(S) AND ADDRESS(ES) AFRL/MLQE (Dr. Joe Wander) 139 Barnes Drive, Suite 2 Tyndall AFB, FL 32403-5323	10. SPONSORING/MONITORING AGENCY REPORT NUMBER AFRL-ML-TY-TR-1999-4550

11. SUPPLEMENTARY NOTES
POC: Joseph D. Wander, Ph.D, AFRL/MLQE, (850) 283-6240

12a. DISTRIBUTION AVAILABILITY STATEMENT Approved for Public Release: Distribution Unlimited	12b. DISTRIBUTION CODE A

13. ABSTRACT *(Maximum 200 words)*

Corona technology is based upon the application of an electric discharge to produce highly reactive free radicals in a gaseous medium.

In this study, a pulsed streamer corona discharge reactor was designed, constructed, and operated to study the removal of NO containing gases. Different physical characteristics of the discharge such as the rise time, peak voltage, and pulse width of the voltage pulse were measured.

A kinetic model was developed to characterize the chemical reactions taking place in the pulsed streamer corona reactor. The kinetic rate constants for the production of highly reactive free radicals such as O, N, and OH were obtained by fitting the model to the NO removal experimental data.

14. SUBJECT TERMS Pulsed streamer corona, NOx, nitrogen oxides, pulsed corona nitric oxide, ethylene			15. NUMBER OF PAGES
			16. PRICE CODE

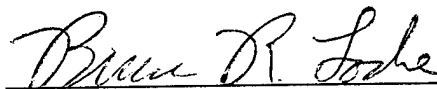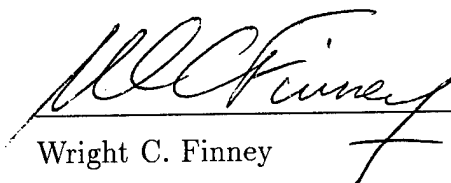| 17. SECURITY CLASSIFICATION OF REPORT UNCL	18. SECURITY CLASSIFICATION OF THIS PAGE UNCL	19. SECURITY CLASSIFICATION OF ABSTRACT UNCL	20. LIMITATION OF ABSTRACT UL

CLASSIFIED BY:

DECLASSIFY ON:

Preface

This thesis was prepared by Florida State University (FSU), Department of Chemical Engineering, under a subcontract with Applied Research Associates (contract No. F08635-93-C-0020), for the Air Force Research Laboratory (AFRL), Airbase and Environmental Technology Division, Tyndall AFB, FL 32403. The work was performed from May 1994 to May 1996. The AFRL project officer was Joseph D. Wander, Ph.D.

This thesis is submitted to the Defense Technical Information Center for publication exactly as it was submitted to Florida State University. This format does not conform to the usual style standards for AFRL reports but is acceptable. '
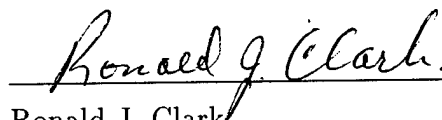
The members of the Committee approve the thesis of Swaminathan Kalyana
defended on July 25, 1996.

Bruce R. Locke
Professor Directing Thesis

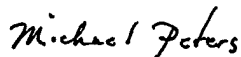Wright C. Finney
Committee Member

Ronald J. Clark
Committee Member

Srinivas Palanki
Committee Member

Approved:

Michael H. Peters, Chair, Department of Chemical Engineering

To

Thatha, Patti, Appa, Amma, Subha

&

Friends ...

ACKNOWLEDGEMENTS

CONTENTS

LIST OF TABLES

LIST OF FIGURES

xii

ABSTRACT

The removal of NO from air streams using pulsed streamer corona discharge, a type of non-thermal plasma, is considered in the present study. Pulsed streamer corona technology is based upon the application of an electric discharge to produce highly reactive free radicals in a gaseous medium.

In this study, a pulsed streamer corona discharge reactor was designed, constructed, and operated to study the removal of NO containing gases. Different physical characteristics of the discharge such as the rise time, peak voltage, and pulse width of the voltage pulse were measured. NO removal was considered from gases of various compositions including pure nitrogen, and dry and humid air. In an atmosphere of nitrogen, the main reaction mechanism for the removal of NO was through reduction of NO to molecular nitrogen, while in the case of dry air, NO was oxidized to NO_2. In humid air, NO_2 removal was also observed.

A kinetic model was developed to characterize the chemical reactions taking place in the pulsed streamer corona reactor. The kinetic rate constants for the production of highly reactive free radicals such as O, N, and $OH^.$ were obtained by fitting the model to the NO removal experimental data.

The addition of 500 ppm of carbon monoxide to the test gas did not have a significant effect on the NO and NO_2 removal efficiencies. The addition of 500 ppm of ethylene had a dramatic effect on the removal efficiency of NO and NO_2. Complete breakdown of 500 ppm of ethylene was noticed at 50 kV at a gas residence time of 44.0 seconds. Identification of byproducts must be undertaken as future work to confirm the validity of the kinetic model predictions in this case.

CHAPTER 1

INTRODUCTION

Nitrogen oxides released into the atmosphere arise primarily from the combustion of fossil fuels from both stationary and mobile sources. In 1992, U.S emissions of anthropogenic nitrogen oxides were estimated to be 23 million tons. Of this, 45% was from mobile sources and the remainder came from stationary sources (Ozkan et al., 1995). The seven oxides of nitrogen that may be present in ambient air are NO, NO_2, N_2O, NO_3, N_2O_3, N_2O_4 and N_2O_5. Of these nitrogen oxides, the only ones subject to regulatory control are NO and NO_2, and these are together referred to as NO_x. Though N_2O is not considered to be an air pollutant, it is considered to be a stratospheric ozone destructor and a greenhouse gas (U.S EPA, 1993).

Nitric oxide (NO) is an odorless gas and is only slightly soluble in water (0.006 g/100 g of water at 24 °C and 1 atm pressure). It is toxic and makes up 90-95% of the NO_x emissions from fossil fuel combustion. Nitrogen dioxide (NO_2) is a reddish brown gas with a characteristic pungent odor. It is corrosive and highly oxidizing. It is formed rapidly in the atmosphere from the oxidation of NO, and it is a toxic agent which can negatively affect human health. Nitrous oxide (N_2O), or laughing gas, is a colorless gas with a slight odor at high concentrations (U.S EPA, 1993).

NO and NO_2 are highly toxic if inhaled in high concentrations. NO entering the body forms nitrite which oxidizes the iron in haemoglobin, rendering it ineffective as an oxygen carrier. In 1986, the World Health Organization recommended that the exposure of humans to NO_2 should not exceed 200 ppbv for more than one hour a

month. Long-term exposure at 50 ppbv can cause pulmonary damage and increased airway resistance in healthy individuals (U.S EPA, 1993).

NO_x gases are one of the main contributors to the formation of photochemical smog. This smog is primarily due to the reaction of NO_x and hydrocarbons which, at high concentrations, contribute to a reduction in visibility. Under the influence of UV light these compounds produce a variety of harmful compounds such as peroxyacetyl nitrate (PAN) and ozone. Ozone is a highly toxic substance which leads to breathing problems above concentrations of 500 ppbv. NO_x emissions are one of the primary contributors to acid rain, which is associated with a number of effects including acidification of lakes and streams, and accelerated corrosion of buildings and monuments (Leslie et al., 1992).

The two main mechanisms that are primarily responsible for NO_x formation during combustion process are *thermal* NO_x and *fuel* NO_x. *Thermal* NO_x results from the oxidation of N_2 contained in combustion air, whereas *fuel* NO_x originates from the oxidation of chemically bound nitrogen in the fuel. Abatement of NO emissions can be achieved by (1) modifying the combustion process, such as using low-NO_x burners, gas recirculation, and staged combustion, and (2) using post-combustion removal methods (Chang et al., 1992).

Among the post-combustion control methods, selective catalytic reduction (SCR) is the most advanced technology currently used to remove NO_x from gas streams. One disadvantage with the SCR process is that the particulate matter commonly found in flue gas streams generated by the combustion of fossil fuels tend to "poison" catalysts, and therefore lower SCR performance. Another post-combustion removal method for NO_x is selective non-catalytic reduction (SNCR). SNCR relies on the injection of ammonia into the gas stream to chemically reduce NO to N_2 and H_2O in the presence of O_2. However, SNCR is effective only between 900 and 1100° C (Kokkinos et al., 1991).

One alternative to SCR and SNCR processes that has been studied since the 1970s is the gas phase plasma oxidation of NO using an electric discharge. Electric discharges initiate electron-gas reactions that in turn produce highly reactive radicals. The application of an electric discharge to a gas can lead to the creation of a thermal or a non-thermal plasma.

A thermal plasma is a "hot" or "equilibrium" plasma, which is characterized by a high gas temperature and approximately equal gas and electron temperatures. Typical examples are those produced in arcs and plasma torches. A "non-thermal plasma", as the name implies, is a plasma in which the electron temperature is considerably higher than that of the components of the ambient gas. The electrons produced are short-lived and rarely collide with a pollutant molecule, but they undergo many collisions with the predominant gas molecules, producing radicals that in turn lead to the removal of the toxic molecules (Penetrante, 1993). Hence, the essence of the non-thermal plasma technique is the efficient use of electrical energy to generate gas phase radicals by electron impact excitation, ionization and dissociation.

The different types of non-thermal plasmas that have been investigated are:

1. Electron Beam

2. Dielectric Barrier Discharge

3. Corona Discharge.

The electron beam process involves the direct irradiation of gases by an external source beam of highly energetic electrons to produce active radicals and atoms which react with NO_x to form nitric acid as well as other products. The use of electron beams to prevent pollution was initiated in the 1970's in Japan by the Japan Atomic Energy Research Institute and the Ebara Corporation, and pilot scale studies are currently being done in several countries such as the U.S, Germany, and Poland (Frank et al., 1993).

In a dielectric barrier discharge, the plasma is sustained between one or more dielectric surfaces backed by a conductor. A repetitively pulsed or ac voltage is applied to the electrodes, resulting in a filamentary periodic pulsed plasma (Chang et al., 1992). The dielectric barrier discharge is currently being used in industry for ozone synthesis (Dhali et al., 1991).

Corona discharges such as pulsed streamer corona, AC corona, and DC corona have been studied for the treatment of flue gas, VOC's, and for the synthesis of gases such as ozone. In the present study, the removal of NO from dry and humid air streams is investigated using positive pulsed streamer corona. The effect on NO removal of additives such as carbon monoxide and ethylene is also considered. The exhaust gases coming out of jet engines (F101 engine with JP4 fuel) have four compounds (ethene, acetylene, propene, and formaldehyde) accounting for 27% of volatile organic emissions at idle power (Spicer et al., 1992). Ethylene is used in the present study as a model hydrocarbon to consider the effect of hydrocarbons on NO_x chemistry.

1.1 Research Objectives

The specific goals of this research are:

1. To study the physical characteristics of the discharge, including voltage, current, and power waveforms of the discharge in order to characterize the power input into the reactor.

2. To study the effect of different discharge voltages and reactor gas residence times on NO removal.

3. To identify the byproducts formed from NO breakdown in dry and humid air streams, and also in the presence of additives such as ethylene and carbon monoxide.

4. To develop a kinetic model describing the chemical reactions taking place in a pulsed streamer corona discharge.

5. To identify the important reaction mechanisms for ethylene breakdown in a pulsed streamer corona discharge.

The literature review given in Chapter 2 describes previous work that considered the application of non-thermal plasmas to the removal of waste gases. Experimental setup and the methods are discussed in Chapter 3. The reaction modeling is explained in Chapter 4. The experimental results and discussion of the experiments along with the modeling results are given in Chapter 5. The conclusions are presented in Chapter 6, followed by recommendations for future work in Chapter 7. Experimental data tables and computer codes are reported in the appendices.

CHAPTER 2

LITERATURE REVIEW

This chapter discusses previous research on pollutant removal from waste streams using non-thermal plasma techniques such as electron beams, dielectric barrier discharge, and corona discharge.

2.1 Electron Beams

Electron beam treatment to prevent pollution was first initiated in Japan in 1970 by the Japan Atomic Energy Research Institute in collaboration with Ebara Corporation. Several pilot plant studies of electron beam process applications to coal-fired powered plants have been made in Europe and in the U.S. This process is particularly attractive for the treatment of large volumes of gaseous effluents such as those coming out of utility power plants (Frank et al., 1993).

In the electron beam process, irradiation of the flue gas with energetic (300-800 keV) electrons initiates electron-gas reactions to produce radicals that have high enough energy to oxidize NO_x and SO_2 to nitric acid and sulfuric acid, respectively. In the presence of ammonia (NH_3), these acids are converted into ammonium sulfate and ammonium nitrate. These salts are later recovered as a dry powder using a conventional particle collector (Frank et al., 1993, Matzing, 1991).

The reaction mechanism involved in the removal of NO_x and SO_2 in electron beam treatment was investigated by Tokunaga et al. (1984). Reactions of NO_x and SO_2

were studied under the irradiation of electron beams using various gas compositions ranging from a simple system (nitrogen-NO) to a more complex system (nitrogen-oxygen-water vapor-NO-SO$_2$) which is close to the composition of an actual flue gas. For the NO-nitrogen gas mixture at a gas temperature of 100° C, a dose of 3 Mrad, and an initial NO concentration of 250 ppm, 10% of the NO was converted into NO$_2$ and 3% of the NO was converted to N$_2$O. The remaining NO was anticipated to be decomposed mainly to nitrogen and oxygen. In the case of a NO$_2$-nitrogen mixture at a dose of 6 Mrad, 60% of the NO$_2$ formed NO and N$_2$O, and 40% of the NO$_2$ was decomposed to nitrogen and oxygen.

For different NO and NO$_2$ concentrations in a gas containing 3% oxygen and 97% nitrogen at 100° C, the final concentrations of NO and NO$_2$ were represented by the following equation:

$$\frac{[NO]}{[NO_2]^2} = 0.027 ppm^{-1}. \tag{2.1}$$

The total NO$_x$ concentration was observed to increase with dose rate for initially low concentrations of NO (50-100 ppm), and was not observed to follow the above empirical relation. The presence of water vapor (2.2% to 12.9%) enhanced the NO removal and the formation of HNO$_3$ at a gas temperature of 120° C. The addition of additives such as carbon monoxide (0-1.13%) and ammonia (0-2000 ppm) were observed to have a positive effect on the removal of NO. For a 1.13% addition of carbon monoxide, NO removal was enhanced by 50% at 1 Mrad, and an increase of 14% was found in the NO removal efficiency with the addition of 2000 ppm of NH$_3$.

A kinetic model for the radiation-induced oxidation of nitrogen oxides to include temperature dependence and the presence of sulfur dioxide was developed by Busi et al. (1987). An increase in temperature from ambient to 120 °C decreased the removal efficiency of NO. Matzing (1991) considered detailed theoretical and model results for the electron beam dry scrubbing process (EBDS). The major radical source was shown to come from positive ion formation, which led to NO$_x$ removal

by both oxidative and reductive reaction pathways. The relative humidity of the gas played a crucial role in the removal efficiencies. The addition of ammonia led to the formation of aerosols, and a linear correlation was found between N_2O formation and the stoichiometric ratio of added ammonia.

Among the disadvantages of using the electron beam process are high cost, large physical size of electron beam generators, X-ray hazards, the necessity of ammonia addition, and aerosol formation (Frank et al., 1993).

2.2   Dielectric Barrier Discharge

Dielectric barrier discharge (DBD) or silent discharge has been studied for the removal of SO_2 (Sardja et al., 1990; Dhali et al., 1991) and NO_x (Chang et al., 1992). In DBD, a repetitive pulsed or AC voltage is applied in order to sustain a discharge between two separated electrodes having a dielectric material covering each. Ions produced by the discharge traverse the space between the electrodes, and are then stored in the surface of the dielectric materials. Hence, a sparkless reactive plasma with a high electron temperature and a low gas temperature is produced which enhances the chemical reactions desired for SO_2/NO_x removal.

In DBD, the gas is exposed to many such discharge pulses. Excitation of an atmospheric pressure plasma in this fashion is quite efficient because arcs between electrodes are prevented by the short duration of the individual current pulses, and the electron energy of the plasma is well matched with the energy required to produce the electronic and dissociative states of molecular gases (Chang et al., 1992). Chang et al. (1992) found that under dry conditions the NO removal efficiency decreased under with an increasing concentration of O_2 at room temperature. Also, the efficiency of NO removal increased in the presence of water vapor in the system at room temperature. At elevated temperatures (130-160° C), increasing $H_2O_{(g)}$ (> 9%) concentration and decreasing CO_2 (< 3%) concentration resulted in increasing NO

removal efficiencies. NO removal efficiency was found to be sensitive to gas temperature, gas composition, and power deposition.

Dielectric discharge can also be produced by utilizing a reactor filled with ferroelectric material between two metal electrodes connected to a high voltage AC power supply. An electric field of high intensity is formed around each dielectric pellet, thereby producing high energy free electrons (Mizuno et al., 1987).

2.3   Corona Discharge

Corona discharge exists in several forms including DC corona, AC corona, pulsed corona, and positive corona or negative corona, depending on the type and polarity of the electric field and on the electrode geometry (uniform or non-uniform). Pulsed streamer corona discharges have been considered for the removal of pollutants both in the gas phase (Clements et al., 1989; Dinelli et al., 1990; Masuda et al., 1990) and in the liquid phase (Clements et al., 1985; Sharma et al., 1993; Joshi et al., 1995). The use of pulsed corona for flue gas treatment is being pursued industrially in several places such as at a coal burning thermal power station at ENEL (Dinelli et al., 1990).

DC corona has been used in the removal of NO_x in place of an electron beam, and it was found that the removal rate was enhanced but the power consumption was very high. DC corona consumes high electric power since it accelerates negative ions as well as electrons. Since oxidizing species such as OH· and O· are produced in a very short time only by electrons with a sufficient energy, it is imperative to electrically accelerate only the electrons, and not the ions, in order to reduce the power consumption. An effective method is to use a very sharp high voltage pulse with a nanosecond range duration time, because this allows strong acceleration of electrons with minimum ion acceleration even under ordinary gas pressure (Masuda

et al., 1990). Due to the nanosecond duration of the applied pulse, much higher electric fields can be applied without causing sparking between the electrodes.

Simultaneous removal of NO_x and SO_2 from flue gas by the application of short duration voltage pulses was considered in an electrode geometry similar to that of an electrostatic precipitator (Dinelli et al., 1990). A nitrogen oxides removal efficiency of 33% together with a sulfur dioxide removal efficiency of 75% was obtained when both contaminants were present at levels of 420 ppmv and 360 ppmv, respectively, in $90°$ C air containing ammonia for 6 Wh/Nm^3 energy input into the gas. The energy efficiency of this process is such that with 1 kWh input to the gas a removal of about 25 g of nitrogen oxide and about 70 g of sulfur dioxide was achieved with the addition of 40 g of ammonia. The use of hydrated lime was also considered as a possible substitute for ammonia for the neutralization of the nitrogen and sulfuric acidic compounds to form salts. Optimization of ammonia injection and gas temperature along with better electrical design of the reactors was suggested to improve the energy efficiency .

In a negative pulsed streamer corona process, NO_x concentration remained unchanged up to a critical peak field intensity for a $NO-NH_3$-air mixture (NH_3: 180 ppm) (Masuda et al., 1990). Beyond this critical field intensity, NO_2 was also removed, and its removal depended upon the gas residence time and the amount of ammonia addition. Ammonia addition enhanced the removal of NO_2 but not that of NO. The efficiency of NO removal by using negative pulsing was found to be a function of the specific power of pulsing P/Q (corona power/ gas flow rate) divided by the inverse of the square root of the residence time.

NO_x removal from dry air mixed with ammonia in a pipe/nozzles-to-plate electrode corona discharge system has also been considered (Ohkubo et al., 1994). The gases were introduced into the discharge zone through the pipe electrode coming out of the nozzles. The addition of ammonia led to the formation of ammonium nitrate

aerosol particles which were deposited on the electrodes. The characteristics of the corona discharge were significantly affected by the addition of inert gases such as argon. The addition helped in obtaining a stable streamer corona for higher NO_x removal efficiency.

Mizuno et al. (1995) noted that the removal of NO_x gases can be achieved by using square-wave voltages having frequencies on the order of several hundred Hz for the energization of cylinder-type plasma chemical reactors. The performance was noted to be better at lower gas temperatures, and the use of ethylene as an additive to the flue gas significantly enhanced the NO_x removal efficiency. They observed the formation of acetic acid in the analysis of the reaction products, but it was not quantified.

Simultaneous removal of NO_x, SO_x, and fly ash (RO_x) using the application of a semi-wet type corona discharge reactor has been considered (Okazaki et al., 1995). The semi-wet type discharge reactor consisted of a cylindrical pyrex glass tube and a stainless steel discharge wire electrode at the center, with a water film covering the inner surface of the glass tube. For an initial concentration of 300 ppm of NO and 500 ppm of SO_2, 90% of NO_x and nearly 100% of SO_2 were removed at the same time, even in a gas containing high oxygen concentration of about 15%.

Tas (1995) investigated the plasma-induced conversion of NO as a function of several parameters including the composition of the gas mixture, the presence of catalyst materials, and the type of catalyst material. The energy efficiency of the conversion of NO to NO_2 can be increased by a factor of 2 for pure bulk gas of helium or nitrogen with 1000 ppm of NO by using a silica catalyst. The energy input was varied by controlling the pulsing frequency of the discharge in the reactor. The addition of oxygen to the bulk gas depressed the dissociative conversion of NO, and at a high power input and for an initial concentration of 1000 ppm, Equation 2.1

corresponded well with the measured conversion of NO. With the addition of water, NO_2 was expected to be converted to HNO_3, however HNO_3 was not detected.

Figure 2.1 compares the energy efficiency of NO removal at high concentrations of NO by Mizuno et al. (1995) and Tas (1995), and Figure 2.2 shows a summary of energy efficiency of NO removal at low concentrations of NO by Masuda et al. (1990) and Ohkubho et al. (1994). As seen in Figure 2.1, the addition of 500 ppm of ethylene increased the NO removal for the same power per unit volume divided by the square root of time in dry air. The data points of Mizuno et al. (1995) and Tas (1995) for the case of NO removal in the presence of water almost falls in the same region.

In Figure 2.2, the NO removal in the presence of ammonia considered by Masuda and Nakao (1990) was far different from that observed by Ohkubho et al (1994). Although, in all the of the cases NO removal was considered by pulsed streamer corona discharge, there were certain dissimilarities such as the nature of the electrode and the polarity of the field. No theoretical justification for this type of plot is available at present, however it serves as a convenient means to compare data under a variety of power conditions.

Modeling of the chemical reactions taking place during the pulsed streamer corona process has been developed in order to understand the evolution of the concentrations of different chemical species (Penetrante et al., 1993). For a power input of 0.05 W/cm^3 and for an initial concentration of 400 ppm NO at 300° K, 200 ppm of the initial NO was converted back to N_2 and 200 ppm to NO_2. Of this 200 ppm of NO_2, 180 ppm was converted to N_2O and 20 ppm to N_2O_5. When the temperature was increased to 400° K, only 100 ppm of the initial NO was converted to NO_2 and another 100 ppm was converted to N_2O. With the addition of 10% water and 15% CO_2, from an initial 400 ppm NO about 120 ppm was converted to HNO_3 and 50 ppm was converted to N_2O. The ozone produced is about 50 ppm and the residual
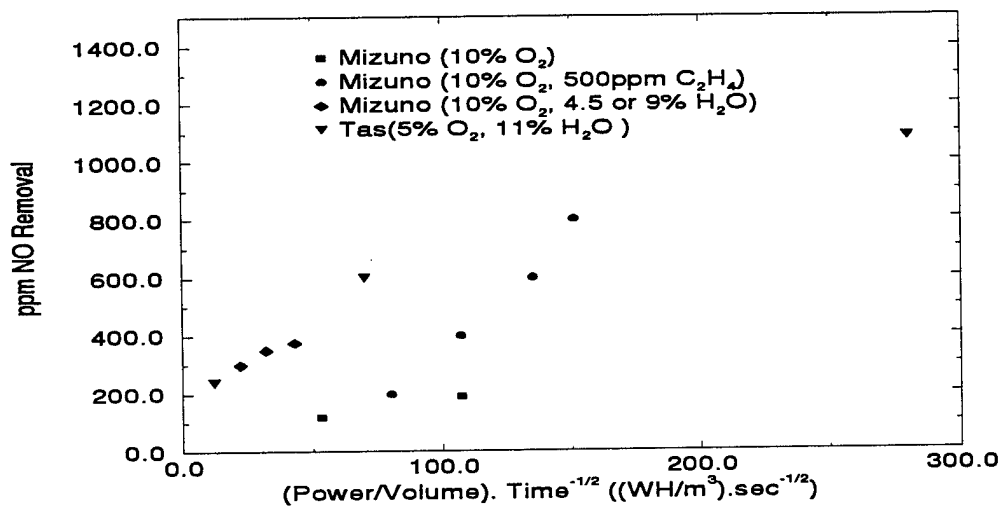
Figure 2.1: Summary of Energy Efficiency of NO Removal at High Concentrations
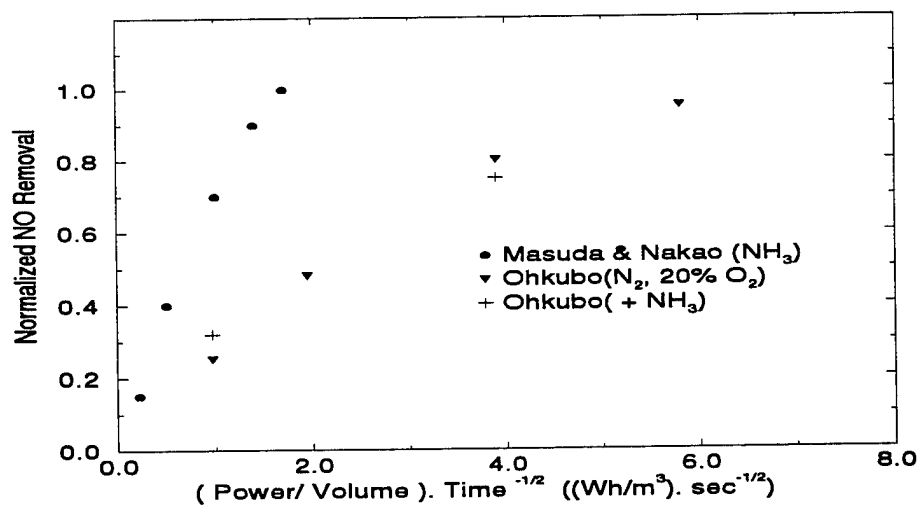
Figure 2.2: Summary of Energy Efficiency of NO Removal at Low Concentrations

NO_x present was around 10 ppm. This model prediction, however, has not yet been confirmed by experimental results.

2.4 Physical Characteristics of the Pulsed Corona Discharge

Different types of corona discharges can occur in non-uniform electric fields, depending upon the polarity and the nature of the applied electric field. Positive pulsed corona proceeds from corona onset to a burst pulse corona to streamer corona, then to glow corona and finally spark discharge as the applied voltage is increased. In the case of negative pulsed corona, the initial form is Trichel pulse corona, followed by pulseless corona and then spark discharge as the voltage is increased. A Trichel pulse refers to the regular current pulse produced when the voltage applied to a negative electrode is gradually increased to produce ionization. These pulses are extremely regular in both their magnitude and repetition rate. The frequency of the Trichel pulse repetition starts with 2 kHz near onset, and it may attain a few MHz before the onset of glow corona (Naseer, 1971). Positive corona depends more on photoionization for its propagation, while the negative corona propagates by impact ionization of the gas molecules (Chang et al., 1993).

In *pulsed streamer corona*, the ionization grows from the high voltage electrode into a background field which is purely geometric. The discharge assumes the form of a number of branched, tree-like streamers, whose starting points are discrete and distributed over the highly stressed region with a specific density (Dinelli et al, 1990). Photoionization is generally assumed to be the mechanism that supplies secondary seed electrons and triggers the avalanches.

The streamer formation in a DC anode (positive) corona can be described as a Townsend avalanche which is a conceptual description of the electron multiplication processes. The process begins with free electrons in a strong electric field gaining energy to collide with gas molecules and lose energy by a variety of collision pro-

cess (e.g. elastic scattering, excitation, ionization), thereby producing secondary electrons and positive ions (Creyghton, 1994). The electrons produced through collision further produce electrons through secondary reactions, resulting in an electron avalanche. As a result, the head of the electron avalanche and the positive ions, which are left behind the avalanche, form a sort of dipole. The electron avalanche is said to be "critical" when the dipole field reaches a value comparable to the external applied field. The electric field is enhanced in front of the head of the electron avalanche, while the electric field is reduced in between the avalanche head and the positive ions which are left behind. Still further back in the avalanche, the electric field between the positive ions and the cathode is enhanced.

Now the electron avalanche has an increased velocity and light emission intensity. These avalanches are referred to as anode directed streamers (ADS). Also, as the electrons propagate towards the anode there is a buildup of positive ions. In the presence of a space charge field and initial free electrons at the cathode side of the avalanche, cathode directed streamers (CDS) can be formed. The CDS propagate as a result of secondary avalanches which neutralize the positive concentration of the previous avalanches, leaving a new positive ion concentration behind at a shorter distance from the cathode (Creyghton, 1994). During the primary avalanche, propagation excited gas molecules are also produced which act as a source for electrons. These electrons serve as a source for secondary avalanches required for CDS propagation.

Streamer discharges are hence highly localized "space charge waves" which enhance the applied field in front of the wave (active region) and propagate because of electron avalanche formation in this high field. Along the track of the wave there remains a weakly ionized plasma filament (passive region), along which the conduction current flows to the high voltage electrode, supplying the energy for streamer advancement (Nasser, 1971). In the case of corona at impulse voltages, the ionic

space charge drift and accumulation can be neglected due to the short duration of the pulse width. In the case of non-uniform electrode geometry, the streamer growth assumes radial directions, increasing the number of branches.

The major characteristics of streamers include the length, number, speed of propagation, width, number of electrons and ions, time lag, and electric field distribution. Typical values of streamer width are in the range of 25 to 100 μm and the speed of propagation is in the range of 0.7-0.9 mm/ns (Creyghton, 1994). Recent experimental and theoretical studies have also shown that the propagation characteristics of positive streamers depend very much upon the degree of electronegativity of the carrier gas. In weakly electronegative gases like atmospheric air, the streamers appear much longer and more branched than in strongly electronegative gas such as SF_6. Hence, with large concentrations of CO_2 and H_2O, the discharge characteristics are very near to those of highly electronegative gases (Gallimberti, 1988).

2.5 Modeling Pulsed Streamer Corona Discharge

In order to model the streamer discharge in a pulsed corona, an understanding of the elementary processes such as ionization, attachment, and photoionization is essential.

A 1-D streamer propagation model has been developed in which the streamer is assumed to possess cylindrical symmetry (Gallimberti, 1972, 1988). The densities of the charged particles along the central axis (x-axis) of the streamer can be calculated solving the continuity equations, i.e., for electrons, positive ions, and negative ions. It is possible to solve for the electric field by solving the Poisson equation once the densities of the charged particles are known:

$$\nabla \cdot E = \frac{(n_p - n_e - n_n)}{\epsilon_o},$$

(2.2)

where E is the electric field, n_p is the concentration of positive ions, n_e is the concentration of electrons, n_n is the concentration of negative ions and ϵ_o is the permittivity of the gas medium considered.

2-D models, in which the radial distribution of charged particles is calculated, have been performed to simulate streamer formation in a uniform electric field (Wang et al., 1990). A 1-D streamer model with an approximation of the Poisson equation has been used to calculate the streamer properties (Creyghton, 1994). The current pulse, net charge injection, and energy loss have also been calculated for an impulse corona (Gallimberti, 1988).

The solution of the Boltzmann equation is necessary to calculate the electron transport coefficients and kinetic rate coefficients for various inelastic electron-gas collision reactions. The Boltzmann equation is the continuity equation for electrons in six-dimensional phase space and it describes the time evolution of the electron energy distribution function. The most common technique used to solve the Boltzmann equation has been the moment method in which a spherical harmonic expansion (or Legendre series) of the angular dependence of the velocity is assumed with truncation after the first two terms (Huxley at al., 1974). The electron transport properties were significantly affected by the composition of gas considered.

The kinetic rate coefficients for the electron-gas reactions are functions of the electron energy distribution function. The kinetic rate coefficients can be calculated by:

$$k_{eij} = \int_0^\infty [\frac{\epsilon}{2m_e}]^{\frac{1}{2}} \sigma_{ij}(\epsilon) f(\epsilon) d\epsilon, \tag{2.3}$$

where k_{eij} is the kinetic rate constant for the electron-gas reaction, ϵ is the electron energy, m_e is the mass of an electron, σ_{ij} is the collisonal cross section, and $f(\epsilon)$ is the electron energy distribution function.

The collision cross section (σ_{ij}) is defined as a measure of the probability of a given type of interaction between a gas molecule and an electron. The cross section

is a function of the relative velocity of particles and the energy of the electrons. It varies over several orders of magnitudes according to the type of interaction being considered.

The densities of chemical reactive dissociation products has been calculated using a numerical model for streamer-induced chemical kinetics as discussed above (Alekseev et al., 1993, McFarlane et al., 1991). Modeling of the electrostatic corona discharge reactor has been done by solving the Boltzmann's equation for the electron energy distribution function and to determine the kinetic rate constants for the electron gas collisional reactions (Mukkavilli et al., 1988). For a dry air system, 58 reactions were considered and 96 reactions were considered for the wet air system. Increase of moisture in the feed air had a negligible effect on the input gases (N_2 and O_2), but it was found to reduce the ozone concentration by more than two orders of magnitude and that of NO_x by a factor of two.

Ozone generation in pulsed corona reactors having point-to-plane and cylindrical geometries have been considered with discrete injection of electrons and also with time-varying electronic density (Pignolet et al., 1990; Loiseau et al., 1994). The shape of the electronic injection time profile did not affect the concentration profile of ozone production. The temperature gradient between the electrodes in the wire-to-cylinder geometry had a drastic effect on the electron densities near the wire, directly through ozone destruction at high temperatures and indirectly by viscosity, which affects the velocity profile (Loiseau et al., 1994).

Past work in the field of pulsed streamer corona has focused on either primarily experimental results or on purely theoretical modeling. The present work will try to combine both experimental and computational aspects in order to develop an understanding of the basic chemistry taking place during pulsed streamer corona process. Removal of NO from gases of various compositions including pure nitrogen and air, and the addition of water vapor, ethylene and carbon monoxide will

be considered. A kinetic model will be utilized in order to develop a quantitative understanding of the reaction pathways occurring in the system.

CHAPTER 3

EXPERIMENTAL APPARATUS AND PROCEDURES

Non-thermal plasma reactors operated at low temperature, low power consumption, and atmospheric pressure can be classified by their physical geometry and by their method of electrical energization. Among the various types are point-to-plane, point-to-point, packed bed, coaxial, and wire-cylinder electrode geometries. The methods of energization include direct current, alternating current, or pulsed current. In this study, a pulsed power delivered to a wire-cylinder geometry reactor was used.

3.1 Power Supply

The pulsed power supply used in this investigation is shown in Figure 3.1. It consists of two major units: 1) a high voltage transformer/rectifier (T-R) set and 2) a pulse generating apparatus. The power supply used was similar to the configuration used by Clements et al. (1989). The high voltage DC T-R set was modified by eliminating the internal rectifier, thereby producing 0-100 kV AC at 0-28 mA. Output from the T-R set was connected to the pulse generation circuit, where the current passes through a high voltage resistor (333 kΩ) and then through a diode array which acts as a half-wave rectifier. The output from the rectifier charged a bank of capacitors (2700 pF) during the charging cycle. A mechanical rotating spark gap having two fixed stainless steel spherical electrodes and a rotating rod electrode was

20
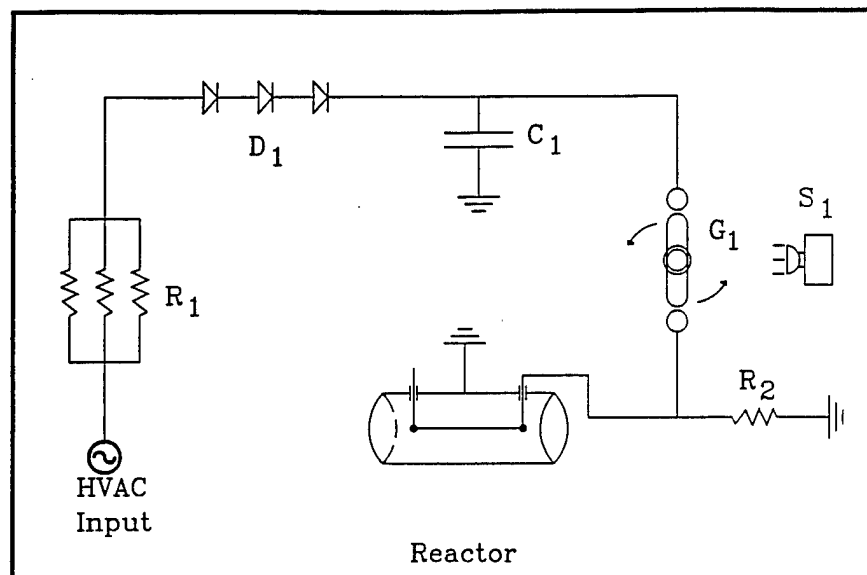
HVAC = 0 - 100 kV, 0 - 28 mA

R_1 = 333 kΩ

R_2 = 300 Ω

D_1 = 60 kV, 12 A max

C_1 = 2700 pF

G_1 = Rotating Spark Gap, 1800 RPM, 60 discharges / sec

S_1 = Strobe Lamp

Figure 3.1: Pulsed Power Supply Diagram

employed to discharge the capacitor bank twice per shaft revolution, synchronized with the AC current (60 Hz). From the output of the spark gap the circuit had two parallel pathways. One of them passed through a load resistor (300 kΩ) which enabled the gap to fire. The other was connected to the central wire within the cylindrical reactor, from which the discharge emanated. The generation of pulsed corona discharge by a rotating spark gap was a source of electromagnetic interference, therefore the pulse generating apparatus was encased in an aluminum box to reduce RF noise.

3.2 Reactor Specifications

The pulsed streamer corona reactor used in this study was a stainless steel 4 in diameter and 18 in long cylindrical tube. The high voltage electrode (0.109 in diameter, 12 in long) run concentric to the grounded outer cylinder resulting in a electrode seperation of 2 in. The active pulsed corona treatment volume of the reactor was 2.45 l. The typical gas flow rate, gas velocity, and residence time in the reactor are from 2.5 to 40 l/min, from 321 to 5134 cm/s, and from 3.6 to 60.0 s, respectively. The high voltage ceramic feed through conductors as well as the center electrode were fabricated of # 304 stainless steel to prevent any corrosion and rust formation inside the reactor.

3.3 Analytical Instrumentation

Analysis of the outlet gases from the reactor included the measurement of NO, NO_2, O_3, N_2O, and hydrocarbon breakdown products. Nitrogen oxides (NO and NO_2) were measured using a Thermo-Environmental Instruments, Inc., Model 42H chemiluminescence NO_x Analyzer. Ozone was measured using a PCI Ozone Corporation, Model HC-1 ozone monitor. N_2O and hydrocarbon breakdown products were

measured using a Hewlett-Packard GC/MS instrument located in the Department of Chemistry at Florida State University. HPLC analysis was also performed on liquid water samples in a column through which the reactor exhaust gas was passed. The gas was bubbled with a sparger through a water column of 200 ml. HPLC analysis was used to determine the breakdown products of the ethylene when NO removal was considered in the presence of ethylene. The pulse waveform characteristics were measured using a Tektronix TDX 460 four channel digitizing oscilloscope with a P6015A 1000x 3.0 pF, 1000 MΩ voltage probe and two current probes (P6016 & P6021). A Cole-Parmer TriSense velocity/temperature/humidity measurement system was used to measure the gas velocity, temperature, and humidity in the gas system. The different analytical instrumentation used along with the reactor and the gas feed system is shown in Figure 3.2.

3.4   Feed Gas System

The feed gas system (see Figure 3.2) consisted of: 1) a compressed air source and pure nitrogen gas cylinders which act as carrier gases, 2) gas cylinders and high pressure regulators containing 1% NO in dry N_2, 1% NO_2 in dry N_2, pure C_2H_4, pure CO, 3) gas cylinders and high pressure regulators containing calibration gases of 100 ppm NO in N_2 and 113 ppm NO_2 in N_2, 4) a water tank through which the air and the other gas can be bubbled for humidification, 5) flow meters, valves, and mass flow controllers, and 6) a stainless steel mixing chamber upstream from the reactor.

The gas cylinders and the regulators were manufactured by Air Products Inc. The water tank used to humidify the air was 26 in long and 7 in diameter. The air was introduced at the bottom of the tank, and was made to bubble through the water column. Flow meters used to monitor the flow rate of the air into the reactor were purchased from Dwyer Inc. Mass flow controllers used to control the flow of air and the trace gases sent into the reactor, were purchased from MKS Instruments Inc. Two
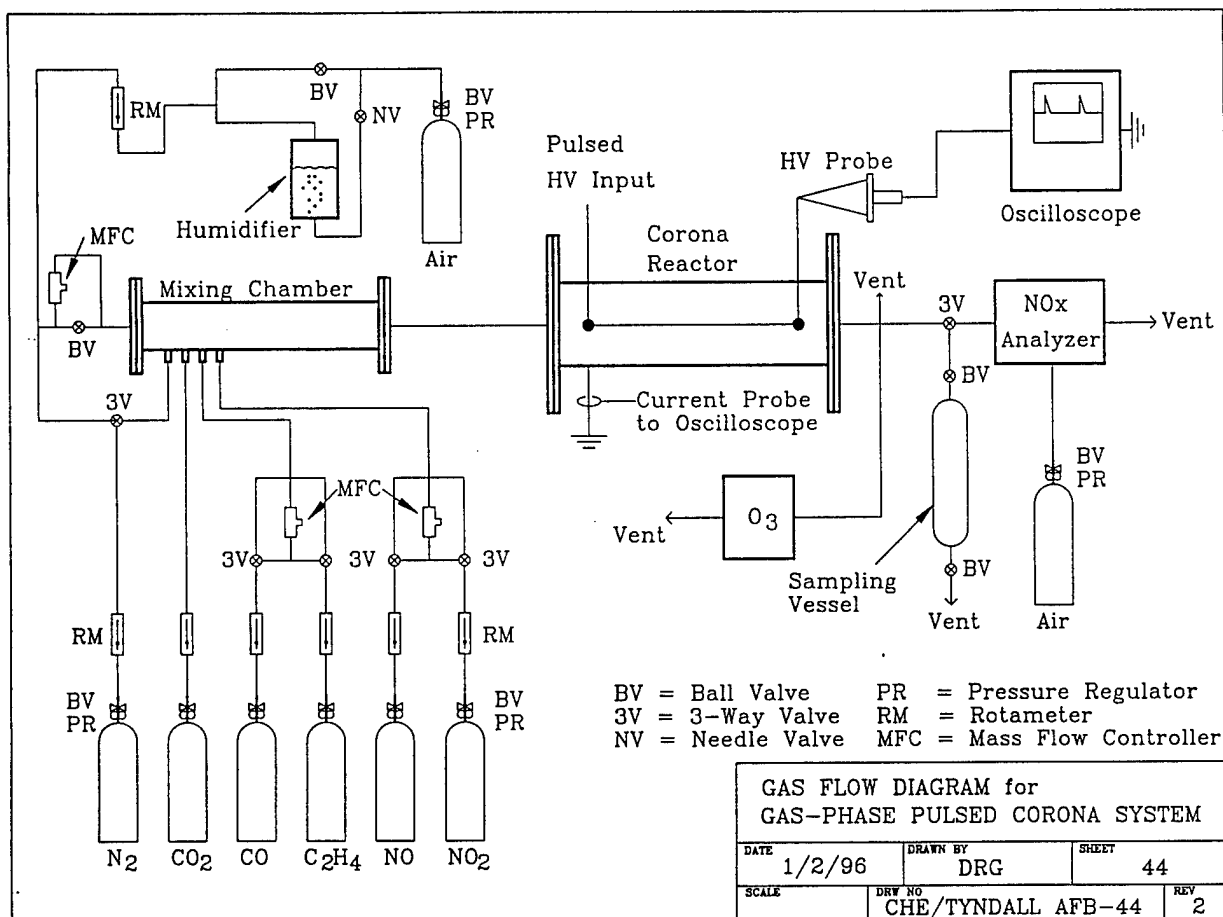
Figure 3.2: Experimental Setup

controllers of Type 1259C were used to control the flow of NO and ethylene gas. A mass flow controller of Type 1559A was used to control the amount of air or N_2 flowing into the reactor. Trace gases such as NO, ethylene and CO were mixed with the air in a stainless steel mixing chamber before passing into the reactor. The mixing chamber was 23.5 in long and had a diameter of 2.5 in.

3.5   Experimental Procedures

In order to conduct a typical experiment to consider the NO removal at a particular voltage and residence time, the NO_x monitor as well as the mass flow controllers were turned on at least 2 hours before the start of the experiment for them to stabilize. Later calibration for the NO_x monitor was performed by passing the calibration gases of known concentrations of NO and NO_2 into the monitor and calibrating the monitor reading to the corresponding value. Once the mass flow controllers stabilize, the readings were zeroed if necessary.

The feed air used in the experiments was produced by a central compressed air source in the building. A dedicated regulator/valve assembly was adjusted so that the pressure of the air delivered to the gas distribution system was 20 psig. The air flow rate through the reactor was then adjusted with needle valves and with the mass flow controller corresponding to the required gas residence time in the reactor. The two spherical electrodes and the rod electrode on the rotating spark gap were cleaned using ethanol and sandpaper before running every experiment. The spherical electrodes tended to corrode during the course of an experiment. The rotating mechanical spark gap was engaged and adjusted such that it was aligned perpendicular to the discharge position when the strobe lamp is in line frequency mode (60 Hz). This ensured full charging of the capacitors by the power supply.

The feed air delivered to the reactor was first passed through a drier (calcium sulphate packed columns) to remove any residual water vapor present in the com-

pressed air. In case where water vapor was required for an experiment in the system, air was bubbled through a water tank. The flow rate of all feed and trace gases were continually monitored by mass flow controllers and/or by flow meters.

To measure the voltage waveform of the pulsed voltage, the high voltage probe was connected to the central wire electrode to which the high voltage input was connected. The current probe was attached across a wire connecting the outer cylinder of the reactor to the ground. The exact locations at which the voltage and the current were measured are shown in Figure 3.2. Both the probes were connected to the oscilloscope to measure the different characteristics of the waveforms. Once the flow rate of all the gases had stabilized, the pulsed corona discharge was applied to the reactor.

The pulsed voltage, current, and power waveform characteristics were noted from the oscilloscope and adequate time was allowed for all the analytical instruments to stabilize. The exhaust gases coming out of the reactor were either passed through the NO_x monitor or the ozone monitor to record the concentration of NO and NO_2 or the ozone concentration. For trace gas sample analysis, the outlet gases from the reactor were passed through a glass sampling vessel. The gases in the sampling vessel were analyzed by GC/MS for the breakdown products of NO_x gases and also for the concentration of ethylene in experiments for which the ethylene was present in the feed gas. For liquid sample analysis, the exhaust gases were bubbled through a water column; these water samples were then analyzed by HPLC and ion chromatography.

Once the readings of the 1) NO_x concentration, 2) the rise time, 3) the peak voltage, 4) the pulse width of the voltage waveform, 5) the peak current and 6) the pulse width of the current waveform, are measured the power to the reactor was turned off and the reactor and the spark gap were grounded with a grounding rod. The valves of the gas cylinders were closed and the reactor was then purged for several minutes with clean, dry compressed air.

CHAPTER 4

REACTION MODELING

In a pulsed corona discharge in a gaseous medium, free electrons gain energy from an imposed electric field and lose energy through collisions with neutral gas molecules. This transfer of energy to the gas molecules leads to the formation of a variety of new species including ions, metastables, atoms, and free radicals. These products are chemically active and react with the other gas molecules to form new stable compounds. The modeling of the reactor is a complicated process and certain assumptions are made to analyze the system.

The kinetic rate constants for the electron-gas reactions depend upon the imposed electric field and also on the gas composition. In this work, a simple model was constructed with the help of experimental data to consider the evolution of different molecular species during the pulsed corona discharge. A global approach was adopted where only dissociation reactions of major constituents of the gas were considered in the reaction model. The kinetic rate constants for the dissociation reactions were obtained from the experimental data of NO removal and NO_2 formation and removal in various gas streams.

The modeling effort here accounted for the chemistry in pulsed streamer corona discharge by considering two chemical reaction sets. During the time frame of pulsing, the electron concentration was assumed to be fixed, and the reaction set included the gas molecule dissociation reactions in order to calculate the concentration profile of different species. During the time between the pulsing, the electron concentration

27

was assumed to be zero, and so the reaction set which did not have the dissociation reactions was used to calculate the concentration profile. These two reaction sets were interchanged repeatedly to simulate the pulse-on, pulse-off aspect of the discharge.

The pulse width of the voltage pulse which was the time at the half maximum, varied between 500-700 nanoseconds. The total pulse duration from the inception of the rise time to the complete decay of the voltage peak was 1 microsecond. In the present modeling, the pulse width was hence assumed to be 1 microsecond and the time between the two pulses was assumed to be 16.667 milliseconds, corresponding to a pulse frequency of 60 Hz. Hence the reaction set with electron dissociation reactions was used to calculate the concentration profile for 1 microsecond followed by the reaction set which did not include the dissociation reactions to calculate the concentration profiles for the next 16.667 milliseconds repeatedly until the final total time equaled the residence time in the reactor.

This method was similar to the model used by Loiseau et al. (1994) for computing ozone production in a cylindrical oxygen-fed ozonizer. For example Figure 4.1 shows the concentration profile of ozone computed by the code used in the present study that alternately employed the two reaction sets to simulate the pulse-on and pulse-off aspect of the discharge. As in the figure, during the pulse-on period the oxygen radicals are produced and hence ozone formation increased rapidly, and during the pulse-off period the ozone production level was flat.

The following were the assumptions made for the model used here:

1. Isothermal system. There is no appreciable heating of the gas during the residence time in the reactor.

2. Plug-flow model. The model does not account for the axial and radial dispersion in the reactor.
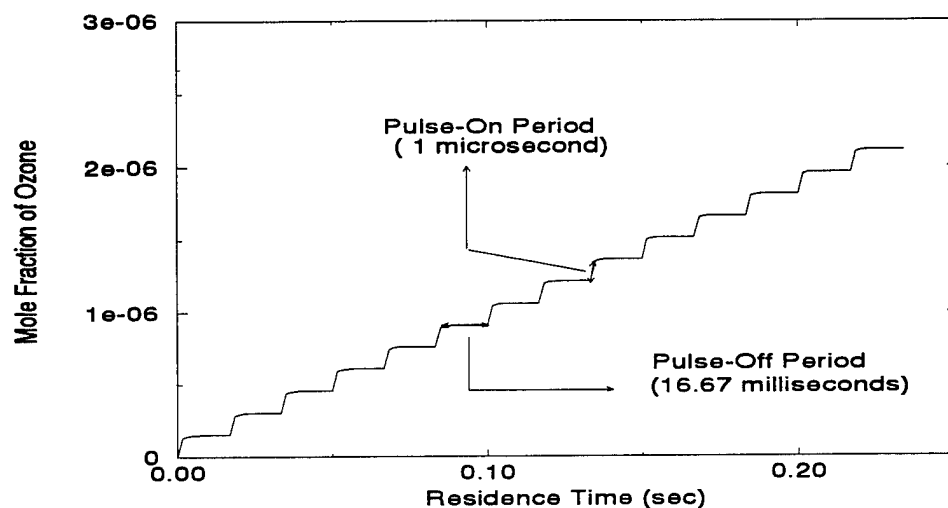
Figure 4.1: Ozone Concentration Profile to Illustrate the Modeling

3. There is no variation in the concentration of electrons during the pulse-on period either in space or in time.

4. Reactions involving metastables, ions, and photoionization are neglected.

5. The model does not account for the variation in electric field strength from the anode wire to the cathode cylinder.

The molar species continuity equations for all the species is given by:

$$\frac{\partial c_i}{\partial t} + \vec{v} \cdot \nabla c_i = D_i \nabla^2 c_i + \sum_j v_{ij} R_{ij}, \qquad (4.1)$$

where c_i is the concentration of species i, t is the time, $\vec{v}$ is the molar average velocity vector, D_i is the diffusional coefficient, v_{ij} is the stoichiometric coefficient of the ith species in jth reaction and R_{ij} is the reaction rate. For a plug flow reactor model without axial dispersion or molecular diffusion the equation reduces to:

$$v_x \frac{dc_i}{dx} = \sum_j v_{ij} R_{ij}, \qquad (4.2)$$

In terms of residence time $(\tau = x/v_x)$ in the reactor, the equation becomes:

$$\frac{dc_i}{d\tau} = \sum_j v_{ij} R_{ij}. \tag{4.3}$$

The above system of ordinary differential equations has been solved using the software CHEMKIN (Kee et al., 1994). A simple set of reactions was considered which included only one electron-molecule collision reaction per each major constituent (N_2, O_2, H_2O). The dissociation reactions considered which were dependent upon the electric field are:

$$N_2 \xrightarrow{K_1[E]} N^{\cdot} + N^{\cdot}, \tag{4.4}$$

$$O_2 \xrightarrow{K_2[E]} O^{\cdot} + O(^1D), \tag{4.5}$$

$$H_2O \xrightarrow{K_3[E]} H^{\cdot} + OH^{\cdot}. \tag{4.6}$$

Reaction 4.4 represents the production of nitrogen free radicals by all possible mechanisms including dissociation, ionization and excitation. The kinetic rate constant for this global reaction is dependent upon the electric field applied and hence varied with the external applied field. Similarly, the rate constants for Reactions 4.5 and 4.6 represent the global kinetic rate constants for the production of oxygen and hydroxyl radicals, respectively. Although ionization is a major process taking place in the corona discharge, it was assumed in the present model that the ions do not play a major role in the chemistry of the neutral gas molecules.

The set of reactions used for modeling NO removal in the case of nitrogen, dry air, and humid air is shown in the Table 4.1. The rate constants for these reactions are obtained primarily from the atmospheric chemistry literature (Willis & Boyd, 1976, Baulch et al., 1983, Demore et al., 1987, and Atkinson et al., 1989), and is cross-checked with the NIST Database (NIST Standard Reference Data Base 17.0, 1994). The criterion for choosing the reactions was to consider reactions of neutral species having significant kinetic rate constants ($> 1.0 \times 10^7$).

Table 4.1: List of Chemical Reactions Considered for Modeling

Chemical Reactions	Rate Constants $(cm^3.mole^{-1}.sec^{-1})$	Source
$N_2 \longrightarrow 2N\cdot$	$K_1[E]$	Expt. Data.
$O_2 \longrightarrow O\cdot + O(^1D)$	$K_2[E]$	Expt. Data.
$N\cdot + N\cdot \longrightarrow N_2$	6.38×10^{10}	Willis & Boyd, 1976.
$N\cdot + O\cdot \longrightarrow NO$	1.45×10^{11}	Willis & Boyd, 1976.
$N\cdot + NO \longrightarrow N_2 + O\cdot$	2.04×10^{13}	Willis & Boyd, 1976.
$N\cdot + O_2 \longrightarrow NO + O\cdot$	5.36×10^7	Atkinson et al., 1989.
$N\cdot + NO_2 \longrightarrow 2NO$	1.81×10^{12}	Atkinson et al., 1989.
$N\cdot + NO_2 \longrightarrow N_2O + O\cdot$	1.81×10^{12}	Atkinson et al., 1989.
$O\cdot + O\cdot \longrightarrow O_2$	1.02×10^{11}	Willis & Boyd, 1976.
$O\cdot + O_2 \longrightarrow O_3$	7.83×10^9	Willis & Boyd, 1976.
$O\cdot + O_3 \longrightarrow 2O_2$	4.82×10^9	Willis & Boyd, 1976.
$O(^1D) \longrightarrow O\cdot$	6.95×10^8	Demore et al., 1987.
$O(^1D) + NO_2 \longrightarrow NO + O_2$	2.95×10^{13}	Schofield, 1979.
$O(^1D) + O_3 \longrightarrow 2O_2$	7.23×10^{13}	Atkinson et al., 1989.
$O(^1D) + O_3 \longrightarrow 2O\cdot + O_2$	7.23×10^{13}	Atkinson et al., 1989.
$O(^1D) + N_2O \longrightarrow N_2 + O_2$	2.95×10^{13}	Demore et al., 1987.
$O(^1D) + N_2O \longrightarrow 2NO$	4.04×10^{13}	Demore et al., 1987.
$NO + O_3 \longrightarrow NO_2 + O_2$	8.43×10^9	Demore et al., 1987.
$NO + O\cdot \longrightarrow N\cdot + O_2$	2.77×10^9	Demore et al., 1987.

Chemical Reactions	Rate Constants $(cm^3.mole^{-1}.sec^{-1})$	Source
$NO + O\cdot \longrightarrow NO_2$	1.40×10^{12}	Atkinson et al., 1989.
$NO + NO_3 \longrightarrow 2NO_2$	1.75×10^{13}	Demore et al., 1987.
$NO + NO_3 \longrightarrow 2NO + O_2$	1.84×10^{11}	Sutherland et al., 1975.
$NO_2 + O_3 \longrightarrow NO_3 + O_2$	1.93×10^{7}	Atkinson et al., 1989.
$NO_2 + O\cdot \longrightarrow NO + O_2$	5.84×10^{12}	Atkinson et al., 1989.
$NO_2 + NO_3 \longrightarrow$		
$NO + NO_2 + O_2$	6.45×10^{8}	Baulch et al., 1983.
$N_2O_4 + M \longrightarrow 2NO_2 + M$	2.06×10^{9}	Baulch et al., 1983.
$2NO_3 \longrightarrow 2NO_2 + O_2$	1.92×10^{8}	Baulch et al., 1983.
$NO_3 + O\cdot \longrightarrow NO_2 + O_2$	1.02×10^{13}	Demore et al., 1987.
$O_3 + N\cdot \longrightarrow NO + O_2$	6.02×10^{7}	Baulch et al., 1983.
$2NO_2 + M \longrightarrow N_2O_4 + M$	3.06×10^{14}	Baulch et al., 1987.
$NO_2 + O\cdot \longrightarrow NO_3$	1.29×10^{12}	Atkinson et al., 1989.
$H_2O \longrightarrow H\cdot + OH\cdot$	$K_3[E]$	Expt. Data
$N\cdot + OH\cdot \longrightarrow NO + H\cdot$	1.45×10^{13}	Demore et al., 1987.
$O(^1D) + H_2 \longrightarrow H\cdot + OH\cdot$	6.02×10^{13}	Demore et al., 1987.
$O(^1D) + H_2O \longrightarrow 2OH\cdot$	1.33×10^{14}	Demore et al., 1987.
$O\cdot + H\cdot \longrightarrow OH\cdot$	1.08×10^{12}	Willis & Boyd, 1976.
$O\cdot + HO_2 \longrightarrow OH\cdot + O_2$	3.4×10^{13}	Atkinson et al., 1989.
$O\cdot + OH\cdot \longrightarrow O_2 + H\cdot$	1.99×10^{13}	Atkinson et al., 1989.
$OH\cdot + H_2 \longrightarrow H_2O + H\cdot$	4.03×10^{9}	Atkinson et al., 1989.
$OH\cdot + OH\cdot \longrightarrow H_2O + O\cdot$	1.08×10^{12}	Atkinson et al., 1989.

Chemical Reactions	Rate Constants $(cm^3.mole^{-1}.sec^{-1})$	Source
$OH \cdot + OH \cdot \longrightarrow H_2O_2$	9.93×10^{12}	Atkinson et al., 1989.
$OH \cdot + HO_2^. \longrightarrow H_2O + O_2$	6.63×10^{13}	Atkinson et al., 1989.
$OH \cdot + H_2O_2 \longrightarrow H_2O + HO_2^.$	1.02×10^{12}	Atkinson et al., 1989.
$OH \cdot + H \cdot \longrightarrow H_2O$	1.45×10^{13}	Atkinson et al., 1989.
$H \cdot + O_2 \longrightarrow HO_2^.$	8.49×10^{11}	Atkinson et al., 1989.
$H \cdot + O_3 \longrightarrow OH \cdot + O_2$	1.67×10^{13}	Atkinson et al., 1989.
$H \cdot + HO_2^. \longrightarrow H_2 + O_2$	3.37×10^{12}	Atkinson et al, 1989.
$H \cdot + HO_2^. \longrightarrow 2OH \cdot$	4.34×10^{13}	Atkinson et al., 1989.
$H \cdot + HO_2^. \longrightarrow H_2O + O \cdot$	1.45×10^{12}	Atkinson et al., 1989.
$H \cdot + H_2O_2 \longrightarrow H_2O + OH \cdot$	6.02×10^{10}	Willis & Boyd, 1976.
$HO_2^. + HO_2^. \longrightarrow H_2O_2 + O_2$	1.02×10^{12}	Demore et al., 1987.
$NO + OH \cdot \longrightarrow HNO_2$	9.03×10^{12}	Atkinson et al., 1989.
$NO_2 + OH \cdot \longrightarrow HNO_3$	1.45×10^{13}	Demore et al., 1989.
$NO_2 + OH \cdot \longrightarrow HO_2^. + NO$	1.39×10^{13}	Atkinson et al., 1989.
$HNO_2 + OH \cdot \longrightarrow NO_2 + H_2O$	2.95×10^{12}	Atkinson et al., 1989.
$HNO_3 + OH \cdot \longrightarrow H_2O + NO_3$	9.03×10^{10}	Atkinson et al., 1989.
$OH \cdot + H \cdot \longrightarrow H_2 + O \cdot$	1.96×10^{7}	Loirat et al., 1987.
$H_2O_2 + H \cdot \longrightarrow HO_2^. + H_2$	3.12×10^{9}	Warnatz, et al., 1984.
$H_2O_2 + O \cdot \longrightarrow OH \cdot + HO_2^.$	1.03×10^{9}	Atkinson et al., 1989.
$O_3 + HO_2^. \longrightarrow OH \cdot + 2O_2$	1.17×10^{9}	Levine et al., 1985.
$O_3 + OH \cdot \longrightarrow HO_2^. + O_2$	3.36×10^{10}	Atkinson et al., 1989.
$HNO_2 + O \cdot \longrightarrow NO_2 + OH \cdot$	1.81×10^{9}	Kaiser et al., 1978.

continued from previous page

Chemical Reactions	Rate Constants $(cm^3.mole^{-1}.sec^{-1})$	Source
$HNO_3 + HNO_2 \longrightarrow$ $NO_2 + H_2O$	9.64×10^6	Kaiser et al., 1977.
$HNO_3 + O^{\cdot} \longrightarrow NO_3 + OH^{\cdot}$	1.81×10^9	Kaiser et al., 1978.
$HNO_3 + H^{\cdot} \longrightarrow HNO_2 + OH^{\cdot}$	6.02×10^{10}	Baulch et al., 1983.
$NO_3 + H^{\cdot} \longrightarrow NO_2 + OH^{\cdot}$	6.63×10^{13}	Boodaghians et al., 1988.
$NO_3 + OH^{\cdot} \longrightarrow NO_2 + HO_2^{\cdot}$	1.39×10^{13}	Boodaghians et al., 1988.
$NO_3 + HO_2^{\cdot} \longrightarrow HNO_3 + O_2$	7.63×10^{11}	Hoffmann et al., 1988.
$NO_3 + HO_2^{\cdot} \longrightarrow$ $NO_2 + OH^{\cdot} + O_2$	3.05×10^{12}	Hoffmann et al., 1988.
$N^{\cdot} + HO_2^{\cdot} \longrightarrow NO + OH^{\cdot}$	1.33×10^{13}	Brune et al., 1983.
$NO + HO_2^{\cdot} \longrightarrow NO_2 + OH^{\cdot}$	4.66×10^{12}	NIST Database.
$NO + HO_2^{\cdot} \longrightarrow HNO_3$	8.43×10^{10}	NIST Database.

CHAPTER 5

EXPERIMENTAL RESULTS & DISCUSSION

5.1 Physical Discharge Characteristics

The physical aspects of the corona discharge including the corona onset voltage, the peak voltage, the pulse rise time, and the pulse width were measured at the location where the pulse was delivered to the centrally located high voltage discharge wire electrode.

First, a power supply calibration was made to find the relation between the applied AC voltage delivered to the pulse forming network and the voltage indicated on the control section of the transformer/rectifier (dial voltage). A plot of the applied voltage versus the dial voltage is shown in Figure 5.1. The applied voltage refers to the peak AC output voltage of the transformer as measured by the high voltage probe and the oscilloscope. This figure shows an apparent linear relationship between the dial voltage and the applied voltage. Linear regression was performed on the data, and the correlation coefficient was found to be 0.9998 and the slope of the line to be 0.964.

Pulsed corona onset (corona initiation voltage) in the reactor was found to occur at a pulsed input voltage of between 13 and 14 kV in an atmosphere of dry air and at about 10 kV in a dry nitrogen atmosphere. Below the onset of corona, the voltage and the current readings measured at the reactor using the oscilloscope were very small. Above the corona onset the peak voltage and the current increased

dramatically. The rise time of the voltage pulse was found to vary between 15 and 30 nanoseconds.
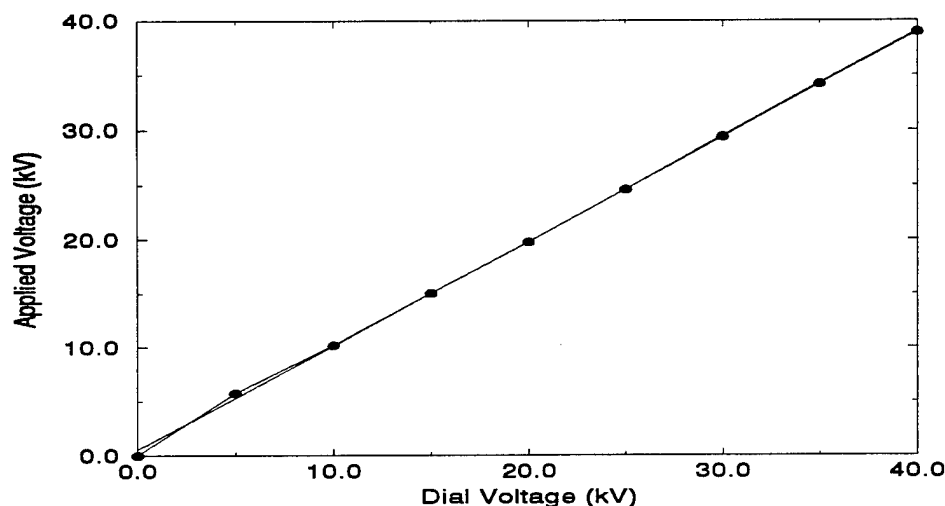
Figure 5.1: Power Supply Calibration

A plot of a typical voltage waveform is shown in Figure 5.2. As seen in the figure, there is a sharp increase in the voltage, i.e., a very short rise time, followed by an exponential decay of the voltage. The pulse width at half-maximum of the voltage pulse varied from 500 to 700 nanoseconds. The current waveform is shown in Figure 5.3. The current pulses were shorter in width (< 300 nanoseconds) when compared to the voltage pulses. The current pulses were measured using two current probes, Tektronix P6021 and P6016. The peak values of current as well as the nature of the waveforms varied distinctly for each probe. Values from both probes are reported because a standard was not available to check the results. The power input per pulse was calculated by multiplying the voltage and the current waveforms and measuring the area under the resulting waveform. A plot of the pulsed power waveform is shown in Figure 5.4. Table 5.1 summarizes the peak voltage, the rise time and the pulse width of the pulsed voltage as a function of dial voltage in a dry air atmosphere.
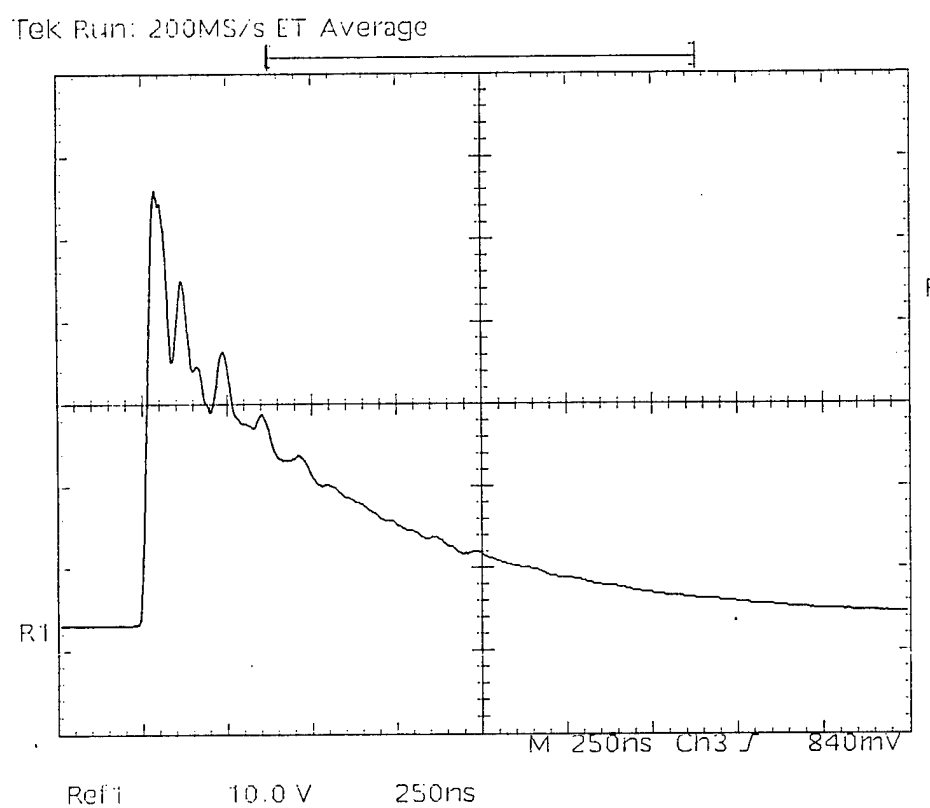
Figure 5.2: Voltage Waveform in an Atmosphere of Dry Air at 40 kV
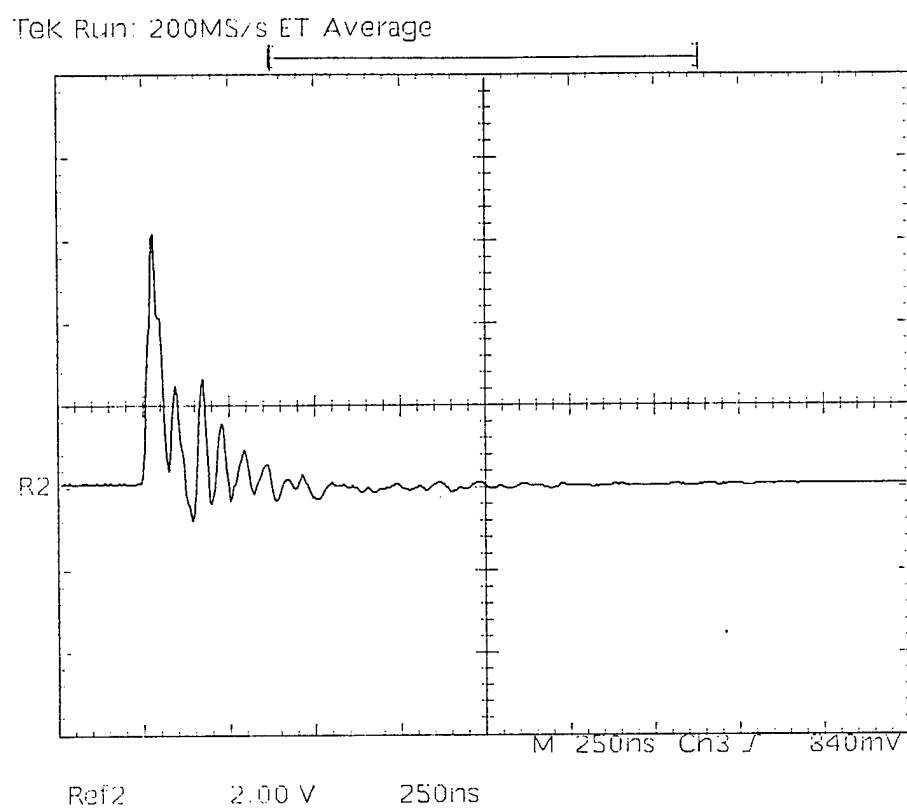
Figure 5.3: Current Waveform in an Atmosphere of Dry Air at 40 kV
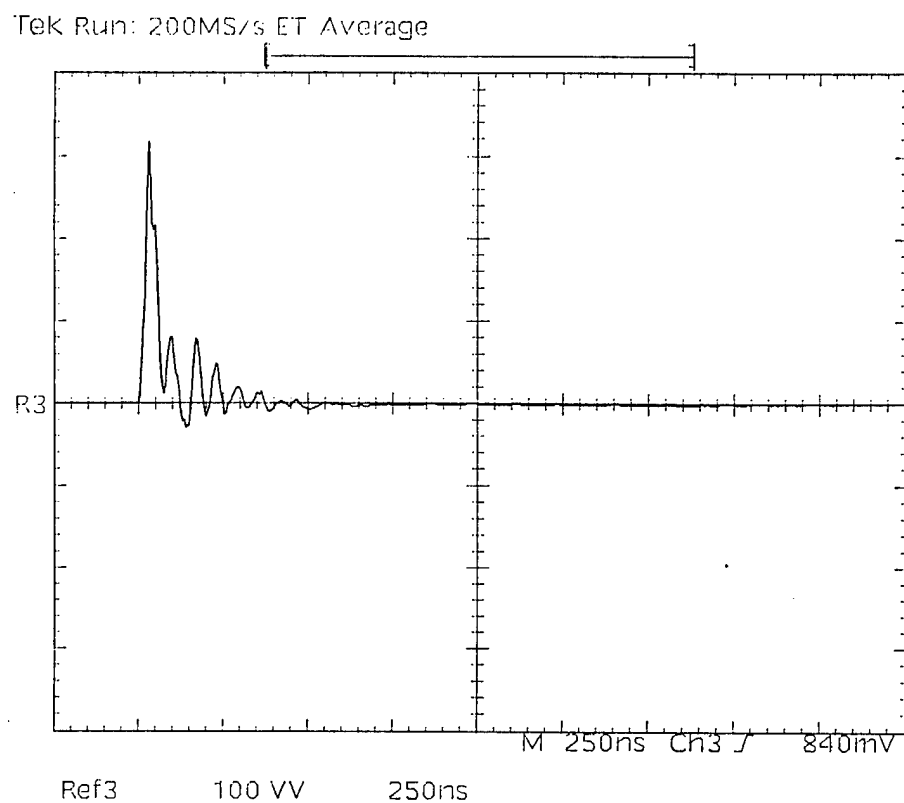
Figure 5.4: Power Waveform in an Atmosphere of Dry Air at 40 kV

Table 5.1: Voltage Characteristics of the Pulse in Dry Air

Dial Voltage (kV)	Peak Voltage (kV)	Rise time (ns)	Pulse Width (ns)
30	43.4	13.5	449
35	49.4	16.5	616
40	53.6	18.0	627
50	58.4	29.0	694

As the table shows, the peak pulsed voltage was significantly higher than the dial voltage, and both the rise time and the pulse width increased with the increase in the applied voltage.

As originally conceived, the pulse generating circuit did not include a load resistor in parallel with the reactor electrodes (see Figure 3.1). However, it was found that the spark gap would not fire even at high input voltages because the effective resistance of the gap between the reactor electrodes was too high. In order to decrease the effective resistance of the gap between the outer grounded cylinder and the high voltage wire electrode, a load resistance was connected from the spark gap output to ground in parallel to the two reactor electrodes. The nature of the voltage waveform was affected by the value of the load resistance (Lucas 1995). As the resistance of the load resistor was decreased from 300 Ω to 77.1 Ω, the decay time (time required for the voltage to drop from its maximum value to its minimum value) for the voltage pulses increased. A load resistor of 300 Ω was used in all the experiments conducted for NO removal.

In this study, the pulse frequency was kept constant at 60 Hz and the voltage was varied in order to increase the energy input into the reactor. Table 5.2 shows the peak value of the current waveform and the corresponding energy per unit pulse calculated

Table 5.2: Current & Power Characteristics of the Pulse in Dry Air Using the Current Probe P6021 and the Probe P6016

Dial Voltage (kV)	Probe P6021			Probe P6016		
	Peak Current (A)	Energy per Pulse (mJ)	Power (watts)	Peak Current (A)	Energy per Pulse (mJ)	Power (watts)
30	48	74.7	4.48	10.5	32.1	1.9
35	58.8	109.0	6.54	12.9	44.0	2.65
40	60.8	149.4	8.96	20.1	77.0	4.6
50	55.6	246.7	14.8	26.7	107.0	6.3

as a function of applied voltage using the two current probes. The power delivered to the reactor was determined by multiplying the energy per pulse by the frequency of pulsing. Using the Tektronix current probe P6016, the energy input varied from 32.1 mJ/pulse to 107 mJ/pulse in an atmosphere of dry air. With the Tektronix current probe P6021, the energy input varied from 74.7 mJ/pulse to 246.7 mJ/pulse in the case of dry air. Hence, there is a significant difference in the measurement of the peak current and the corresponding energy per pulse measurement using the two current probes. Calibration of the two current probes must be conducted to determine the status of each of those probes.

The energy delivered per pulse was somewhat higher than that reported by Tas (1995) (6-7 mJ/pulse). The power was found to vary from 1.9 to 6.3 watts in case of probe P6016 and in case of P6021 the power input varied from 4.48 to 14.8 watts. Mizuno et al. (1995) reported an input power of 20 to 40 watts which is higher than the values obtained from both the current probes.

Experiments were designed to determine the extent of NO removal from several gases with different compositions in order to study the reaction mechanisms for NO removal. The experiments were conducted at four different residence times and at four different voltages. All of the experiments were repeated twice to ensure the reproducibility of the results. The average concentration determined in the two runs was used to plot the figures of NO and NO_2 concentrations as functions of residence time and operating voltages. As an initial case, experiments on NO removal in an atmosphere of nitrogen, was considered. This was followed by experiments in dry air, humid air, and finally in the presence of gas additives such as carbon monoxide and ethylene.

5.2 NO Removal in Nitrogen

NO removal experiments in an atmosphere of dry nitrogen were conducted at different residence times (7.2, 14.5, 29.0, and 44.0 seconds) and at different dial voltages (30, 35, 40, and 50 kV). The initial concentration of NO during the experiments was 100 ppmv.

The NO removal data as a function of residence time for different voltages is shown in Figure 5.5. It was observed that the NO concentration decreased as the residence time in the reactor was increased at a particular voltage. Also, as the applied voltage was increased for a particular residence time, the NO concentration decreased. Complete removal of NO was observed at the higher voltages of 40 and 50 kV at a residence time of 44.0 seconds. The NO_2 concentration profile as a function of residence time for different dial voltages is shown in Figure 5.6. A maximum of 8 ppm NO_2 formation was measured with the NO_x monitor at the voltages of 40 and 50 kV. The concentration profile of NO_2 at 35, 40, and 50 kV passed through a maximum as the residence time in the reactor was increased. Also, as the voltage was increased, the time corresponding to the maximum concentration decreased. At
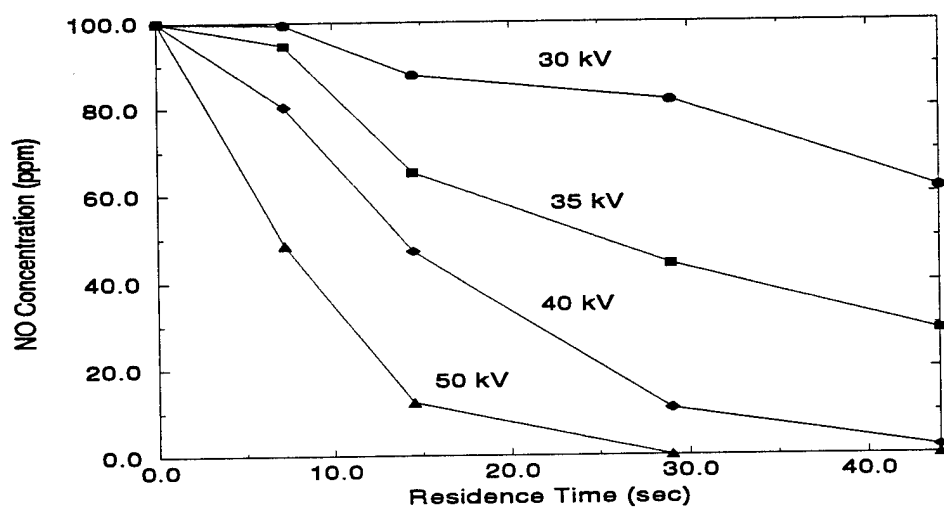
Figure 5.5: NO Concentration Profile in an Atmosphere of Nitrogen
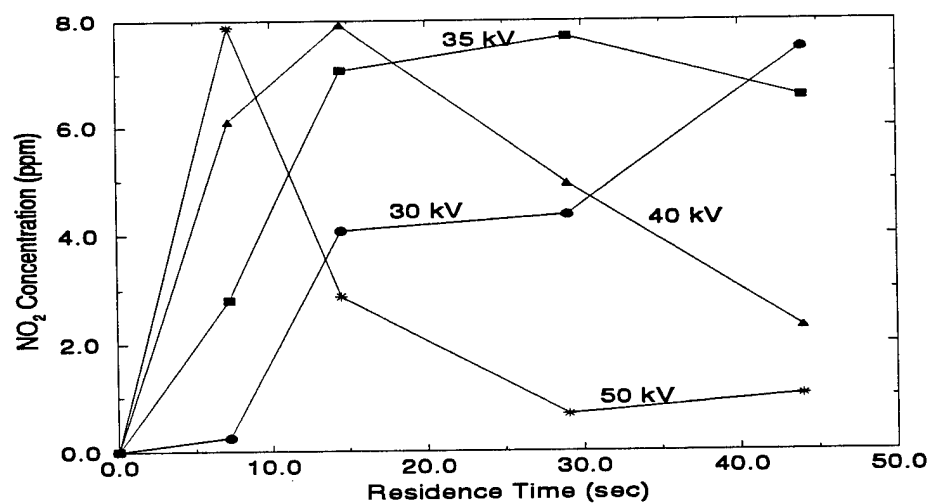
Figure 5.6: NO$_2$ Concentration Profile in an Atmosphere of Nitrogen

30 kV the NO_2 concentration was steadily increasing with the residence time. These profiles indicate that at high voltages (35, 40, & 50 kV) NO_2 is an intermediate product, and at longer residence times NO_2 was reduced back to molecular nitrogen and oxygen. At 30 kV, the amount of power input was not sufficient to reduce the NO_2 formed. Approximately 97% removal of NO_x was obtained at high voltages (40 & 50 kV) and at a residence time of 44.0 seconds.

The kinetic model described earlier was used to determine the rate constant for the nitrogen dissociation reaction by fitting the model to the NO experimental data. The number of chemical reactions considered to calculate the concentration profiles of different species was 31. Figure 5.7 shows the mole fractions of NO, NO_2, and N_2O calculated by the model as a function of residence time at 50 kV. Experimental values of the NO_2 concentration profile at 50 kV in Figure 5.6 qualitatively matches well with the model profile of NO_2 at 50 kV shown in Figure 5.7 (100 ppm = 0.0001 in terms of mole fraction). The maximum value of NO_2 concentration in the model profile is around 17 ppm whereas the maximum value found by the experiments at 50 kV was around 8 ppm. Figure 5.7 also shows a small formation of N_2O. Essentially the model predicts around 90% reduction of initial NO to molecular nitrogen and oxygen in an atmosphere of nitrogen at 50 kV.

The model profile of NO and the experimental data is shown in Figure 5.8. As seen in Figure 5.8, the model profiles match very well with the experimental values at 35, 40 and 50 kV at longer residence time. There is a slight deviation of the model from the experimental points at 30 kV. The experimental data of NO removal at 7.2 seconds residence time for all the voltages except 50 kV were less than that predicted by the model.

The rate constant of the nitrogen dissociation as a function of applied voltage thus obtained by fitting the model to the experimental data is shown in Figure 5.9. This figure shows an almost linear relation of the rate constant as a function
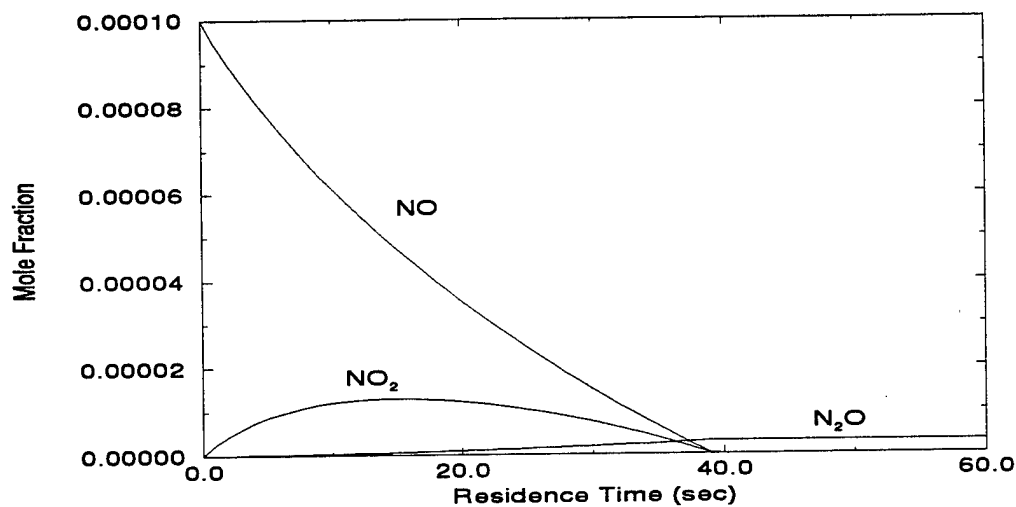
Figure 5.7: Model Profile of Different Species in an Atmosphere of Nitrogen
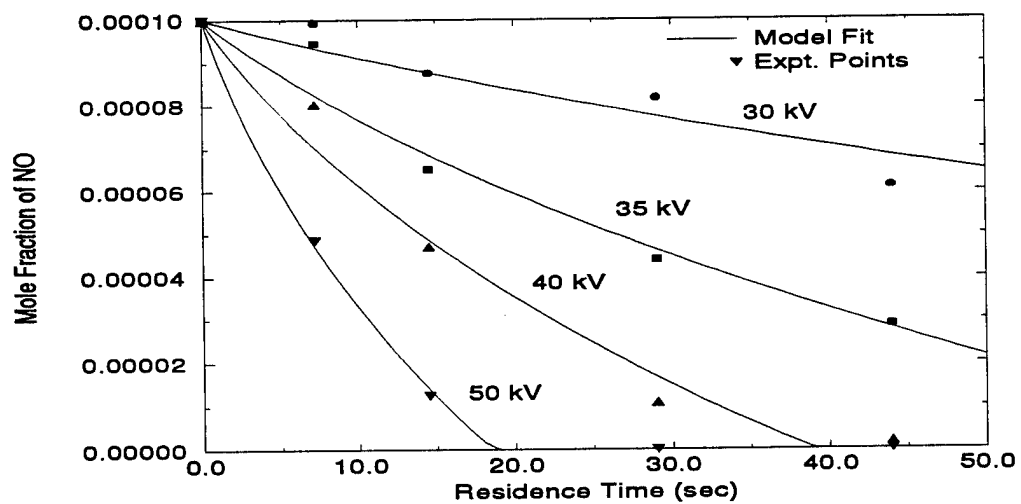
Figure 5.8: Model Fit for NO Concentration Profile in an Atmosphere of Nitrogen
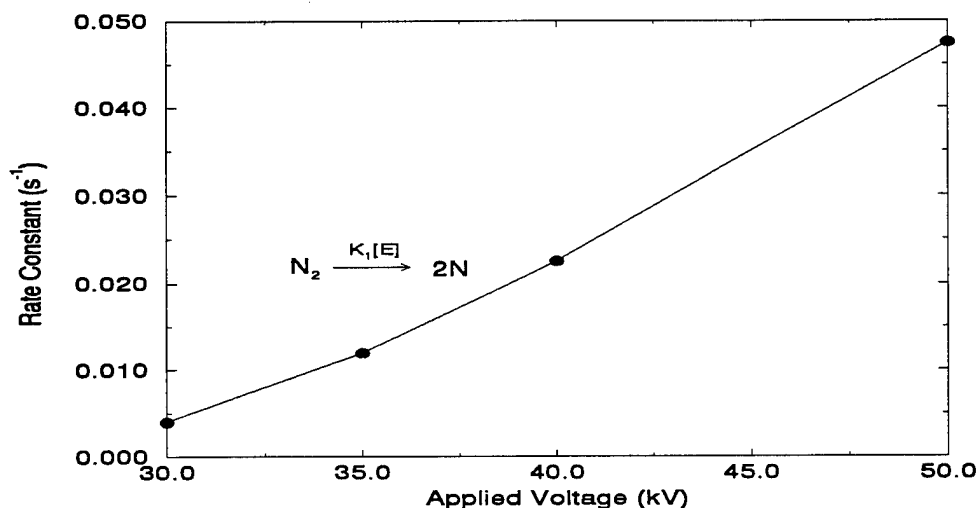
Figure 5.9: Rate Constants of Nitrogen Dissociation as a Function of Applied Voltage in an Atmosphere of Nitrogen

of dial voltage. The rate constant determined is a pseudo first-order rate constant, which is essentially the electron concentration multiplied by the actual second order dissociation rate constant.

Both experimental and modeling results indicate that the main reaction pathway for NO removal in nitrogen is through reduction to molecular nitrogen. The main reactions responsible for the removal are:

$$N_2 + e^- \longrightarrow N^{\cdot} + N^{\cdot} + e^-, \tag{5.1}$$

$$NO + N^{\cdot} \longrightarrow N_2 + O^{\cdot}, \tag{5.2}$$

$$NO + O^{\cdot} \longrightarrow NO_2, \tag{5.3}$$

$$NO_2 + N^{\cdot} \longrightarrow N_2 + O_2, \tag{5.4}$$

$$NO_2 + N^{\cdot} \longrightarrow N_2O + O^{\cdot}. \tag{5.5}$$
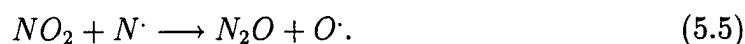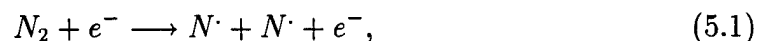
As the applied voltage is increased, the amount of nitrogen radicals produced by Equation 5.1 increases. The reaction responsible for the NO removal is Equation 5.2. Equation 5.3 results in the formation of NO_2 but the Equations 5.4 and 5.5 are fast enough to reduce the NO_2 formed back to N_2 and to N_2O.

Tokunaga et al. (1984) used an electron beam to consider NO removal as a function of dose rate in an atmosphere of nitrogen, and concluded that the NO was mainly decomposed to nitrogen and oxygen. The products from the discharge were analyzed and NO_2 and N_2O were present in very small amounts (NO_2=10%, N_2O=3%). Tas (1995) used pulsed streamer corona discharge to consider the NO removal in an atmosphere of nitrogen, and concluded that the reduction pathway was the main path for the removal of NO.

Penetrante et al. (1995) considered in detail the kinetics of corona discharge by solving for the electron energy distribution function to calculate the kinetic rate constants for the electron-gas reactions in order to predict the profile of different species for the case of NO removal in an atmosphere of nitrogen. The chemical kinetics calculation included 287 reactions and 37 species involving charged as well as neutral species. His model also predicts the reduction of NO as the main pathway for NO removal. It is important, however, to note that in this study the model developed for the case of NO removal in nitrogen has considered only 13 neutral species and 31 chemical reactions as compared to the vast number of reactions considered by Pentrante et al. (1995). It is, therefore, possible to characterize the chemical reactions taking place in the pulsed streamer corona reactor by considering the neutral species reactions.

5.3 NO Removal in Dry Air

Experiments on NO removal in an atmosphere of dry air at various voltages (30, 35, 40, and 50 kV) and at different gas residence times (3.6, 7.2, 14.5, 29.0, and 60.0) were conducted to study the effect of oxygen addition on the NO and NO_2 concentration profiles.

The feed air used for the study was from a compressed air source from the building. The compressed air source was passed through a series of drier columns (anhydrous calcium sulphate) to remove the water vapor in the air. The initial NO concentration was about 116 ppm.

The concentration of NO_2 varied from 0 ppm to 25 ppm as the residence time in the reactor (without corona) increased. This indicated that the initial NO was being oxidized into NO_2 when mixed with air in the reactor even in the absence of corona discharge. The temperature of the gas varied from 12.9 to 19 °C during the experiments.

NO concentration profiles as a function of residence time for different voltages are shown in Figure 5.10. NO concentration decreased as the applied voltage was increased for a particular residence time. It also decreased as the residence time was increased for a particular voltage. Comparing Figures 5.5 and 5.10, the rate of NO removal was faster in the case of dry air than in nitrogen. At 50 kV in an atmosphere of nitrogen 90% of NO was removed whereas in dry air almost 100% removal was observed at 14.5 seconds residence time. Using an initial concentration of 250 ppmv of NO, Chang et al. (1992) observed that at room temperature, the addition of oxygen reduces the NO removal rate in case of dielectric barrier discharge. This is in contradiction to what was observed in the experiments conducted in this study. Tas (1995) also observed that for an initial concentration of 1200 ppm, the NO removal decreased with an increase in the oxygen composition on the feed gas.
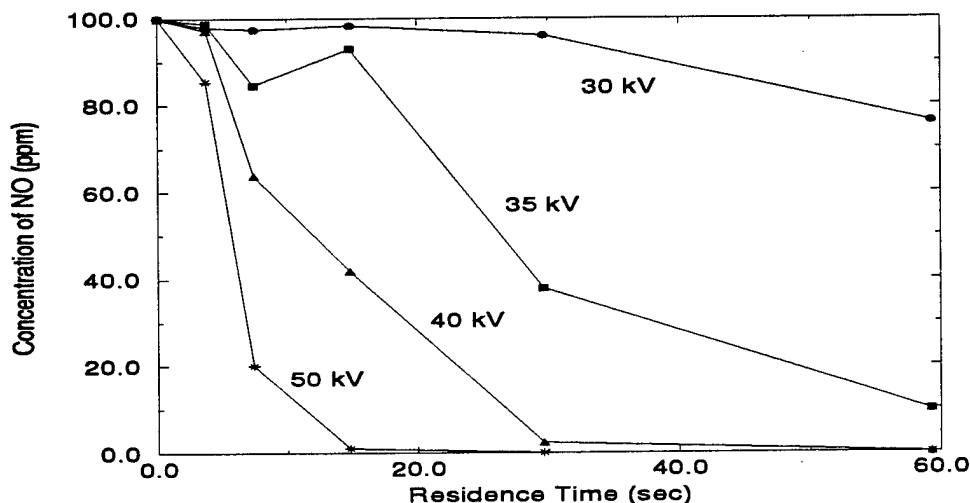
Figure 5.10: NO Concentration Profile in an Atmosphere of Dry Air

The NO_2 concentration profiles are shown in Figure 5.11. The NO_2 concentration increased with the voltage for short residence times as residence time was increased. The NO_2 profiles at 40 and 50 kV go through a maxima and the concentrations decrease slightly at longer residence time. NO_2 concentration profiles at 30 and 35 kV increase steadily with residence time. Unlike the NO_2 profile in the case of NO removal in nitrogen, the removal of NO_2 in dry air was not observed at longer residence time and at high voltages.

The results indicate that most of the NO was converted into NO_2 at the tested voltages and residence times. The total NO_x was higher than the initial NO concentration at 14.5 and 29.0 seconds residence time and at 50 kV. This indicated that there was NO_x formation from the dry air itself during the discharge. To confirm this, an experiment to consider the formation of NO and NO_2 in the pulsed corona discharge in dry air was conducted. It was observed that at 60 seconds residence time and at an applied voltage of 50 kV, the formation of NO_2 was 10 ppm. Tokunaga et al. (1984) also noticed an increase in the total NO_x concentration when the
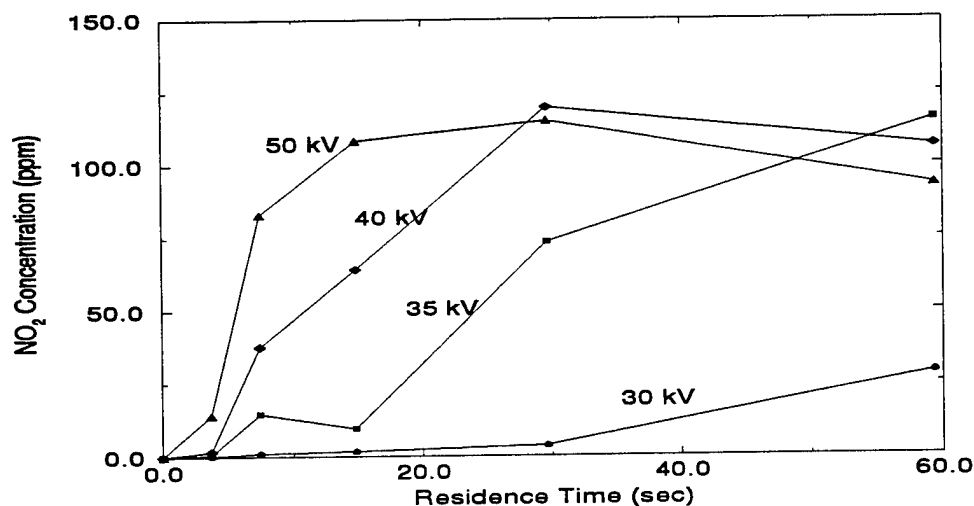
Figure 5.11: NO$_2$ Concentration Profile in an Atmosphere of Dry Air

initial concentration of NO was around 50-100 ppm. For an initial concentration of 100 ppm of NO, the NO$_x$ concentration at a dose rate of 5 Mrad was 120 ppm, and it was found to increase with dose rate for a gas composition of 3% oxygen in an atmosphere of nitrogen.

A measurement of N$_2$O was made for the 44.0 second residence time experiment at 50 kV, and the concentration was found to be 17 ppm. The measurement was made by a GC/MS analysis of the gas sample coming out of the outlet of the reactor.

For the case of NO removal in dry air, the two unknown rate constants corresponding to the nitrogen and oxygen dissociation were obtained by fitting the model profiles with the experimental data of NO and NO$_2$. The model profiles of NO, NO$_2$, N$_2$O, and O$_3$ are shown in Figure 5.12 for the case of 50 kV. NO removal corresponded with NO$_2$ formation at shorter residence times and at the longer residence times the NO$_2$ concentration leveled out at 80% of the initial NO. The O$_3$ concentration increased only after a significant lag time where the NO concentration decreased. This is due to the fact that in the presence of NO, the amount of
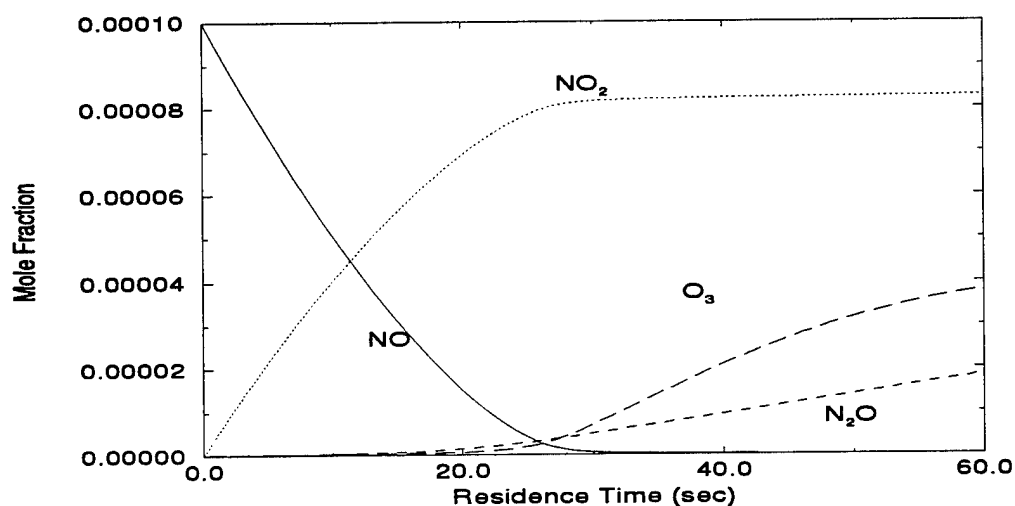
Figure 5.12: Model Profile of Different Species in an Atmosphere of Dry Air

ozone formation due to oxygen radicals reacting with oxygen molecules is very small when compared to oxygen radicals reacting with NO to produce NO_2. Once the NO molecules were removed, the ozone formation was unhindered and the slope of the ozone concentration as a function of residence time started increasing. The N_2O concentration as predicted by the model for a residence time of 44.0 seconds at 50 kV is around 15 ppm which matches well with the experimentally observed value. This is a significant observation since N_2O data was not used in fitting the model, i.e., the N_2O measurement provides an independent check of the model. There was around 20% deviation between the model profile and the experimental values in case of NO_2 concentration at 50 kV.

The model profile for NO and the experimental points used to fit the model are shown in Figure 5.13. As seen in the figure, there is a deviation between the experimental points and the model at short residence time (3.6 seconds). One reason for this behavior could be that at short residence time, the flow pattern in the reactor
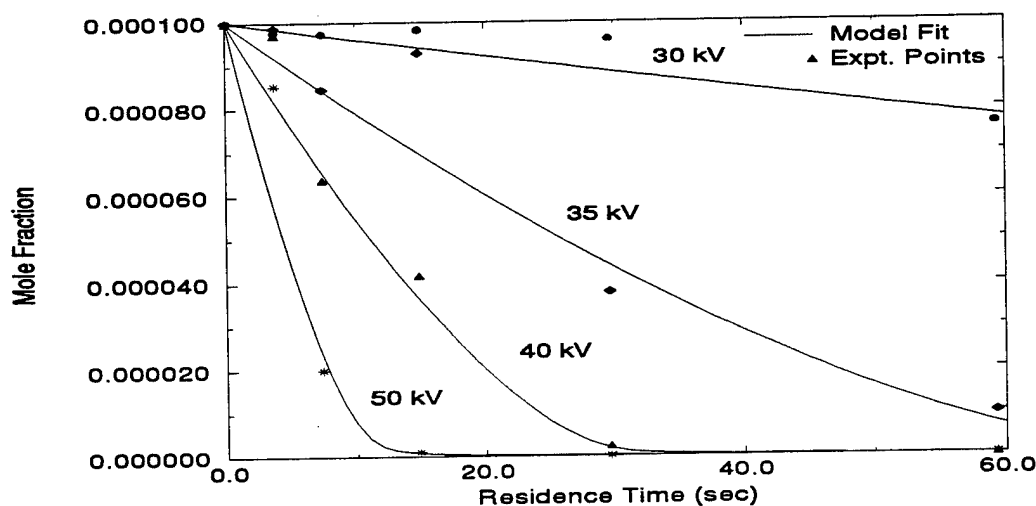
Figure 5.13: Model Fit for NO Concentration Profile in an Atmosphere of Dry Air

was highly turbulent and hence the reactor would operate more as a well mixed reactor than as a plug-flow reactor. The model profile for NO fits well with the experimental points at longer residence times.

The main reaction mechanisms for the removal of NO in an atmosphere of dry air was through the oxidation of NO to NO_2 and the main reactions in addition to Reactions 5.2 to 5.5 are:

$$O_2 + e^- \longrightarrow O^{\cdot} + O(^1D) + e^-, \tag{5.6}$$

$$O_2 + O^{\cdot} \longrightarrow O_3. \tag{5.7}$$
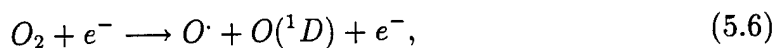
Reaction 5.6 produces the necessary oxygen radicals required for the oxidation of NO. Reaction 5.3 converts the NO to NO_2 and Reaction 5.5 converts the NO_2 formed into N_2O. The ozone formation was significant once the NO molecules are removed and Reaction 5.7 is the corresponding reaction pathway.
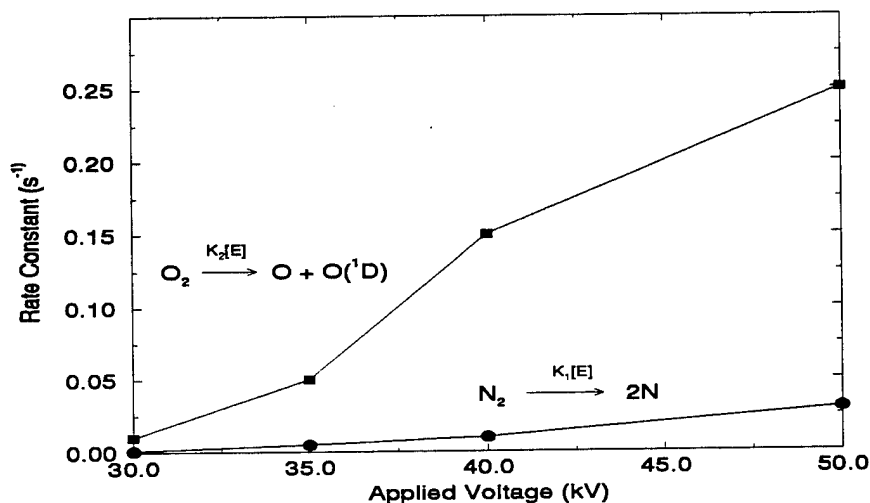
Figure 5.14: Rate Constants of Nitrogen and Oxygen Dissociation as a Function of Applied Voltage in an Atmosphere of Dry Air

The rate constants obtained for nitrogen and oxygen dissociation as a function of applied voltage are shown in Figure 5.14. The slope for the oxygen dissociation is higher than that for nitrogen dissociation in air. The nitrogen dissociation rate constant in dry air was not the same as in the case of a pure nitrogen feed gas. The rate constant was 0.0475 s^{-1} in an atmosphere of nitrogen at 50 kV but in dry air the rate constant was reduced to 0.03 s^{-1} at the corresponding voltage. The presence of electronegative gas such as oxygen does have an effect on the nitrogen dissociation (Chang et al., 1992).

Tokunaga et al. (1984) conducted experiments for NO removal in a dry mixture of nitrogen and oxygen (N_2 97%, O_2 3%) using an electron beam, and they concluded that for high initial concentrations of NO and at high dose rate, the ratio of the final concentrations of NO and NO_2 after the treatment were given by the empirical relation of Equation 2.1. Tas (1995) also considered the removal of NO from dry air

and concluded that the empirical relation holds true. However experiments and the modeling conducted in this work do not follow the empirical relation suggested by Tokunaga et al (1984). This relation holds true only for cases in which the initial concentration of NO was very high (500-1000 ppm). Penetrante (1993) considered modeling the concentration profiles of NO and NO_2 in an atmosphere of dry air at room temperature, and he concluded that for an initial concentration of 400 ppm of NO, 50% of the initial NO was converted into NO_2 which was later again converted to N_2O and N_2. In this study, the model prediction for an initial concentration of 100 ppm is 80% conversion of the initial NO to NO_2 and 20 ppm N_2O formation. Efforts to remove the NO_2 formed due to the oxidation of NO must be considered.

5.4   Ozone Formation in Dry Air

The formation of ozone in dry air with pulsed streamer corona treatment was considered for various voltages (30, 35, 40, and 50 kV) and at different residence times (7.2, 14.5, 29.0, and 44.0 seconds) in order to have an independent check of the model. The experiments were performed without any addition of NO to the dry air. Ozone production was not detected at voltages below 30 kV. Concentration profiles of ozone as a function of applied voltage and residence time are shown in Figure 5.15. The ozone concentration increased monotonically with an increase in the residence time at a particular voltage. The increase in ozone concentration with the voltage was nonlinear for a particular residence time.

The amount of ozone predicted by the model is shown in Figure 5.16. The model predicts 200 ppmv of ozone to be produced at a gas residence time of 44.0 seconds and at 50 kV, whereas the value observed in the experiment was 1300 ppmv.

The model predicts less formation of ozone than that observed by the ozone monitor. Some of the reasons for this discrepancy between the experimental and modeling results could be due to the fact that the ozone monitor measurement capability (0.1%
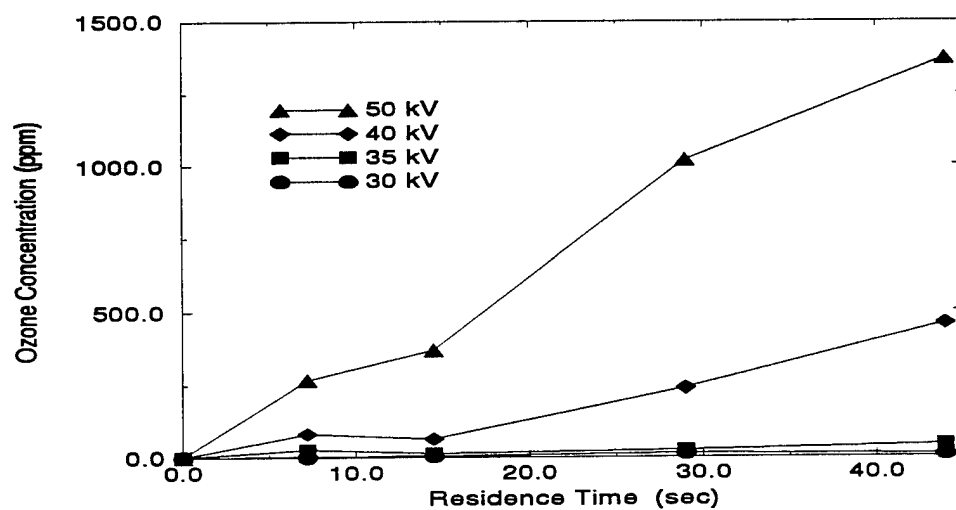
Figure 5.15: O_3 Concentration Profile in an Atmosphere of Dry Air
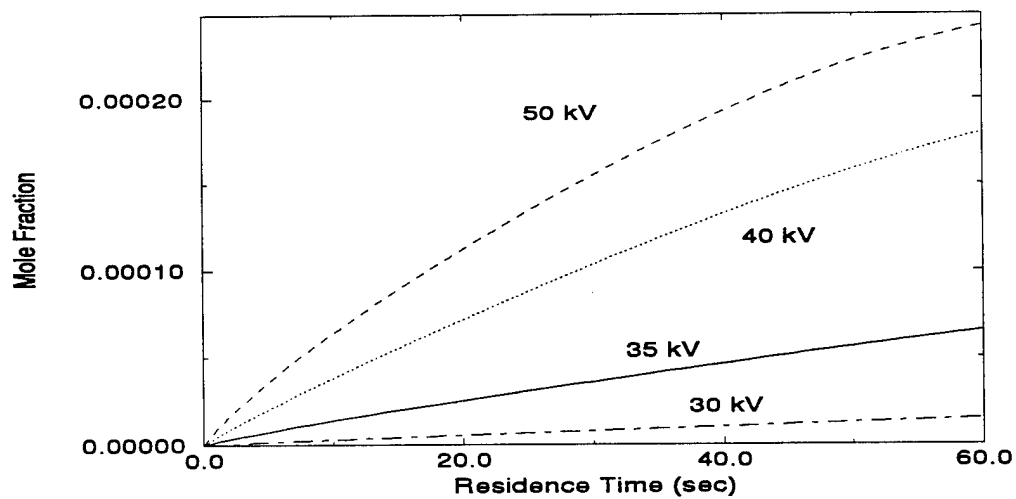
Figure 5.16: O_3 Concentration Profile Predicted by the Model

to 9.9% wt) was not in the range of concentrations produced by the discharge. At high voltages, the readings measured by the montior were significantly different for the two runs conducted at the same operating conditions. Also, when a comparison was done between the value observed by the ozone monitor and the amount obtained by doing an indigo-test method, the difference in the concentrations was more than a factor of 2 (Lincoln, 1995).

5.5   NO Removal in Humid Air

Water vapor is present in concentrations of up to 5 % by mole in the exhaust gases coming out of combustion of fossil fuels or from jet cell engines (Spicer et al., 1992). The hydroxyl radicals produced from the pulsed corona-induced dissociation of water molecules react with NO_2 to form HNO_3.

Experiments were conducted in order to test the removal of NO in humid air. The feed air was humidified by passing it through a humidifier bringing the water content to 83% relative humidity at 18° C. This corresponds to 1.5% of gas composition by volume. As in previous experiments the voltage was varied at different residence times (7.2, 14.5, 29.0, and 44.0 seconds) and the NO and NO_2 outlet concentrations from the reactor were monitored.

Figure 5.17 shows the concentration profile of NO as a function of residence time for different dial voltages. When compared with Figure 5.10 corresponding to NO removal in dry air, the amount of NO removal for the operating voltages of 35, 40 & 50 kV in humid air was less than that of dry air. At an operating voltage of 50 kV, 80% removal of NO was observed at a residence time of 7.2 seconds in dry air. In the presence of water at the same operating conditions, 75% removal of NO was observed. Hence the addition of water did not enhance the NO removal. However, with dielectric discharge Chang et al. (1992) reported an increase in the removal
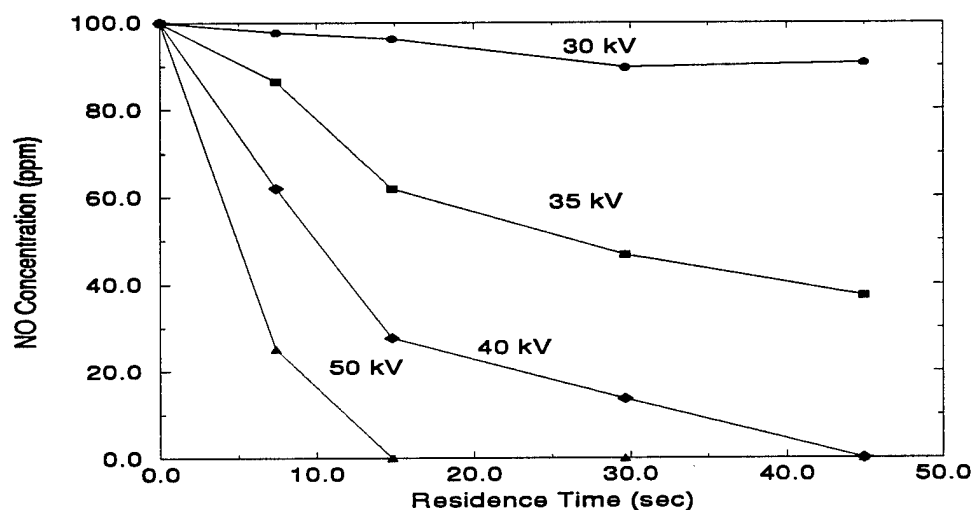
Figure 5.17: NO Concentration Profile in an Atmosphere of Humid Air

efficiency of NO with the addition of water for a initial concentration of 250 ppmv of NO.

Figure 5.18 shows the concentration profiles of NO_2 as functions of residence time and operating dial voltage. The NO_2 concentration undergoes a maximum at about 14.5 seconds residence time for 35 and 40 kV. The maximum for 50 kV was at 7.2 seconds while the 30 kV profile had a steady increase in the concentration. The concentration of NO_2 was less than 5 ppm for all the voltages at a residence time of 44.0 seconds. The maximum concentration of NO_2 attained was 22 ppm for the case of 50 kV. Around 95% removal of NO_x was observed for 40 and 50 kV voltages at a gas residence time of 44.0 seconds. Thus with the addition of water, the NO_2 concentration has decreased significantly. The NO_2 concentration was 2.5 ppm at 50 kV at a residence time of 29.0 seconds in case of humid air as compared to 86.4 ppm in case of dry air at corresponding conditions.

In order to measure the possible formation of HNO_3 from NO_2, the exhaust gases from the reactor were made to bubble through a water column of 500 ml of water for
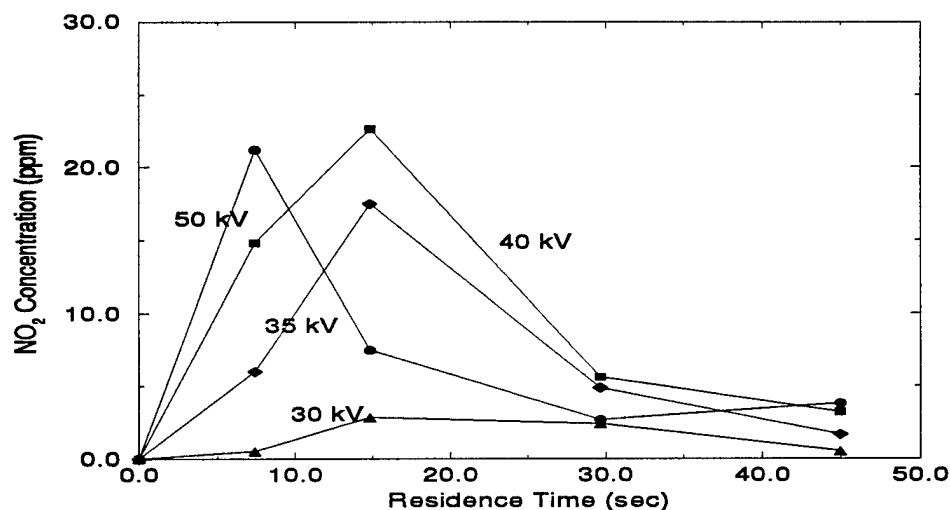
Figure 5.18: NO_2 Concentration Profile in an Atmosphere of Humid Air

1 hour. The gases were bubbled through the column using a sparger. The operating voltage was 50 kV and the gas residence time was 44.0 seconds. The liquid sample was then analyzed for nitrate samples by the ion chromatography technique. The concentration of NO_3^- in the sample was 900 ppb by weight which corresponds to 1.64 ppmv of HNO_3 in the gas sample. The amount measured as nitrates is significantly lower when compared with the removal of NO_2.

The important reactions which are responsible for the reduced concentration of NO_2 are:

$$H_2O + e^- \longrightarrow H\cdot + OH\cdot + e^-, \tag{5.8}$$

$$NO_2 + OH\cdot \longrightarrow HNO_3, \tag{5.9}$$

$$NO + OH\cdot \longrightarrow HNO_2. \tag{5.10}$$
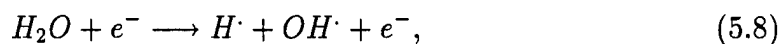
The model profiles of NO, NO_2, HNO_2 and HNO_3 are shown in Figure 5.19 corresponding to 50 kV. The number of chemical reactions considered was to model the reactions taking place in the presence of water in the system was 74. The
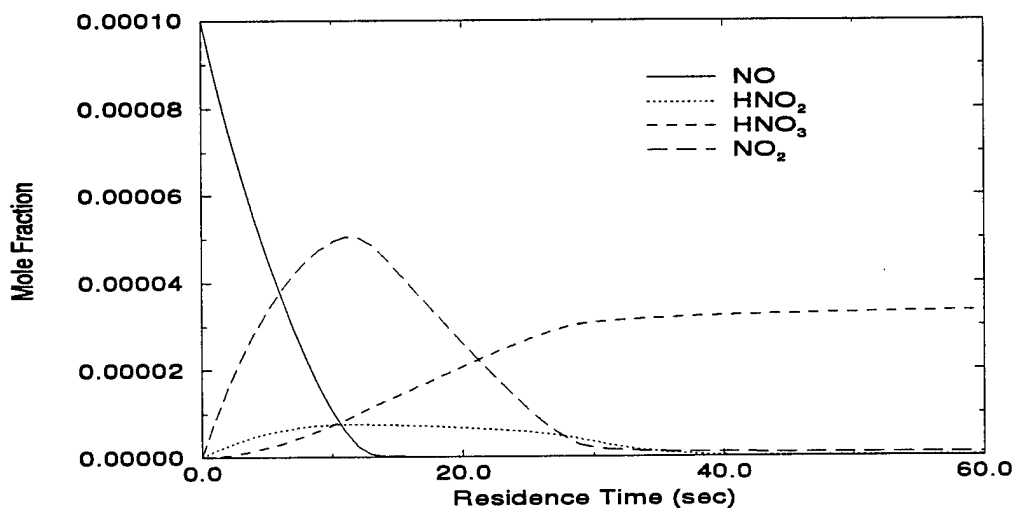
Figure 5.19: Model Profile of Different Species in an Atmosphere of Humid Air

NO_2 profile undergoes a maximum concentration of 50 ppm at 16 seconds residence time. The model predicts up to 35% conversion of initial NO to HNO_3. HNO_2 is an important intermediate product and is an important route for NO removal. The nitric acid produced tends to form aerosols, and as such proper quantification of the acid produced by the discharge has not been done. Future work should consider the study of aerosol formation.

Figure 5.20 shows the NO model profile versus the experimental data used to fit the model to calculate the rate constant for water dissociation. As the graph shows, the model matches from the experimental points at short residence times but deviates from it at longer residence times. In calculating the rate constant for the water molecule dissociation, an assumption has been made that the rate constants for oxygen and nitrogen dissociation were not affected by the addition of water. That could possibly explain the reason as to why there is a deviation of the model from the experimental points.
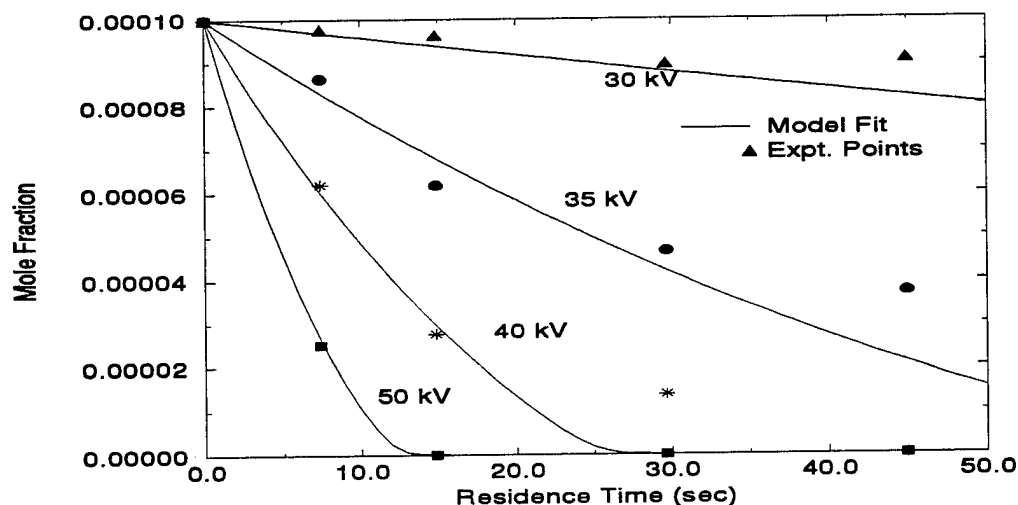
Figure 5.20: Model Fit for NO Removal in an Atmosphere of Humid Air

The maximum concentration of NO_2 as observed in the experiments was around 20 ppm for the case of 50 kV while the model predicts a maximum of 50 ppm. The NO_2 concentration profile predicted by the model for various voltages is shown in Figure 5.21. As shown in Figure 5.21, the NO_2 concentration for the cases of 40 and 50 kV goes through a maximum, while in the cases of 30 and 35 kV there is a steady increase in the concentration of NO_2. But the experimental data as shown in Figure 5.18 indicate that at all of the voltages except 30 kV, the NO_2 concentration goes through a maxima.

The kinetic rate constant for the water dissociation obtained by fitting the model with the experimental data is shown in Figure 5.22 as a function of operating dial voltage. The rate constant increases monotonically with the applied voltage. Tokunaga et al. (1984), Chang et al. (1992), and Tas (1995) observed that the addition of water enhances the NO removal as well. But in this study the addition of water did not enhance the NO removal. One of the reasons is that at high concentrations of initial NO and NO_2 the final concentrations of NO and NO_2 come to equilibrium
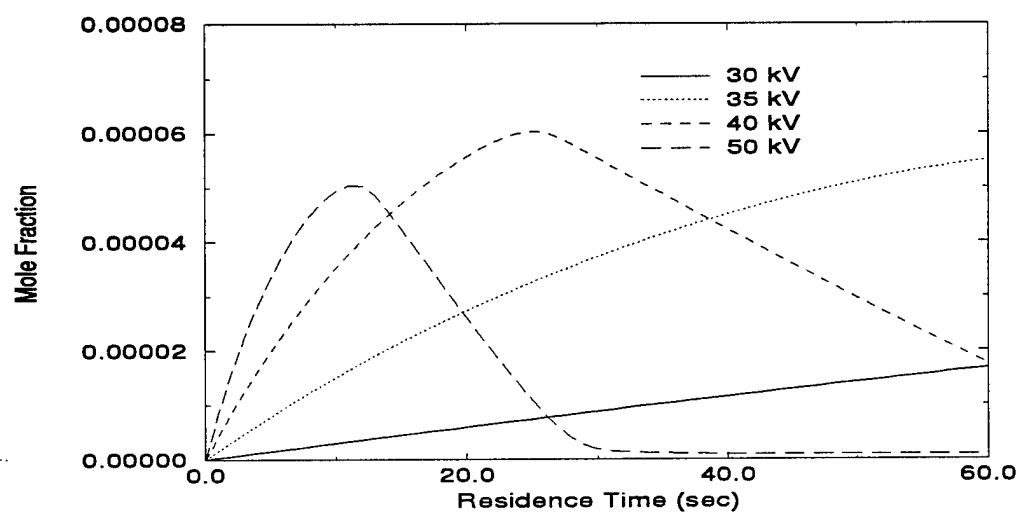
Figure 5.21: NO_2 Model Profile in an Atmosphere of Humid Air
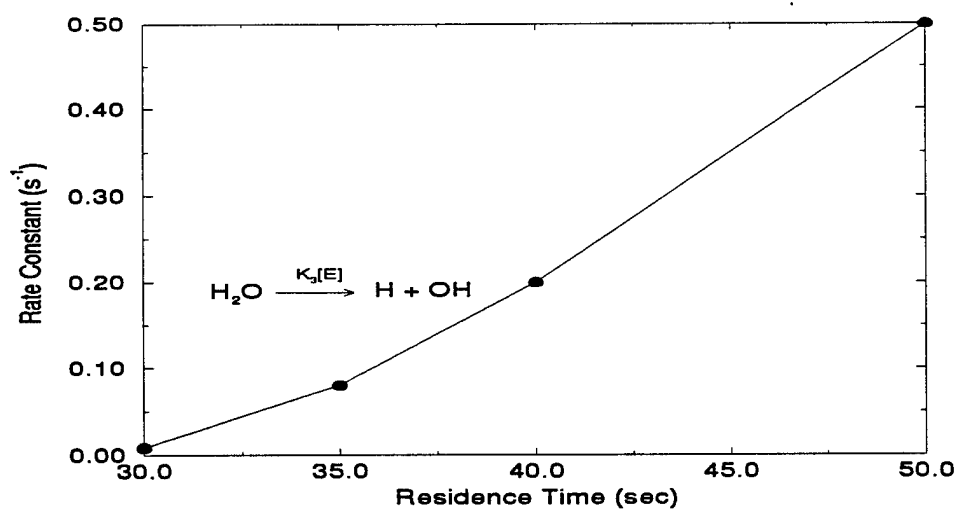
Figure 5.22: Rate Constants of Water Dissociation as a Function of Applied Voltage in an Atmosphere of Humid Air

as suggested by the empirical relation given by Equation 2.1 in the case of dry air. With the addition of water, NO_2 removal takes place due to the formation of HNO_3 from NO_2. Since there is a drop in the NO_2 level, the corresponding equilibrium concentration of NO also drops according to the Relation 2.1. Hence the enhanced removal of NO noticed in the presence of water is not due to the direct reactions of NO with the hydroxyl radicals. However, the experiments conducted in this study indicate that the empirical relation 2.1 does not hold when the initial concentration of NO is low.

5.6 The Effect of CO on NO Removal in Humid Air

Carbon monoxide is one of the important constituents of combustion gases. The addition of 500 ppm of CO to humid air was studied to consider NO removal under these conditions.

Tokunaga et al. (1984) showed that the addition of CO enhanced the NO removal due to the production of $HO_2^{\cdot}$ radicals by the following reaction mechanism:

$$CO + OH^{\cdot} \longrightarrow CO_2 + H^{\cdot}, \tag{5.11}$$

$$H + OH^{\cdot} \longrightarrow HO_2^{\cdot}, \tag{5.12}$$

$$NO + HO_2^{\cdot} \longrightarrow NO_2 + OH^{\cdot}. \tag{5.13}$$
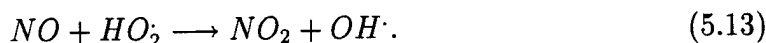
Experiments to determine NO removal with the addition of CO were performed at different voltages (30, 35, 40, and 50 kV) and at different gas residence times (7.2, 14.5, 29.0, and 44.0 seconds). The inlet concentration of CO was maintained at 500 ppm. The concentration of NO and NO_2 as a function of residence time for different operating voltages are shown in Figures 5.23 and 5.24, respectively. Comparing the concentration profiles of NO removal without CO (Figure 5.17) and with CO (Figure 5.23), CO did not have any effect on the NO removal. The NO concentrations at 7.2
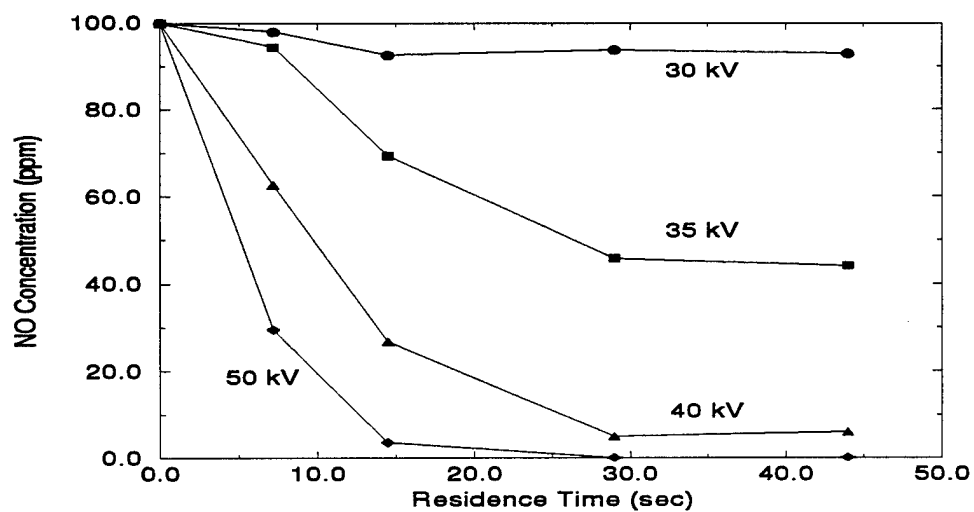
Figure 5.23: NO Concentration Profile in an Atmosphere of Humid Air and CO
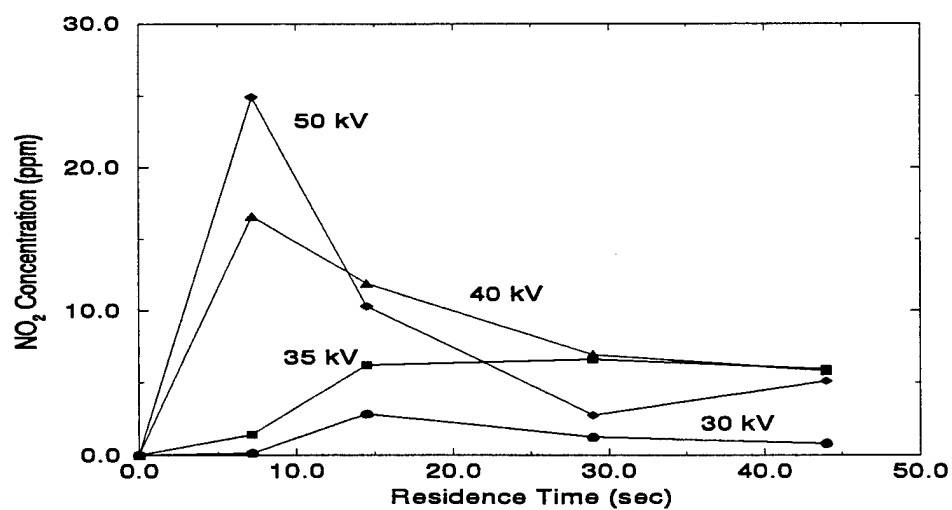
Figure 5.24: NO_2 Concentration Profile in an Atmosphere of Humid Air and CO

seconds residence time were 62.6 ppm and 29.5 ppm at 40 and 50 kV, respectively, in the presence of CO. In the absence of CO in the system (see Figure 5.17) the NO concentration at these voltages for the same residence time were 62.0 and 25.6 ppm.

Figures 5.18 and 5.24 can be compared for NO_2 concentration profiles to conclude that the presence of CO at 500 ppm does not affect the NO_2 profile too. The NO_2 concentrations at 7.2 seconds residence time were 16.6 and 24.9 ppm for 40 and 50 kV, respectively, in the presence of CO in the system. The corresponding NO_2 concentrations in the absence of CO in the system at 7.2 seconds residence time was 14.8 and 21.8 ppm for the cases of 40 and 50 kV

The amount of CO added might be too small to provide a significant improvement in the NO removal. The minimum concentration with which Tokunaga et al. (1984) observed any change in the NO removal was 0.29% (2900 ppm) of CO. The kinetic model profiles of NO, NO_2 and HNO_3 for NO removal in humid air in the presence CO for the case of 50 kV are shown in Figure 5.25. To consider the concentration profile in this case, the additional Reaction 5.11 was considered. The model profile obtained in this case is very similar to the model profiles obtained in case of NO removal in humid air (see Figure 5.19). The addition of a single reaction of carbon monoxide has not significantly affected the species concentration profiles at this concentration.

Figure 5.26 compares the NO profile predicted by the model to the experimental points. As seen in the figure, the profile of NO matches matches well with the experimental points. The NO_2 profile of the model qualitatively matches the experimental points but the values are significantly different from each other. The maximum concentration predicted by the model is around 50 ppm whereas the maximun observed concentration of NO_2 was around 22 ppm. Addition of high concentrations of CO (> 0.5 %) to consider the removal of NO must be considered for future work.
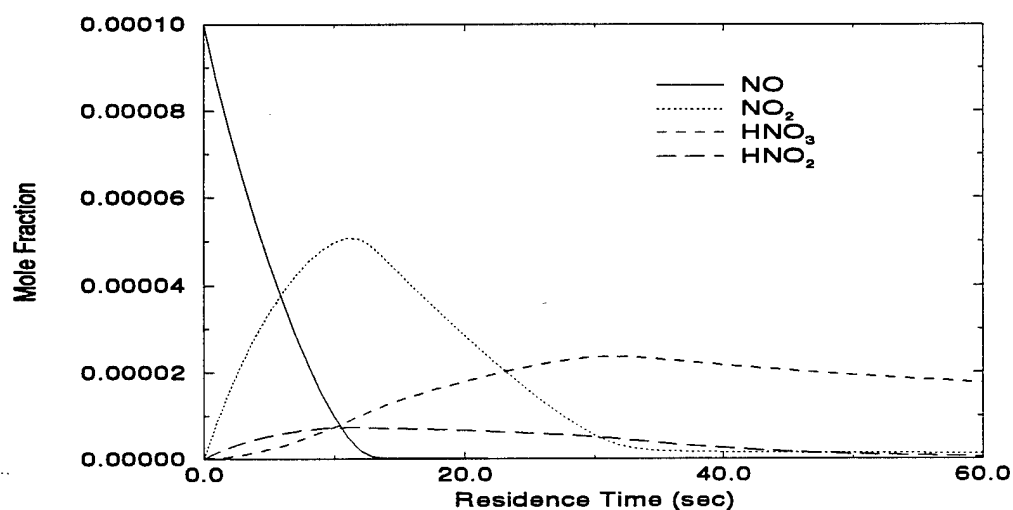
Figure 5.25: Model Profile of Different Species in the Presence of 500 ppm of CO in Humid Air
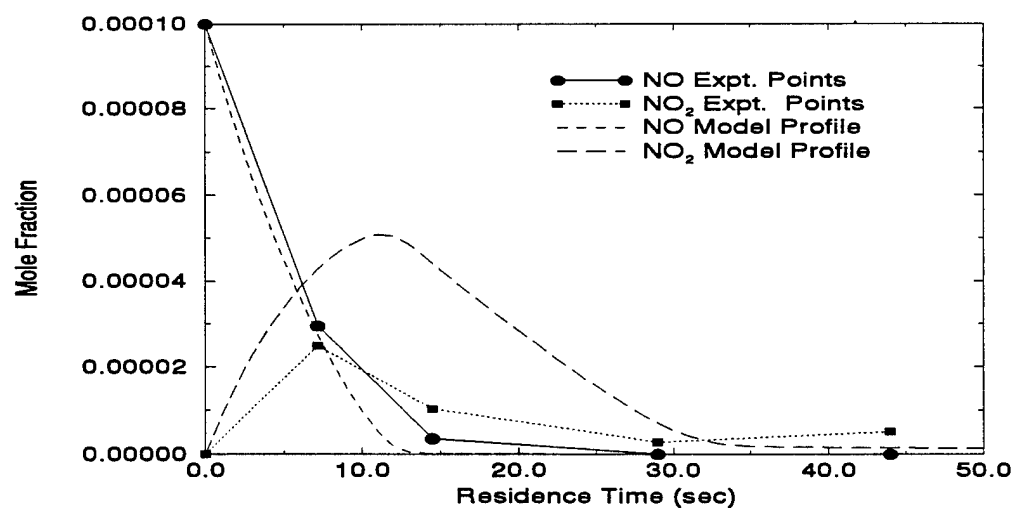
Figure 5.26: Comparison of the Model Prediction of NO and NO_2 Profile with Experimental Data in Case of NO Removal in the Presence of 500 ppm of CO in Humid Air

5.7   NO Removal from Air in the Presence of Ethylene

The atmospheric chemistry of NO_x and hydrocarbons has been well characterized by Atkinson et al. (1984) and Seinfeld (1986). The reactions of ethylene in the atmosphere with hydroxyl radicals, ozone, and dissociated oxygen may also be applicable in the pulsed streamer corona reactor.

Mizuno et al. (1993) considered the effect of hydrocarbons on the removal efficiency of NO_x from the exhaust of a diesel engine. They observed that at a gas temperature of $30°$ C the NO_x removal efficiency was 22% for an input power of 37.5 W. With the addition of 500 ppm of ethylene a rapid increase in the NO_x removal rate was observed. The NO_x removal rate with ethylene was 60% for an input power of 35 W. Among the additives considered, ethylene had the greatest effect on the removal efficiency of NO_x over other additives such as methane and propane.

Vogtlin and Penetrante (1993) conducted experiments on the removal of NO_x in the presence of hydrocarbon additives such as ethylene and octane at high gas temperatures of 100 to $200°$ C. Octane was the hydrocarbon used as an additive at a concentration ranging from 0.8 to 8 times the initial NO_x concentration. At a ratio of 8:1, 93.75% of the initial NO was removed and 45.5% of the initial NO_x from room air was removed at an energy cost of 29 eV per NO_x molecule removed. When the molar ratio was lowered to 4:1 for a gas composition of 5% O_2, 10% H_2O, 15% CO_2, and 70% N_2 (flue gas composition), almost 100% NO was removed and 45% of NO_x was removed at an energy consumption of 80 eV per removed NO_x molecule. No byproducts identification was made during the study. The hydrocarbon additives were found to be recycling the hydroxyl radicals during the oxidation and reduction of NO. Hence, the efficiency of a particular hydrocarbon was therefore limited by the reaction rate of this hydrocarbon with hydroxyl radicals.

In the natural atmosphere, ethylene reacts primarily with hydroxyl radicals since the concentration of ozone and dissociated oxygen is very small. Hydroxyl radicals

directly attack ethylene to produce peroxyl radicals which further react with oxygen molecules through the following reactions:

$$C_2H_4 + OH^{\cdot} \longrightarrow HOCH_2CH_2^{\cdot}, \tag{5.14}$$

$$HOCH_2CH_2^{\cdot} + O_2 \longrightarrow HOCH_2CH_2O_2^{\cdot}. \tag{5.15}$$
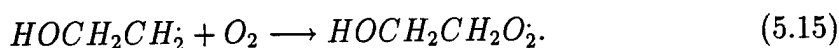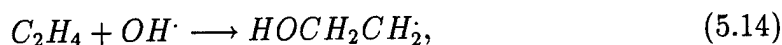
NO is converted to NO$_2$ through the following reaction:

$$HOCH_2CH_2O_2^{\cdot} + NO \longrightarrow NO_2 + HOCH_2CH_2O^{\cdot}. \tag{5.16}$$
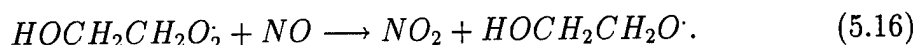
The HOCH$_2$CH$_2$O$^{\cdot}$ radical is known to react with oxygen to give glycolaldehyde (HOCH$_2$CHO) and formaldehyde (CH$_2$O). The formaldehyde produced in the above reactions can further react with hydroxyl radicals to produce hydroperoxy radicals. Direct reactions of ethylene with ozone also leads to the production of formaldehyde, formic acid, carbon dioxide, and carbon monoxide in the atmosphere (Seinfeld, 1986).

$$\begin{aligned}
C_2H_4 + O_3 \longrightarrow \ & HCHO + 0.4HCOOH + 0.18CO_2 + 0.42CO \\
& 0.12H_2 + 0.42H_2O + 0.12HO_2^{\cdot}
\end{aligned}$$
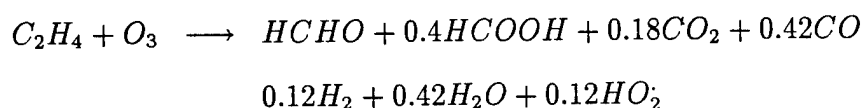
Ethylene also reacts with dissociated oxygen and hydrogen through the following reactions:

$$C_2H_4 + O^{\cdot} \longrightarrow CH_3^{\cdot} + HCO^{\cdot}, \tag{5.17}$$

$$C_2H_4 + O^{\cdot} \longrightarrow CH_2 + CH_2O, \tag{5.18}$$

$$C_2H_4 + O^{\cdot} \longrightarrow C_2H_3^{\cdot} + OH^{\cdot}, \tag{5.19}$$

$$C_2H_4 + H^{\cdot} \longrightarrow C_2H_5^{\cdot}. \tag{5.20}$$
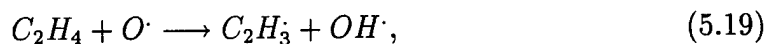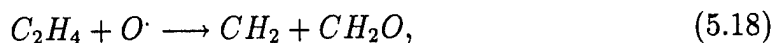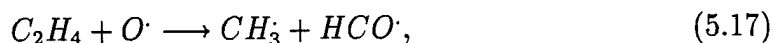
The radicals such as HCO$^{\cdot}$, CH$_3$$^{\cdot}$, and HOCH$_2CH_2$$^{\cdot}$ react with NO and NO$_2$ to form other products.

5.7.1 Dry Air

A series of NO_x removal experiments at different voltages (30, 35, 40, and 50 kV) and residence times (7.2, 14.5, 29.0, and 44.0 seconds) with 500 ppm of ethylene present in dry air was considered.

In dry air, the main reaction mechanism for ethylene breakdown was through reactions with oxygen radicals to produce other radicals such as $HCO\cdot$, CH_3, CH_2 and CH_2O. Figure 5.27 shows the variation of NO concentration as a function of residence time for various operating voltages. As can be seen in the figure, the NO concentration quickly decreased at higher voltages. When Figures 5.10 and 5.27 are compared, it can be seen that the presence of ethylene greatly enhances NO removal. NO removal in case of dry air and in the absence of ethylene at 7.2 seconds residence time and at an operating voltage of 50 kV was 80%. The addition of ethylene increases the removal efficiency to almost 100% at the same operating conditions. The CH_3 and $HCO\cdot$ radicals produced from ethylene breakdown react with NO to form a variety of compounds such as CH_3NO and HNO thereby enhancing the NO removal. Also, $HCO\cdot$ radicals increase the production of hydroperoxy radicals, which are known to enhance the NO removal:

$$HCO\cdot + O\cdot \longrightarrow H\cdot + CO_2, \qquad (5.21)$$

$$H\cdot + O_2 \longrightarrow HO_2\cdot. \qquad (5.22)$$
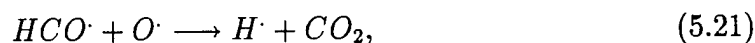
Figure 5.28 shows the NO_2 concentration profile as a function of residence time for various operating voltages. NO_2 concentration increased monotonically with the residence time for the lower voltages (30 & 35 kV), and at higher voltages (40 & 50 kV) the concentration passes through a maximum. When Figures 5.11 and 5.28 are compared the NO_2 concentration in the presence of ethylene (Figure 5.28) is significantly smaller at higher voltages (40 & 50 kV) and at longer residence times
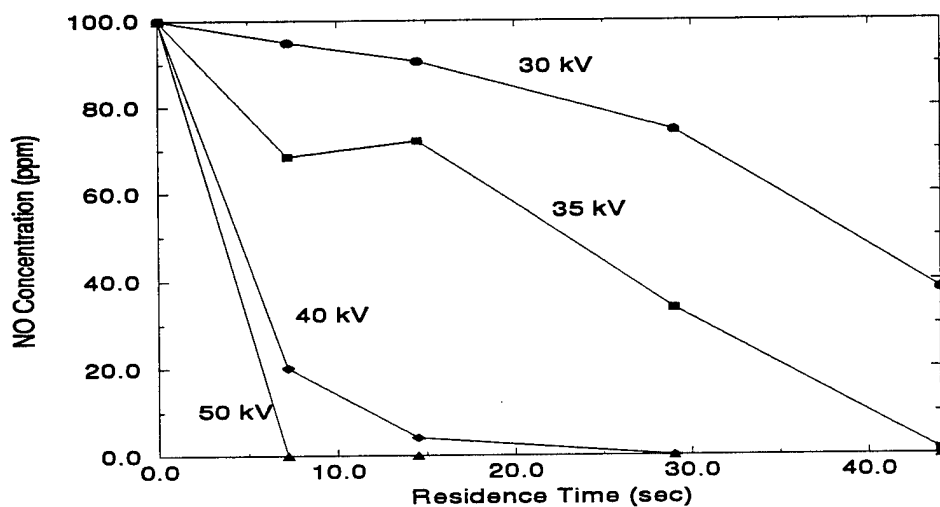
Figure 5.27: NO Concentration Profile in an Atmosphere of Dry Air and 500 ppm of Ethylene
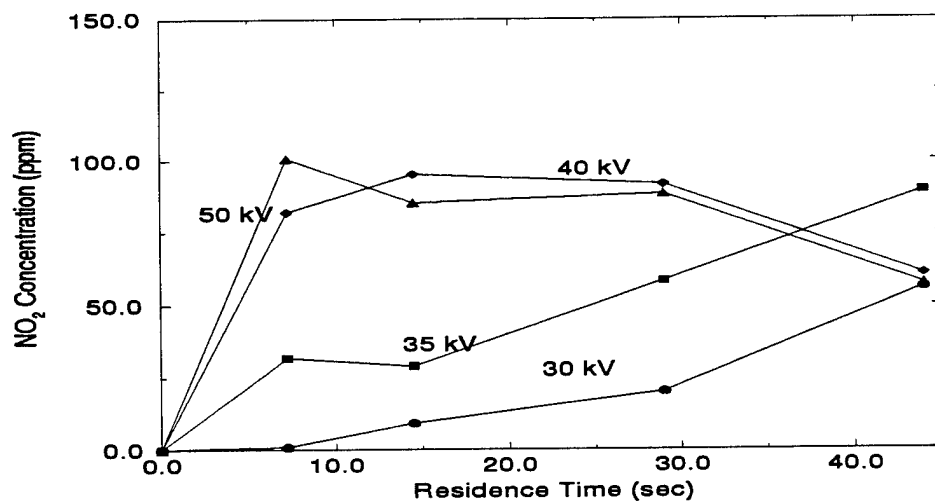
Figure 5.28: NO_2 Concentration Profile in an Atmosphere of Dry Air and 500 ppm of Ethylene

as compared to profile in Figure 5.11 (no ethylene). The HCO· radicals react with NO_2 to form HNO_2. The HCO· radicals also produce OH· radicals by reaction with oxygen radicals. The corresponding reactions are:

$$HCO· + NO_2 \longrightarrow HNO_2 + CO, \tag{5.23}$$

$$HCO· + O· \longrightarrow CO + OH·. \tag{5.24}$$
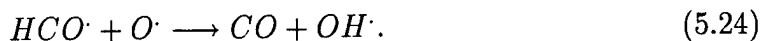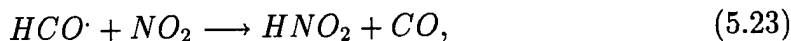
The hydroxyl radicals produced help in the breakdown of ethylene and also in the removal of NO_2. Thus, HCO· is a very important reactive radical which acts as a pathway for hydroxyl and hydroperoxy radicals and also acts as a source for the removal of NO_2. Some of the NO_2 is also reduced by the methyl radicals to NO. But, the main reaction mechanism for the removal of NO_2 is through conversion to HNO_2.

At the highest voltage of 50 kV and at longest residence time of 44.0 seconds, 45% removal of NO_x is observed in the presence of 500 ppm of ethylene as compared to 5% removal of NO_x in dry air without ethylene.

A list of additional reactions that are considered for modeling NO removal in the presence of ethylene is shown in Table 5.4 at the end of Chapter 5. The model concentration profiles for various chemical species for the case of 50 kV are shown in Figures 5.29 and 5.30. Figure 5.29 shows the concentration profiles of NO, NO_2, HNO_2 and O_3 as functions of residence time for the case of 50 kV along with the experimental data of NO and NO_2. The rate constants for the oxygen and nitrogen dissociation are assumed to be the same as those calculated from the NO experimental data for the dry air case. There is a significant formation of HNO_2. As shown in Figure 5.29, experimentally observed NO removal was faster than that predicted by the model. At a residence time of 7.2 seconds for an operating voltage of 50 kV, 70% removal of NO is predicted by the model as compared to 100% removal of NO found in the experiment. Also, in the model 10 ppm of NO_2 is observed for a voltage of 50 kV and at a residence time of 29.0 seconds. The amount of NO_2 corresponding to
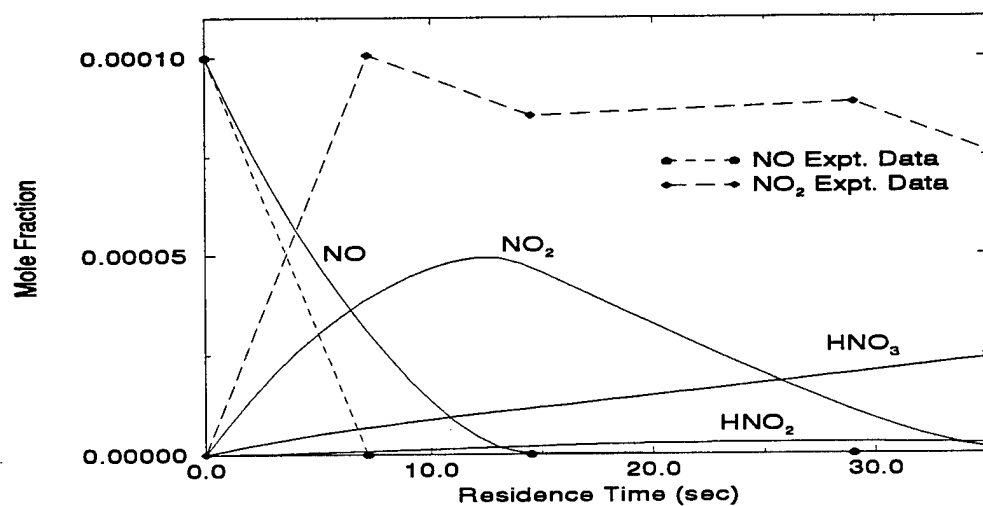
Figure 5.29: Concentration Profile of Different Species Predicted by the Model for NO Removal in the Presence of 500 ppm Ethylene in Dry Air With the Experimental Data
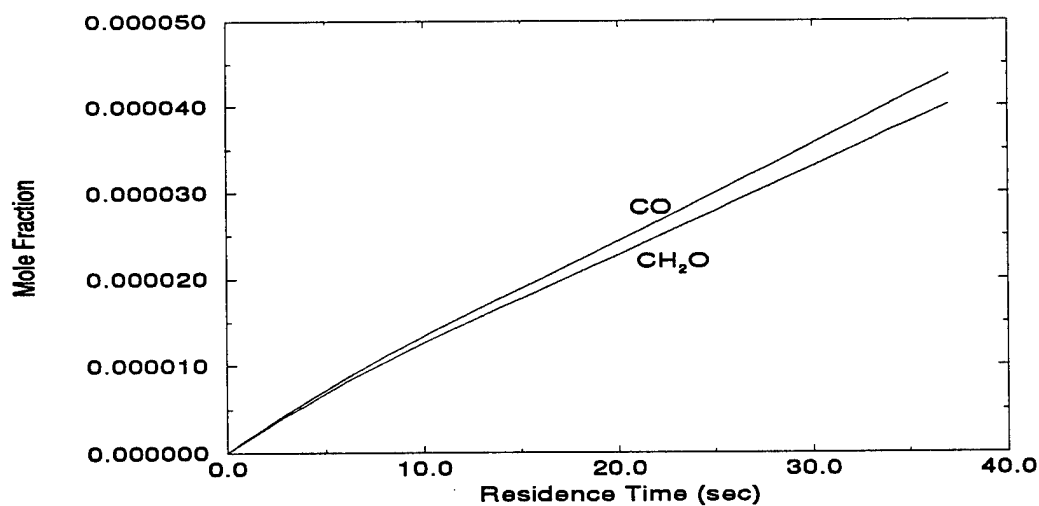
Figure 5.30: Concentration Profile of Breakdown Products Predicted by the Model for NO Removal in Dry Air with 500 ppm Ethylene

the experiment at the same operating conditions is 91.6 ppm. There is a significant difference between the model and the experiments in this case.

Figure 5.30 shows the main products expected from ethylene breakdown in the pulsed streamer corona reactor that were predicted by the model. The concentrations of CO and CH_2O increase steadily with residence time. Future work should focus on analyzing gas samples from the exhaust of the reactor for the formation of CO, CH_2O and HNO_2.

5.7.2 Humid Air

A series of experiments at different voltages (30, 35, 40, and 50 kV) and residence times (7.2, 14.5, 29.0, and 44.0 seconds) was conducted to consider the effect of ethylene on NO removal in humid air. The presence of water leads to the corona-induced production of hydroxyl radicals which should lead to more ethylene removal than that observed for in dry air. Figure 5.31 shows the profiles of ethylene breakdown in the cases of dry and humid air as predicted by the model.

The concentration profiles of NO as a function of residence time in humid air with ethylene for various operating voltages are shown in Figure 5.32. The rate of NO removal is lower compared to the profile obtained for dry air with ethylene (Figure 5.27). The concentration of NO at 7.2 seconds residence time was 17 ppm in humid air case as opposed to almost 0 ppm in the dry air (both with ethylene). The reason for this reduction in the NO removal can be explained in terms of lower external applied electric field caused by an increase in the electronegativity of the gas with the addition of water.

The concentration profile of NO_2 in humid air with ethylene is shown in Figure 5.33. The NO_2 concentration profiles go through maxima similar to the NO_2 profile in humid air without the presence of ethylene (Figure 5.18). The maximum concentration of NO_2 at 50 kV was about 24.4 ppm and at a gas residence time of 7.2 seconds, which compares well with the NO_2 maximum concentration of 21.2 ppm
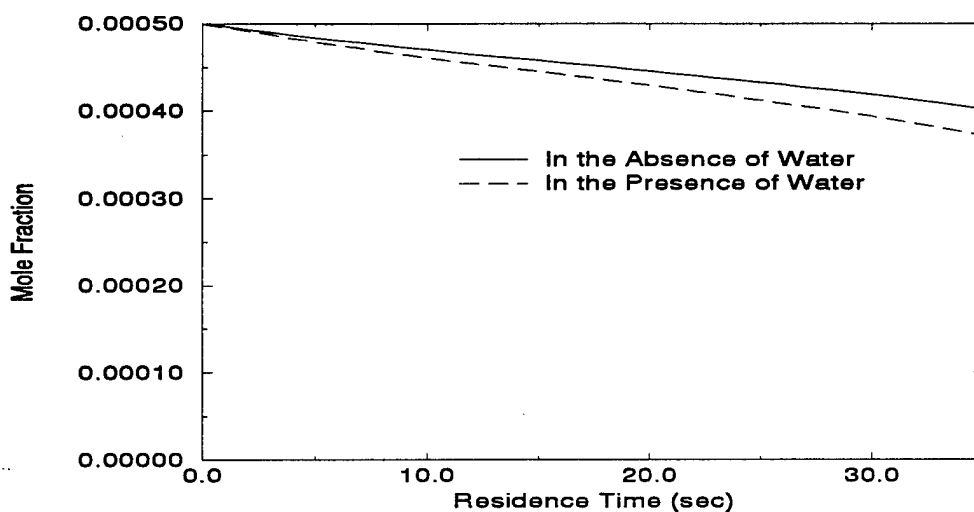
Figure 5.31: Ethylene Model Profile With and Without the Presence of Water in Case of NO Removal from Air
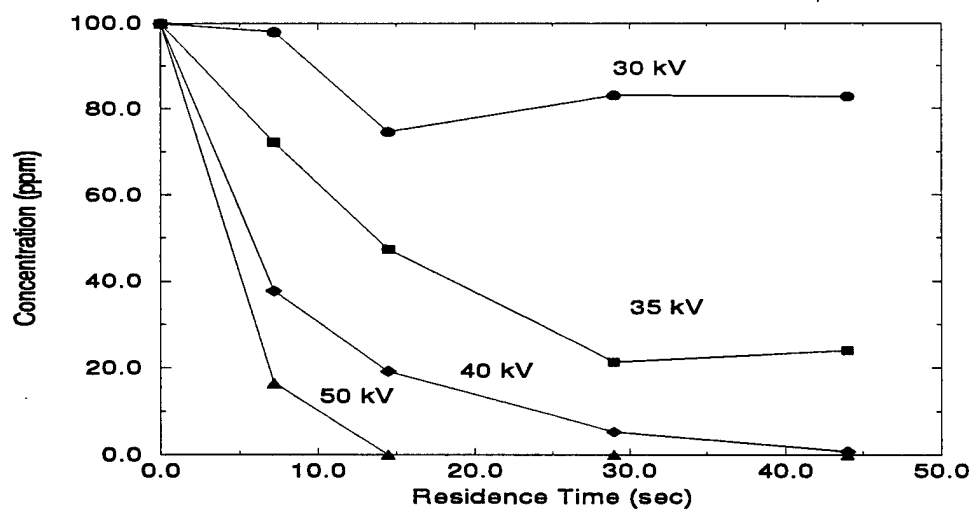
Figure 5.32: NO Concentration Profile in an Atmosphere of Humid Air and 500 ppm of Ethylene
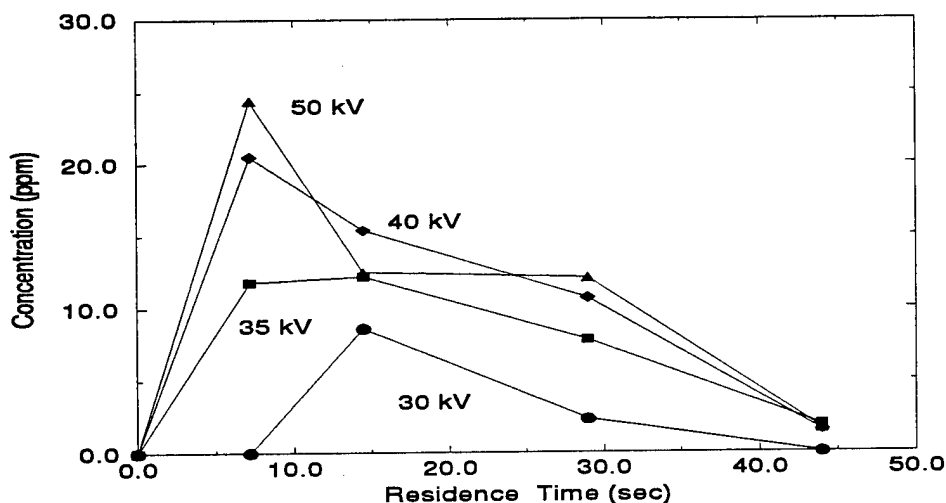
Figure 5.33: NO_2 Concentration Profile in an Atmosphere of Humid Air and 500 ppm of Ethylene

in humid air without ethylene. Hence, ethylene does not significantly affect NO_2 removal in the presence of water. The model profiles indicate that the main break down product formed from NO_2 in the case of humid air and 500 ppm ethylene is HNO_2 as opposed to HNO_3 in humid air with no ethylene.

The concentration profiles of NO, NO_2, HNO_2, and HNO_3 in humid air with 500 pmm of ethylene predicted by the model are shown in Figure 5.34 along with the experimental data of NO and NO_2. The model profile of NO matches very well with the experimental data. The profile of NO_2 predicted by the model also qualitatively matches with the experimental data. The model concentration profiles of the main byproducts formed from ethylene breakdown such as glycolaldehyde ($HOCH_2CHO$), formaldehyde (CH_2O), and CO are shown in Figure 5.35. To calculate the profile, the rate constants for nitrogen, oxygen, and water have been assumed to be the same as that obtained in NO removal from humid air.

To confirm the validity of the model, an experiment to determine the byproducts formed by the dissociation of ethylene in humid air was conducted at 50 kV and at
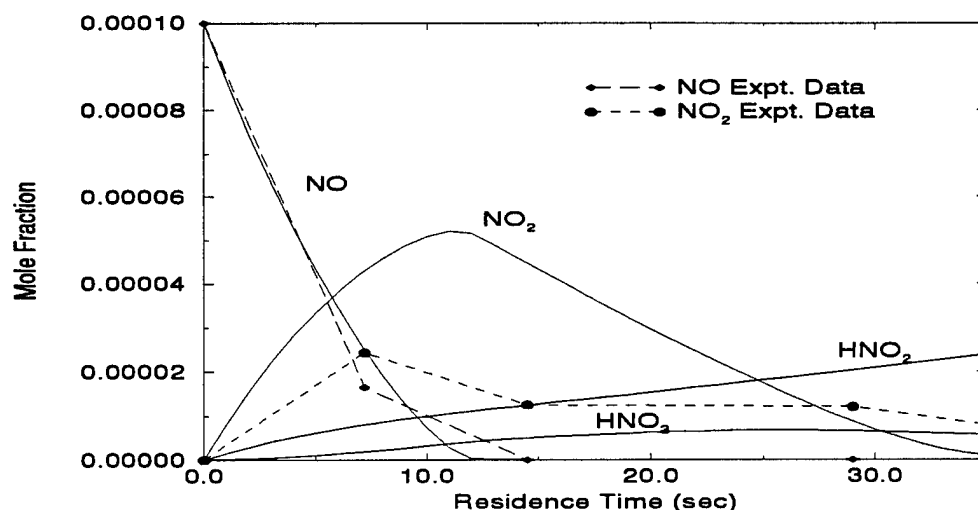
Figure 5.34: Concentration Profile of Different Species Predicted by the Model in Case of NO removal in the Presence of 500 ppm of Ethylene in Humid Air With the Experimental Data

44.0 seconds residence time. The outlet gas from the reactor was collected in a glass sample tube as well through a water column to dissolve the products formed. The gas sample analysis by GC/MS indicated the complete breakdown of ethylene and a significant increase in the concentration of CO_2. This result was in contradiction with the model profiles predicted by the model. HPLC analysis, of the liquid samples showed four peaks. Two peaks were tentatively identified as oxalic acid and formic acid. Mizuno et al. (1995) considered the removal of NO_x gases from dry air and found acetic acid to be an important byproduct. Acetic acid was not identified as one of the byproducts in this analysis.

Future work should focus on the identification and quantification of the byproducts formed. Table 5.3 shows the list of chemical compounds that could be formed from the ethylene removal. More understanding of the ethylene chemistry is necessary to predict accurately the concentration profiles.
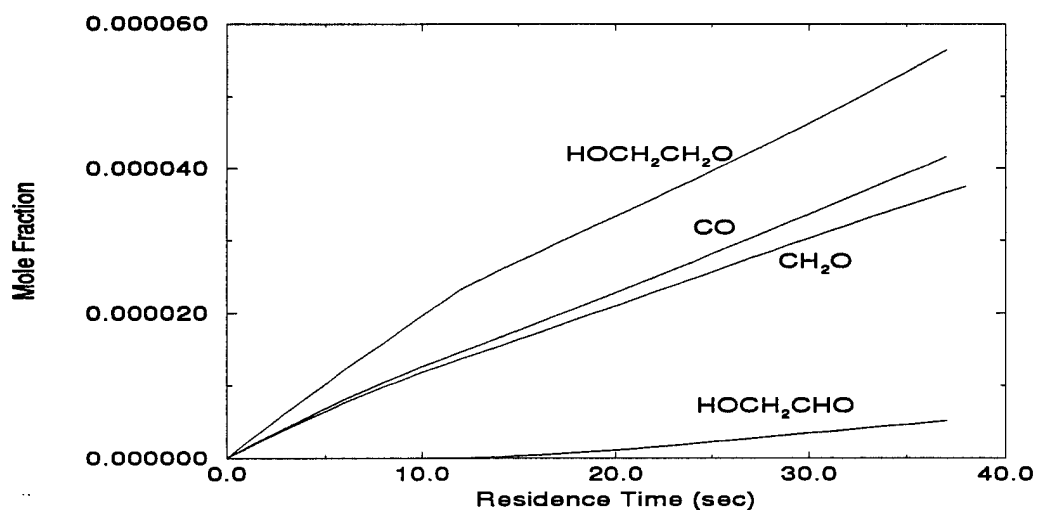
Figure 5.35: Concentration Profile of Breakdown Products Predicted by the Model in Case of NO Removal in Humid Air with 500 ppm of Ethylene

Table 5.3: Byproducts Predicted by the Model Due to Ethylene Breakdown

Name	Chemical Formula
Formaldehyde	CH_2O
Formic Acid	$HCOOH$
Glycolaldehyde	$HOCH_2CHO$
Acetaldehyde	CH_3CHO
Ethylene Glycol	$OHCH_2CH_2OH$
Carbon Monoxide	CO
Carbon dioxide	CO_2
Methyl Nitrate	CH_3NO
Hydrogen Cyanide	HCN

Table 5.4: Additional List of Chemical Reactions Considered for Modeling NO Removal in the Presence of Ethylene

Chemical Reactions	Rate Constants $(cm^3.mole^{-1}.sec^{-1})$	Source
$C_2H_4 + O^{\cdot} \longrightarrow CH_3 + HCO^{\cdot}$	4.39×10^{11}	NIST
$C_2H_4 + O^{\cdot} \longrightarrow CH_2 + CH_2O$	3.98×10^{11}	NIST
$C_2H_4 + O^{\cdot} \longrightarrow H^{\cdot} + CH_2CHO$	3.76×10^{11}	NIST
$C_2H_4 + O^{\cdot} \longrightarrow C_2H_3 + OH^{\cdot}$	1.46×10^{9}	NIST
$C_2H_4 + N^{\cdot} \longrightarrow HCN + CH_3$	9.93×10^{10}	NIST
$C_2H_4 + H^{\cdot} \longrightarrow C_2H_5$	6.88×10^{11}	NIST
$C_2H_4 + OH^{\cdot} \longrightarrow C_2H_4OH^{\cdot}$	5.42×10^{12}	NIST
$HCO^{\cdot} + CH_3 \longrightarrow CO + CH_4$	1.21×10^{14}	NIST
$HCO^{\cdot} + O^{\cdot} \longrightarrow CO + OH^{\cdot}$	3.10×10^{13}	NIST
$HCO^{\cdot} + O^{\cdot} \longrightarrow H^{\cdot} + CO_2$	3.01×10^{13}	NIST
$HCO^{\cdot} + OH^{\cdot} \longrightarrow H_2O + CO$	1.02×10^{14}	NIST
$HCO^{\cdot} + O_2 \longrightarrow HO_2 + O^{\cdot}$	3.31×10^{12}	NIST
$HCO^{\cdot} + NO_2 \longrightarrow CO + HNO_2$	3.27×10^{29}	NIST
$HCO^{\cdot} + NO \longrightarrow CO + HNO$	7.23×10^{12}	NIST
$HCO^{\cdot} + CH_3 \longrightarrow CH_3CHO$	1.81×10^{13}	NIST
$C_2H_4OH^{\cdot} + O_2 \longrightarrow HOCH_2CH_2O_2$	1.81×10^{12}	NIST
$2HOCH_2CH_2O_2 \longrightarrow$ $2HOCH_2CH_2O^{\cdot} + O_2$	5.0×10^{11}	NIST

Chemical Reactions	Rate Constants $(cm^3.mole^{-1}.sec^{-1})$	Source
$2HOCH_2CH_2O_2^{\cdot} \longrightarrow$ $HOCH_2CH_2OH + HOCH_2CHO + O_2$	4.04×10^{11}	NIST
$HOCH_2CH_2O_2^{\cdot} + NO$ $\longrightarrow HOCH_2CH_2O^{\cdot} + NO_2$	5.42×10^{12}	NIST
$CH_3^{\cdot} + HO_2^{\cdot} \longrightarrow CH_3O^{\cdot} + OH^{\cdot}$	1.81×10^{13}	NIST
$CH_3^{\cdot} + O^{\cdot} \longrightarrow CH_3O$	1.58×10^{10}	NIST
$CH_3^{\cdot} + O^{\cdot} \longrightarrow H^{\cdot} + CH_2O$	8.43×10^{12}	NIST
$CH_3^{\cdot} + HO_2^{\cdot} \longrightarrow CH_4 + O_2$	3.61×10^{12}	NIST
$CH_3^{\cdot} + NO \longrightarrow CH_3NO$	1.01×10^{13}	NIST
$CH_3^{\cdot} + NO_2 \longrightarrow CH_3ONO$	7.00×10^{10}	NIST
$CH_3^{\cdot} + NO_2 \longrightarrow CH_3O^{\cdot} + NO$	1.39×10^{13}	NIST
$CH_2O + O^{\cdot} \longrightarrow OH^{\cdot} + HCO^{\cdot}$	1.01×10^{11}	NIST
$CH_2O + OH^{\cdot} \longrightarrow H_2O + HCO^{\cdot}$	6.03×10^{12}	NIST
$CH_2O + OH^{\cdot} \longrightarrow HCOOH + H^{\cdot}$	1.21×10^{11}	NIST
$CH_2 + OH^{\cdot} \longrightarrow CH_2O + H^{\cdot}$	1.81×10^{13}	NIST
$CH_2 + HCO^{\cdot} \longrightarrow CH_3^{\cdot} + CO$	1.81×10^{13}	NIST
$CH_2CHO + O_2 \longrightarrow CH_2O + CO + OH^{\cdot}$	1.81×10^{10}	NIST
$C_2H_5^{\cdot} + O^{\cdot} \longrightarrow CH_3CHO + H^{\cdot}$	8.02×10^{13}	NIST
$C_2H_5^{\cdot} + HCO^{\cdot} \longrightarrow C_2H_5CHO$	1.81×10^{13}	NIST
$C_2H_5^{\cdot} + HCO^{\cdot} \longrightarrow C_2H_6 + CO$	1.21×10^{14}	NIST
$C_2H_3^{\cdot} + OH^{\cdot} \longrightarrow CH_3CHO$	3.01×10^{13}	NIST
$CH_3O^{\cdot} + HCO^{\cdot} \longrightarrow CH_3OH + CO$	9.04×10^{13}	NIST

Chemical Reactions	Rate Constants $(cm^3.mole^{-1}.sec^{-1})$	Source
$H\cdot + CH_3OH \longrightarrow CH_2OH + H_2$	8.39×10^{12}	NIST
$O\cdot + CH_3OH \longrightarrow OH\cdot + CH_2OH$	4.87×10^{9}	NIST
$OH\cdot + CH_3OH \longrightarrow CH_2OH + H_2O$	6.4×10^{11}	NIST
$CH_3O\cdot + CH_3OH \longrightarrow CH_3OH + CH_2OH$	3.1×10^{8}	NIST
$NO_3 + CH_3OH \longrightarrow HNO_3 + CH_2OH$	5.73×10^{6}	NIST
$CH_2OH + CH_2OH \longrightarrow HOCH_2CH_2OH$	4.82×10^{12}	NIST

CHAPTER 6

SUMMARY & CONCLUSIONS

In the present study, it was shown that a pulsed streamer corona discharge can be used to remove NO_x from feed gases such as nitrogen and air containing small amounts of other gases such as water, carbon monoxide, and ethylene. A rotating spark gap pulsed power supply providing fast rise time, narrow width, repetitive high voltage pulses to a wire-cylinder geometry gas phase reactor vessel was constructed and employed in this study. Experiments varying the gas composition, the pulsed voltage value, and the gas residence time were performed to determine the NO and NO_2 removal. The main reaction pathways for NO removal were identified for each of the gas compositions. A model was developed to calculate the concentration profiles of different chemical species under treatment by a pulsed streamer corona discharge. The reaction rate constants for the nitrogen, oxygen and water molecules were obtained by fitting the experimental data of NO removal with the model.

Power input into the pulsed corona discharge reactor was calculated using the voltage and current measurements made during experiments using a fast oscilloscope and high voltage and current probes attached to the pulsed power input. The peak voltage was significantly higher than the applied voltage, and the rise time varied from 15-30 nanoseconds as the applied voltage was increased from 30 to 50 kV. The pulse width varied from 500 to 700 nanoseconds. There was difference in the nature of the current waveforms as obtained from both of the current probes. The energy input varied from 74.7 mJ/pulse at 30 kV to 246.7 mJ/pulse at 50 kV in an atmosphere

80

of dry air. The power input varied from 4.48 w to 14.8 w at the corresponding condtions.

Figure 6.1 shows the summary of NO concentration profile in different atmospheres at a voltage of 50 kV and Figure 6.2 shows the summary of the corresponding NO_2 concentration profile. As seen in Figure 6.1, NO removal in the presence of ethylene in dry air was the fastest. The addition of water did not enhance the NO removal. The concentration profiles of NO removal in humid air, in the presence of 500 ppm of CO in humid air, and in the presence of 500 ppm of ethylene in humid air almost match each other. The NO_2 concentration profile shown in Figure 6.2 indicates that in the presence of water, NO_2 formation is significantly reduced as compared to NO_2 removal in dry air. The addition of ethylene to dry air enhanced the NO_2 removal as shown in the figure. As was observed in case of NO removal profiles, the NO_2 concentration profiles in the case of humid air, 500 ppm of CO in humid air, 500 ppm of ethylene in humid air matched each other well.

For the experimental case of pure nitrogen containing NO under pulsed corona treatment, NO was chemically reduced to N_2. About 99% removal of NO_x was observed at 50 kV pulsed voltage for a gas residence time of 44.0 seconds. The model profiles of NO and NO_2 matched well with the experimental data and the model indicated that there was a small amount of N_2O formation during the process. The rate constant for nitrogen dissociation was determined by fitting the model with the NO experimental data. The experiments, as well as the modeling results, match well with the results indicated in the non-thermal plasma treatment literature. In the experimental case of dry air containing NO, oxidation mechanisms dominate the reduction pathway and hence NO was converted to NO_2. Subsequent removal of NO_2 was not observed under the current operating conditions (maximum of 50 kV pulsed voltage and 60.0 seconds residence time). The addition of oxygen in the form of using dry air as the feed gas increased the rate of NO removal. Chang et al. (1992) reported
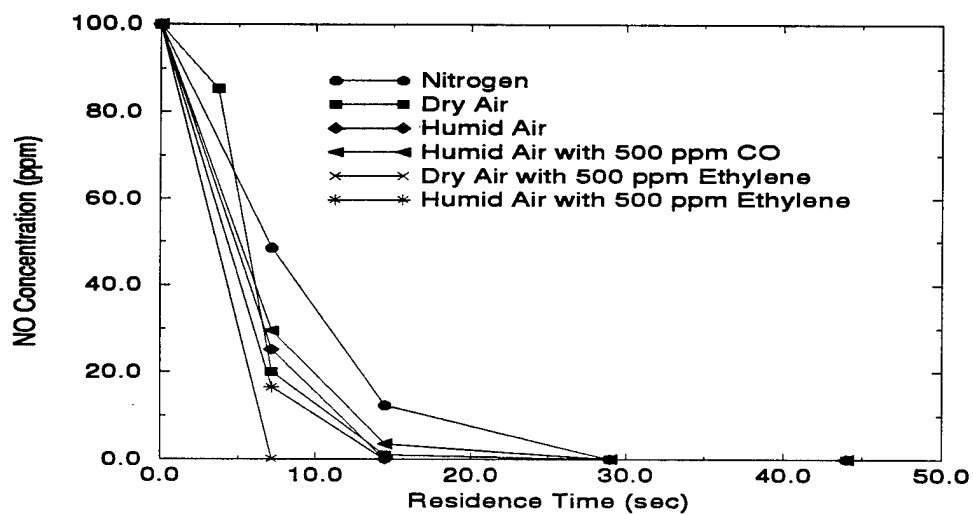
Figure 6.1: Summary of NO Removal in Different Atmospheres
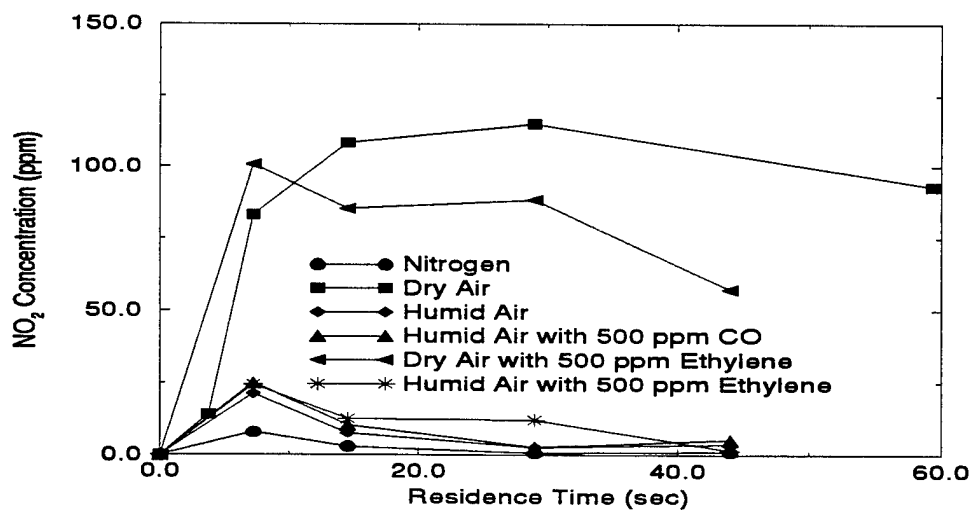
Figure 6.2: Summary of NO_2 removal in Different Atmospheres

that in a dielectric barrier discharge system, the addition of oxygen decreased the rate of NO removal. The model developed in this study predicted 80% conversion of the initial NO to NO_2, while the experimental value showed 95% conversion of NO to NO_2 at 50 kV and at long residence time.

The rate constants for nitrogen and oxygen dissociation were determined from the NO removal and the NO_2 formation data. The reaction rate constant of nitrogen was found to be different from the value obtained in pure nitrogen. The rate constant was 0.0475 s^{-1} in an atmosphere of nitrogen at 50 kV, but in dry air the rate constant was lower at 0.03 s^{-1}. Hence the rate constant depend upon the composition of the gas.

N_2O measurement during the experiment matched well with the model value obtained in this case. This result is significant as this matched very well with the model prediction and acted as an independent check for the model. To have an additional independent check on the model, experiments were conducted to measure ozone formation in dry air under pulsed streamer corona discharge. The model prediction did not match with the experimental value, however the measurement range of the ozone monitor was not in the range of ozone concentrations produced during the discharge. Future work should be done to calibrate the ozone monitor to check the validity of the results.

In the case of NO removal in feed air in the presence of water, the addition of water did not enhance NO removal. NO_2 concentration was significantly lowered due to the water-induced formation of further products from NO_2. A very small amount of HNO_3 was measured as nitrate during the experiments using ion chromatography. No previous research have reported measurements of the formation of HNO_3. The model predict about 35% conversion of the initial NO to HNO_3 at 50 kV and at long residence time (60.0 seconds). The experimental measurements did not find such high

concentrations of nitric acid. The NO_2 concentration profile qualitatively matched with the experimental data, but quantitatively the difference was significant.

The presence of 500 ppm of carbon monoxide in the humid air did not affect the experimental concentration profiles of NO and NO_2. Tokunaga et al. (1984) showed that the removal of NO was enhanced in the presence of 1.13% carbon monoxide by volume. In the present study the amount of carbon monoxide added to the gas may have been too small to have an affect on the concentration of NO. The model profile with and without 500 ppm of carbon monoxide also showed no effect of CO on NO removal.

In the presence of 500 ppm of ethylene, NO_x removal was enhanced. The main reaction pathways for the enhanced removal of NO and NO_2 are due to the production of highly reactive radicals by the reaction of oxygen atoms with ethylene. The formation of radicals such as $HCO\cdot$, and CH_3 react with NO and NO_2 to enhance their removal. In dry air with ethylene about 45% removal of NO_x was observed. The model indicated that the main reaction pathway for the removal of NO_2 in dry air is through reaction with $HCO\cdot$ radical to form HNO_2.

In humid air containing ethylene, additional ethylene breakdown caused by its reaction with hydroxyl radicals aid in the removal of NO_2. Complete removal of ethylene under these conditions was found using by GC/MS analysis of the gas samples. The byproducts formed from ethylene breakdown have yet to be identified properly. Four chromatographic peaks were observed when the sample was analyzed by HPLC. Formic acid and oxalic acid were identified as two of its peaks. Oxalic acid formation is not predicted as a byproduct in the current model. Further analysis is required to confirm the formation of oxalic acid and also to identify the products that are formed.

In conclusion, the use of pulsed streamer corona discharge has been shown to be successful in the removal of NO_x in different gas compositions. The main reaction

mechanisms for NO_x removal in various gas compositions under corona discharge were identified in this work. The addition of ethylene was found to enhance both NO and NO_2 removal even in the case of dry air, while water addition assisted NO_2 but not NO removal. The addition of 500 ppm of CO in humid air did not enhance the NO and NO_2 removal.

CHAPTER 7

FUTURE WORK

As an extension of this work, several aspects of this project should be considered for future work. Among them are:

1. Model Verification. The kinetic model which has been developed using the experimental data obtained could be verified for its applicability in several other experiments. As a simple case, the model could be tested for the removal of NO_2 from a feed gas containing NO_2 in nitrogen, dry air, or humid air.

2. Calibration of Ozone Monitor. Experiments were carried out to determine the amount of ozone being produced from dry air at different residence times and operating voltages. The model prediction did not match well with the experimental values. The calibration of the ozone monitor to check the validity of the experimental data obtained must be undertaken.

3. Byproducts Identification. In the experiments conducted to study the removal of NO in humid air, both NO and NO_2 removal was observed. Further products formed from NO_2 have not yet been quantified. The nitric acid produced tends to form aerosols. The analysis of aerosols is an important area for future work. Better techniques to characterize the aerosols and to measure the concentration of aerosols are necessary. In experiments of NO removal with ethylene and water, the liquid sample collected was analyzed with HPLC. Four

peaks were recorded but not all the peaks have been identified. Two of the peaks was identified to be oxalic acid and acetic acid. Further experiments and analysis should be done using techniques such as the FTIR method used by Mizuno et al. (1995) to determine the byproducts formed.

4. Power Characteristics. To confirm the validity of the current probes used in this study. A plot of NO and NO_x removal as a function of power per unit volume, power/per unit volume divided by the square root of the residence time in the reactor should be done. This will assist in comparing the experimental data obtained in this work with the values reported in the literature.

5. Operating Conditions. Variation of the gas temperature, and gas compositions could be considered. The exhaust gases coming out of power plants or jet cell engines are at high temperature and contain large concentrations of carbon dioxide and water vapor. Addition of such gases and operation of the reactor at high temperatures could be considered. The rate of NO_x gas removal at higher concentrations of NO could be investigated to compare the values obtained with the literature.

6. Use of Catalyst. Tas (1995) has considered the use of a silica catalyst to improve the energy efficiency of NO removal. The use of a catalyst may be considered as a packing in between the electrodes or as a coating for the electrodes.

7. Improvements on Modeling. In terms of modeling, several improvements could be made. The solution of Boltzmann's equation for the electron energy distribution function and subsequent calculation of rate constants for the dissociation reactions would lead to a model which can be independently checked with the experimental data. The model now assumes a constant electric field during the pulsing, both in time as well as in space. Variation of the electric field along the electrode length could be introduced to include the non-uniform aspect of

the electric discharge. Also, there is a definite temperature variation along the distance between the electrodes. Introduction of temperature variation in the model could also be considered.

8. Improvements in Experimental Setup. The power input into the system is increased in our case by increasing the applied voltage. Under the current operating conditions, the pulsed dial voltage could be operated at a maximum of 50 kV. If the dial voltage is increased above 50 kV, sparking takes place near the high voltage connection to the central wire electrode. The insulation provided to the central wire is not sufficient enough, to insulate the wire for voltages higher than 50 kV. For the operation of the reactor at higher voltages above 50 kV, better insulation is required. Also, to increase the power input into the system, the frequency of pulsing could be increased. The rotating spark gap currently has the facility to rotate only at a frequency of 60 Hz. Ability to run the spark gap at different frequencies could be considered to increase the power input into the system.

REFERENCES

[1] Alekseev, G. Y., Leuchenko, A. L, and Bityurin, V. A, "Flue Gas Cleaning of the Electrostatic Corona, Part II Chemical Kinetics and Heat and Mass Transfer in NO_2/SO_2 Removal", *Research Report IVTAN-ANRA* 93/2, MOSCOW, 1993.

[2] Atkinson, R. and Lloyd, A. C., "Evaluation of Kinetic and Mechanistic Data for Modeling of Photochemical Smog", *J. Phys. Chem. Ref. Data*, **13**, 2, 1984, 315-444.

[3] Atkinson, R., Baulch, D. L., Cox, R. A., Hampson, R. F., Kerr, J. A., and Troe, J., "Evaluated Kinetic and Photochemical Data for Atmospheric Chemistry", *J. Phys. Chem. Ref. Data*, **18**, 1989, 881-1097.

[4] Baulch, D. L., Drysdale, D., and Horne, D. G., "Evaluated Kinetic Data for High Temperature Reactions", 1983, Butterworths, London, Vol. 2.

[5] Boodaghians, R., B., Canosa-Mas, C., E., Carpenter, P. J., and Wayne, R., P., "The Reactions of NO_3 with OH and H", *J. Chem. Phys. Farad. Trans.*, 2, **84**, 1988, 931-948.

[6] Brune, Wm., H., Schwab, J., J., and Anderson, J., G., "Laser Magnetic Resonance, Resonance Flourescence and Resonance Absorption Studies of the Reaction Kinetics of $O + OH \longrightarrow H + O_2$, $O + HO_2 \longrightarrow OH + O_2$, $N + OH \longrightarrow H + NO$ and $N + HO_2 \longrightarrow$ Products at 300° K Between 1 and 5 torr", *J. Phys. Chem.*, **87**, 1983, 4503-4514.

[7] Busi, F., Dangelantonio, M., Mulazzani, Q., G., and Raffaelli, V., "A Kinetic Model for Radiation Treatment of Combustion Gases", *The Science of the Total Environment*, **64**, 1987, 231-238.

[8] Chang, M. B., Kushner, M. J., and Rood, M. J., "Gas Phase Removal of *NO* from Gas Streams via Dielectric Barrier Discharges", *Envir. Sci. Technol.*, **26**, 1992, 777-781.

[9] Chang, J. S., "Energertic Electron Induced Plasma Processes for Reduction of Acid and Greenhouse Gases in Combustion of Flue Gases", *Non-Thermal Plasma Techniques for Pollution Control*, Part A, Eds: Penetrante, B., M. and Sculthesis, S., E., Springer-Verlag, 1993, 1-32.

[10] Clements, J., S., Sato., M., Davis, R., H., "Preliminary Investigation of Pre-breakdown Phenomena and Chemical Reactions Using a Pulsed High Voltage Discharge in Water", *IEEE. Trans. Ind. Appl.*, **IA-23**, 1985, 1372.

[11] Clements, J. S., Mizuno, A., Finney, W. C., and Davis, R. H., "Combined Removal of SO_2, NO_x, and Fly Ash from Simulated Flue Gas Using Pulsed Streamer Corona", *IEEE Trans. on Ind. Appl.*, **25**, No. 1, January/February 1989, 62-69.

[12] Creyghton, Y. L. M.,"Pulsed Positive Corona Discharges, Fundamental Study and Application to Flue Gas Treatment", *CIP-DATA Kononkijke biblitheck*, Den Haag, Netherlands, 1994.

[13] Demore, W. B., Molina, M. J., Sander, S. P., Hampson, R. F., Kurylon, M. J., Golden, D. M., Howard, C. J., and Ravishankara, A. R., "Chemical Kinetics and Photochemical Data for Use in Stratospheric Modeling", National Aeronautics and Space Administration, JPL Publication 87-41, 1987.

[14] Dhali, S., K., and Sardja, I., "Dielectric-Barrier Discharge For Processing of SO_2/NO_x", *J. Appl. Phys.*, **69**(9), 1 May 1991, 6319-6324.

[15] Dinelli, G., Civitano, L., and Rea, M., "Industrial Experiments on Pulse Corona Simultaneous Removal of NO_x and SO_2 from Flue Gas", *IEEE Trans. on Ind. Appl.*, **26**, 1990, 535-541.

[16] Frank, W., N., and Hirano, S., "The History of Electron Beam Processing for Environmental Pollution Control and Work Performed in the United States", *Non-Thermal Plasma Techniques for Pollution Control*, Eds: Penetrante, B., M., and Schultheis, S., E., Part B, Springer-Verlag, 1993, 1-26.

[17] Fujii, T., Gobbo, R., Rea, M., "Pulse Corona Characteristics" , *IEEE Tran. on Ind. Appl.*, **29**, No. 1, January/Febuary 1993.

[18] Gallimberti, I., "A Computer Model for Streamer Propagation", *J. Phys. D: Appl. Phys.*, **5**, 1972, 2179-2189.

[19] Gallimberti, I., "Impulse Corona Simulation for Flue Gas Treatment", *Pure Appl. Chem.*, **60**, 1988, 663-674.

[20] Hoffmann, A., and Zellner, R., Paper Presented at the 10th Int. Symposium on Gas Kinetics, Swansey, 1988.

[21] Huxley, L., G., H., and Crompton, R., W., "The Diffusion and Drift of Electrons in Gases", Wiley, New York, 1974, 669.

[22] Joshi, A., A., Locke, B., R., Arce , P., and Finney, W., C., "Formation of Hydroxyl Radicals, Hydrogen Peroxide and Aqueous Electrons by Pulsed Streamer Corona Discharge in Aqueous Solution", *Journal of Hazardous Materials*, **41**, April 1995, 3-30.

[23] Kaiser, E., W., and Wu, C., H., "A Kinetic Study of the Gas Formation and Decomposition Reactions of Nitrous Acid", *J. Phys. Chem*, **81**, 1977, 187-190.

[24] Kaiser, E., W., and Wu, C., H., "Upper Limits to the Gas Phase Reactions of HONO with NH_3 and $O(^3P)$ atoms", *J. Phys. Chem.*, **81**, 1978, 187-190.

[25] Kee, R. J, Rupley, F. M., and Miller, J. A., "Chemkin-II: A Fortran Chemical Kinetics Package for the Analysis of Gas Phase Chemical Kinetics", Sandia Report, SAND89-8009B, 1994.

[26] Kokkinos, A., Cichanowicz, J., E., Hall, R., E., and Sedman, C., B., "Stationary Combustion NO_x Control: A Summary of the 1991 Symposium", *J. Air Waste. Manage. Assoc.*, **41**, 1991, 1252-1259.

[27] Leslie S., L., "Nitrogen Oxides Control Technology", Noyes Data Corporation, 1992, 4-14.

[28] Levine, J., S., "The Photochemistry of Atmospheres", Academic Press, 1985.

[29] Lincoln, D., "Ozone Generation in Gas Phase Pulsed Corona Reactor", *Report Prepared For Department of Chemical Engineering, FAMU-FSU College of Engineering*, 1995.

[30] Locke, B.R, Swaminathan, K., Finney, W.C., "Laboratory Studies of Nitrogen Oxide Removal by Pulsed Streamer Corona." *Final Report Prepared for USAF*, 1995.

[31] Loirat, H ., Caralp, F., Destriau, F., and Lesclaux, R., "Oxidation of CO by N_2O between 1076 and 1288° K: Determination of the Rate Constant ofthe Exchange Reaction", *J. Phys. Chem*, **91**, 1987, 6538-6542.

[32] Loiseau, J., F., Laoassie, F., Monge, C., Peyrous, R., Held, B., and Coste, C., "Numerical Simulation of Ozone Axial and Radial Distribution in a Cylindrical Oxygen-Fed Ozonizer", *J. Phys. D: Appl. Phys*, 1994, 63.

[33] Lucas, S., "Voltage Waveform Characterization of the Pulsed Corona Reactor", *Report Prepared For Department of Chemical Engineering, FAMU-FSU College of Engineering*, 1995.

[34] McFarlane, J., and Wren, J. C., "Modeling Electric Discharge Chemistry", *AECL-10374 Atomic Energy of Canada Limited*, Whiteshell Laboratories, 1991.

[35] Masuda, S., and Nakao, H., "Control of NO_x by Positive and Negative Pulsed Corona Discharges", *IEEE Trans. on Ind. Appl.*, **26**, 1990, 374-383.

[36] Matzing, H., "Chemical Kinetics of Flue Gas Cleaning by Irradiation with Electrons", *Adv. Chem. phys.*, **80**, 1991, 315-402.

[37] Mizuno, A., Ito, H., "Basic Performance of an Electrically Augmented Filter Consisting of Packed Ferroelectric Pellet Layer", *J. Electrostatics.*, **25**, 1987, 97-107.

[38] Mizuno, A., and Kamase, Y., "A High- Voltage Pulse Source for Electron-Beam Generation Using field Emission" *IEEE Trans. on Ind. Appl.*, **25**, No. 1 January/February 1989.

[39] Mizuno, A., Chakrabarti, A, Okazaki, K., "Application of Corona Technology in the Reduction of Greenhouse Gases and Other Pollutants", *Non-Thermal Plasma Techniques for Pollution Control*, Part B, Eds: Penetrante, B., M and Schultheis, S., E., Springer-Verlag, 1993, 165-185.

[40] Mizuno, A., Simizu, K., Chakrabarti, A., Dascalescu, L., and Furuta, S., "NO_x Removal Process Using Pulsed Discharge Plasma", *IEEE Tran. on Ind. Appl.*, **31**, No. 5, September-October 1995, 957-963.

[41] Mukkavilli, S., Lee, C. K., Varghese, K., and Tavalarides, L. L.,"Modeling of the Electrostatic Corona Discharge Reactor", *IEEE Trans. Plasma. Sci.*, **16**, 1988, 656-660.

[42] Naseer, E., "Fundamentals of Gaseous Ionization and Plasma Electronics", Wiley-Interscience, 1971.

[43] NIST Chemical Database 17, version 6.01, 1994, Eds: Mallard, W., G., Westley, F., Herron, J., T., Hampson, R., F.; National Institute of Standards and Technology (NIST), Gaithesburg, USA.

[44] Ohkubho, K., Kanazawa, S., Nomoto, Y., Chang, J. S., and Adachi, T., "NO_x Removal by a Pipe with Nozzle-Plate Electrode Corona Discharge System", *IEEE Tran. on Ind. Appl.*, **30**, No. 4, July/August 1994, 856-860.

[45] Okazaki, K., Mizuno, A., Shimizu, K., Niwa, T., "Application of Semi-Wet Type Corona Discharge Reactor to the Simultaneous Removal of NO_x, SO_x and Fly Ash in Pulverized Coal Combustion", *IEEE Tran. Ind. Appl.*, **31**, Nov/Dec. 1995, 1463-1468.

[46] Ozkan, U., S., Agarwal, S., K., and Marcelin, G., "Reduction of Nitrogen Oxides Emissions", ACS Symposium Series, 1995, 1-52.

[47] Penetrante, B. M., "Plasma Chemistry and Power Consumption in Non-thermal Plasma", *Non-Thermal Plasma Techniques for Pollution Control*, Part A, Eds: Penetrante, B., M., and Schultheis, S., E, Springer-Verlag 1993, 65-89.

[48] Penetrante, B. M., Hsiao, M. C., Meritt, B. T., Vogtlin, G. E., Wallman, P. H., "Comparison of Electrical Discharge Techniques for Nonthermal Plasma Processing of NO in N_2", *IEEE Tran. on Plasma Sci.*, **23**, No. 4, August 1995.

[49] Peyrous, R., Pinolet, P., and Held, B., "Kinetic Simulation of Gaseous Species by an Electrical Discharge in Dry or Humid Oxygen", *J. Phys. D: Appl. Phys.*, **22**, 1989, 1658-1667.

[50] Pignolet, P., Hadj-Ziane, S., Held, B., Peyrous, R., Benas, J., M., and Coste, C., "Ozone Generation by Point to Plane Corona Discharge" *J. Phys. D: Appl. Phys.*, **23**, 1990, 1069-1072.

[51] Sardja, I., and Dhali., S., K., "Plasma Oxidation of SO_2" *Appl. Phys. Lett.*, **56**(1), 1 January 1990, 21-23.

[52] Schofield, K., "Critically Evaluated Rate Constants for Gaseous Reactions of Several Electronically Excited Species", *J. Phys. Chem. Ref. Data*, **8**, 1979, 723-763.

[53] Seinfeld, J. H., "Atmospheric Chemistry and Physics of Air Pollution", John Wiley and Sons, New York, 1986.

[54] Sharma, A., K., Locke, B., R., Arce, P., "A Preliminary Study of Pulsed Streamer Corona Discharge for the Degradation of Phenol in Aqueous Solutions", *Hazardous Waste & Hazardous Materials*, **10** (2), 1993, 209-219.

[55] Spicer, C. W., Holdren, M. W., Smith, L. D., and Hughes, D. P, Smith, M. D., "Chemical Composition of Exhaust From Aircraft Turbine Engines", *Journal of Engineering for Gas Turbines and Power*,**114**, January 1992, 111-117.

[56] Suhr, H., Weddigen, G., "Reduction of Nitric Oxide in Flue Gases by Point to Plane Corona Discharge with Catalytical coatings on the Plane Electrode" *Combust. sci. and Tech.*, **72**, 101-115.

[57] Sutherland, C. D., and Zinn, J., "Chemistry Computations for Irradiated Hot Air", Los Alamos Scientific Laboratory Informal Report LA-6055-MS, 1975, Los Alamos, NM.

[58] Tas, M.A, "Plasma-Induced Catalysis, A Feasibility study and fundamentals", thesis Technische Universiteit Eindhoven, Netherlands, CIP-DATA Koninklijke Bibliotheek, Den Haag, 1995.

[59] Tokunaga, O., and Suzuki, N., "Radiation Chemical Reactions in NO_x and SO_2 Removal from Flue Gas", *Radiat. Phys. Chem.*, **24**, 1984, 145-165.

[60] U.S. EPA, "Air Quality Criteria for Oxides of Nitrogen", Research Triangle Park, 1993.

[61] Vogtlin, G., E., and Penetrante, B., M., "Pulsed Corona Discharge for Removal of NO_x from Flue Gas", *Non-Thermal Plasma Techniques for Pollution Control*, Part B, Eds: Penetrante, B., M, and Schultheis, S., E., Springer-Verlag, 1993, 187-198.

[62] Wang, M., C., and Kunhardt, E., E., "Streamer Dynamics", *Phys. Rev. A*, **42**, 1990, 465-515.

[63] Warnatz, J., "Rate Coefficients in C/H/O System", *Combustion Chemistry*, Ed: Gardinger, Jr., Springer, 1984, 197-360.

[64] Willis, C., and Boyd, A. W., "Excitation in the Radiation Chemistry of Inorganic Bases", *Int. J. Rad. Phys. Chem.*, **8**, 1976, 71-111.

BIOGRAPHICAL SKETCH

Swaminathan Kalyana

Swaminathan Kalyana was born on April 22, 1973 at Poonthotam, Tamil Nadu, India. He finished his junior college from St. Mary's Junior College, Hyderabad, India in 1990. He enrolled in University College of Technology, Osmania University, Hyderabad, India as an undergraduate in the fall of 1990. He graduated in the spring of 1994 with a Bachelor of Technology in Chemical Engineering degree.

In the fall of 1994, he joined FAMU-FSU college of engineering, The Florida State University to pursue a Master of Science degree in Chemical Engineering. During this time he was a graduate research and teaching assistant with the Chemical Engineering Department. His professional interests include areas of environmental engineering and process design.

APPENDIX A

NO REMOVAL DATA FROM NITROGEN, DRY, AND HUMID AIR

The concentrations shown in the tables have been normalized for an initial concentration of NO to be 100 ppm and NO_2 concentration to be 0 ppm.

Table A.1: NO and NO_2 Data at 30 kV in an Atmosphere of Nitrogen

Res. Time (sec)	NO Conc. (ppm)		NO_2 Conc. (ppm)		Mean NO	Mean NO_2
	Run1	Run2	Run1	Run 2		
7.2	99.8	98.8	0	0	99.9	0
14.5	87.6	87.7	3.3	4.8	87.6	4.0
29.0	82.7	80.7	4.1	4.5	81.7	4.3
44.0	57.9	64.5	7.0	7.9	61.2	7.4

Table A.2: NO and NO_2 Data at 35 kV in an Atmosphere of Nitrogen

Res. Time	NO Conc.		NO_2 Conc.		Mean NO	Mean NO_2
(sec)	(ppm)		(ppm)			
	Run1	Run2	Run1	Run 2		
7.26	98.46	90.74	2.6	3.0	94.62	2.80
14.52	64.8	65.43	6.94	7.2	65.11	7.06
29.04	43.85	44.96	8.38	7.02	44.05	4.93
44	28.75	28.55	6.76	7.36	28.65	6.56

Table A.3: NO and NO_2 Data at 40 kV in an Atmosphere of Nitrogen

Res. Time	NO Conc.		NO_2 Conc.		Mean NO	Mean NO_2
(sec)	(ppm)		(ppm)			
	Run1	Run2	Run1	Run 2		
7.2	82.75	78.05	5.17	7.03	80.42	6.10
14.5	47.29	46.95	7.78	8.06	47.12	7.92
29	12.86	8.96	4.46	5.41	10.91	4.93
44	1.58	1.98	2.0	2.06	1.78	2.30

Table A.4: NO and NO$_2$ Data at 50 kV in an Atmosphere of Nitrogen

Res. Time (sec)	NO Conc. (ppm)		NO$_2$ Conc. (ppm)		Mean NO	Mean NO$_2$
	Run1	Run2	Run1	Run 2		
7.2	48.07	49.17	7.78	8.0	48.62	7.87
14.5	12.36	12.4	2.8	3.0	12.38	2.9
29	0	0	0.76	0.6	0	0.68
44	0	0	0.83	1.24	0	1.03

Table A.5: NO and NO$_2$ Data at 30 kV in an Atmosphere of Dry Air

Res. Time (sec)	NO Conc. (ppm)		NO$_2$ Conc. (ppm)		Mean NO	Mean NO$_2$
	Run1	Run2	Run1	Run 2		
3.6	97.5	98.1	0	0	97.8	0
7.2	97.2	97.6	0.65	1.62	97.4	1.13
14.5	97.4	99.2	3.3	0	98.3	1.6
29.0	79.8	94.6	28.0	3.7	87.2	15.8
59.0	77.0	73.0	27.3	22.8	75	25.0

Table A.6: NO and NO$_2$ Data at 35 kV in an Atmosphere of Dry Air

Res. Time (sec)	NO Conc. (ppm)		NO$_2$ Conc. (ppm)		Mean NO	Mean NO$_2$
	Run1	Run2	Run1	Run 2		
3.6	99.0	98.5	0	0	98.7	0
7.2	82.04	87.10	17.5	11.5	84.58	14.5
14.5	90.5	95.4	12.4	6.4	92.9	9.4
29	47.4	28.6	63.4	84.8	38	74.1
59	9.5	10.8	105.1	107.2	10.1	106.1

Table A.7: NO and NO$_2$ Data at 40 kV in an Atmosphere of Dry Air

Res. Time (sec)	NO Conc. (ppm)		NO$_2$ Conc. (ppm)		Mean NO	Mean NO$_2$
	Run1	Run2	Run1	Run 2		
3.6	98.9	95.4	0	3.0	97.1	1.5
7.2	58.56	68.9	42.1	33.0	63.8	37.6
14.5	44.4	39.2	64.1	64.7	41.8	64.4
29	0	3.8	121.9	117.9	1.9	119.9
59.0	1.1	0	99.4	101.9	0.5	100.6

Table A.8: NO and NO$_2$ Data at 50 kV in an Atmosphere of Dry Air

Res. Time (sec)	NO Conc. (ppm)		NO$_2$ Conc. (ppm)		Mean NO	Mean NO$_2$
	Run1	Run2	Run1	Run 2		
3.6	75.0	95.7	24.7	3.3	85.3	14.0
7.2	18.8	21.3	82.5	79.8	20.0	81.2
14.5	0	1.9	108.2	108.6	0.9	108.4
29	0	0	111.9	119.0	0	115.4
44	0	0	85.4	87.4	0	86.4

Table A.9: NO and NO$_2$ Data at 30 kV in an Atmosphere of Humid Air

Res. Time (sec)	NO Conc. (ppm)		NO$_2$ Conc. (ppm)		Mean NO	Mean NO$_2$
	Run1	Run2	Run1	Run 2		
7.2	97.64	97.94	1.0	0	97.79	0.5
14.5	98.66	94.0	2.04	3.62	96.33	2.83
29.0	80.64	88.67	2.42	2.4	84.66	2.4
44	89.59	91.82	1.02	0	90.7	0.5

Table A.10: NO and NO$_2$ Data at 35 kV in an Atmosphere of Humid Air

Res. Time (sec)	NO Conc. (ppm)		NO$_2$ Conc. (ppm)		Mean NO	Mean NO$_2$
	Run1	Run2	Run1	Run 2		
7.2	86.79	86.14	6.52	5.46	86.46	5.95
14.5	66.49	57.23	16.76	18.24	61.86	17.5
29.0	41.72	51.76	4.02	5.72	46.74	4.87
44.0	43.36	31.12	1.81	1.48	37.2	1.65

Table A.11: NO and NO$_2$ Data at 40 kV in an Atmosphere of Humid Air

Res. Time (sec)	NO Conc. (ppm)		NO$_2$ Conc. (ppm)		Mean NO	Mean NO$_2$
	Run1	Run2	Run1	Run 2		
7.2	59.94	64.11	15.66	13.97	62.02	14.82
14.5	29.05	26.36	23.26	22.1	27.7	22.68
29	7.9	19.4	5.29	4.75	13.65	5.62
44.0	0	0	2.88	3.54	0	3.21

Table A.12: NO and NO_2 Data at 50 kV in an Atmosphere of Humid Air

Res. Time	NO Conc.		NO_2 Conc.		Mean NO	Mean NO_2
(sec)	(ppm)		(ppm)			
	Run1	Run2	Run1	Run 2		
7.2	28.1	22.06	20.8	21.58	25.08	21.19
14.5	0	0	4.75	10.26	0	7.5
29.0	0	0	2.76	2.62	0	2.69
44.0	0	0	3.81	3.83	0	3.82

APPENDIX B

NO REMOVAL DATA WITH THE ADDITION OF CO AND C_2H_4

The concentrations shown in the table have been normalized for an initial concentration of NO to be 100 ppm and NO_2 concentration to be 0 ppm.

Table B.1: NO and NO_2 Data at 30 kV in an Atmosphere of Humid Air and CO

Res. Time (sec)	NO Conc. (ppm)		NO_2 Conc. (ppm)		Mean NO	Mean NO_2
	Run1	Run2	Run1	Run 2		
7.2	98.6	97.5	0.2	0	98.0	0.1
14.5	96.3	88.8	1.5	4.0	92.6	2.8
29.0	94.2	93.3	1.2	1.1	93.8	1.2
44.0	93.2	92.6	1.6	0	92.9	0.8

Table B.2: NO and NO_2 Data at 35 kV in an Atmosphere of Humid Air and CO

Res. Time (sec)	NO Conc. (ppm)		NO_2 Conc. (ppm)		Mean NO	Mean NO_2
	Run1	Run2	Run1	Run 2		
7.2	94.6	94.3	1.6	1.2	94.5	1.4
14.5	78.0	60.8	3.4	9.0	69.4	6.2
29.0	50.2	41.3	6.4	6.7	45.8	6.6
44.0	45.6	42.6	5.7	6.1	44.1	5.9

Table B.3: NO and NO_2 Data at 40 kV in an Atmosphere of Humid Air and CO

Res. Time (sec)	NO Conc. (ppm)		NO_2 Conc. (ppm)		Mean NO	Mean NO_2
	Run1	Run2	Run1	Run 2		
7.2	66.3	58.9	13.6	19.5	62.6	16.6
14.5	27.5	26.0	11.5	12.3	26.8	11.9
29.0	5.6	4.2	7.1	6.75	4.9	6.9
44.0	9.6	2.5	5.6	5.9	6.05	5.8

Table B.4: NO and NO$_2$ Data at 50 kV in an Atmosphere of Humid Air and CO

Res. Time (sec)	NO Conc. (ppm)		NO$_2$ Conc. (ppm)		Mean NO	Mean NO$_2$
	Run1	Run2	Run1	Run 2		
7.2	30.5	28.4	25.6	24.3	29.5	24.9
14.5	4.6	2.3	10.8	9.7	3.5	10.3
29.0	0	0	2.5	2.9	0	2.7
44.0	0	0	5.2	5.0	0	5.1

Table B.5: NO and NO$_2$ Data at 30 kV in an Atmosphere of Dry Air and 500 ppm Ethylene

Res. Time (sec)	NO Conc. (ppm)		NO$_2$ Conc. (ppm)		Mean NO	Mean NO$_2$
	Run1	Run2	Run1	Run 2		
7.2	91.8	97.9	1.6	0	94.9	0.8
14.5	92.4	88.9	7.6	10.8	90.65	9.2
29.0	79.0	70.4	20.0	20.1	74.7	20.1
44.0	27.9	48.0	68.5	43.4	38.0	56.0

Table B.6: NO and NO$_2$ Data at 35 kV in an Atmosphere of Dry Air and 500 ppm of Ethylene

Res. Time (sec)	NO Conc. (ppm)		NO$_2$ Conc. (ppm)		Mean NO	Mean NO$_2$
	Run1	Run2	Run1	Run 2		
7.2	65.1	71.9	36.8	27.9	68.5	31.9
14.5	66.4	77.9	34.3	23.9	72.2	29.1
29.0	42.6	24.9	54.0	63.1	33.8	58.5
44.0	1	1.1	91.7	87.0	1.1	89.4

Table B.7: NO and NO$_2$ Data at 40 kV in an Atmosphere of Dry Air and 500 ppm Ethylene

Res. Time (sec)	NO Conc. (ppm)		NO$_2$ Conc. (ppm)		Mean NO	Mean NO$_2$
	Run1	Run2	Run1	Run 2		
7.2	25.5	14.7	77.2	87.0	20.1	82.1
14.5	4.3	3.7	95.6	94.8	4.0	95.2
29.0	0	0	90.0	93.2	0	91.6
44.0	0	0	63.9	57.3	0	60.6

Table B.8: NO and NO_2 Data at 50 kV in an Atmosphere of Dry Air and 500 ppm Ethylene

Res. Time (sec)	NO Conc. (ppm)		NO_2 Conc. (ppm)		Mean NO	Mean NO_2
	Run1	Run2	Run1	Run 2		
7.2	0	0	102.3	99.0	0	100.7
14.5	0	0	86.1	84.6	0	85.4
29.0	0	0	88.6	88.4	0	88.5
44.0	0	0	55.0	59.5	0	57.3

Table B.9: NO and NO_2 Data at 30 kV in an Atmosphere of Humid Air and 500 ppm Ethylene

Res. Time (sec)	NO Conc. (ppm)		NO_2 Conc. (ppm)		Mean NO	Mean NO_2
	Run1	Run2	Run1	Run 2		
7.2	98.3	97.6	0	0	98.0	0
14.5	76.1	73.2	8.3	8.9	74.65	8.6
29.0	92.2	73.9	1.0	3.5	83.1	2.3
44.0	80.0	85.8	0	0	82.9	0

Table B.10: NO and NO_2 Data at 35 kV in an Atmosphere of Humid Air and 500 ppm Ethylene

Res. Time (sec)	NO Conc. (ppm)		NO_2 Conc. (ppm)		Mean NO	Mean NO_2
	Run1	Run2	Run1	Run 2		
7.2	70.3	74.1	13.2	10.4	72.2	11.8
14.5	68.2	26.7	8.5	15.9	47.4	12.2
29.0	20.6	22.2	7.9	7.7	21.4	7.8
44.0	34.6	13.4	1.5	2.4	24	1.9

Table B.11: NO and NO_2 Data at 40 kV in an Atmosphere of Humid Air and 500 ppm Ethylene

Res. Time (sec)	NO Conc. (ppm)		NO_2 Conc. (ppm)		Mean NO	Mean NO_2
	Run1	Run2	Run1	Run 2		
7.2	37.8	36.7	19.9	21.2	37.7	20.5
14.5	22.6	15.8	14.7	16.2	19.2	15.4
29.0	3.6	7.0	10.5	11.0	5.3	10.7
44.0	0	1.4	1.1	2.0	0.7	1.5

Table B.12: NO and NO_2 Data at 50 kV in an Atmosphere of Humid Air and 500 ppm Ethylene

Res. Time (sec)	NO Conc. (ppm)		NO_2 Conc. (ppm)		Mean NO	Mean NO_2
	Run1	Run2	Run1	Run 2		
7.2	15.6	17.4	24.2	24.6	16.5 .	24.4
14.5	0	0	11.3	13.8	0	12.5
29.0	0	0	9.8	14.5	0	12.1
44.0	0	0	2.0	1.2	0	1.6

APPENDIX C

OZONE FORMATION DATA

Table C.1: O_3 Data at 30 kV in an Atmosphere of Dry Air

Res. Time (sec)	O_3 Conc. (ppm)		Mean O_3
	Run1	Run2	
7.2	0	3	1.5
14.5	9	0	4.5
29	12	15	13.5
44.0	6	9	7.5

Table C.2: O_3 Data at 35 kV in an Atmosphere of Dry Air

Res. Time (sec)	O_3 Conc. (ppm)		Mean O_3
	Run1	Run2	
7.2	33	21	27
14.5	15	12	13.5
29.0	27	21	24
44.0	24	78	41

Table C.3: O_3 Data at 40 kV in an Atmosphere of Dry Air

Res. Time (sec)	O_3 Conc. (ppm)		Mean O_3
	Run1	Run2	
7.2	766	96	81
14.5	45	81	63
29.0	294	183	238.5
44.0	453	459	456

Table C.4: O_3 Data at 50 kV in an Atmosphere of Dry Air

Res. Time (sec)	O_3 Conc. (ppm)		Mean O_3
	Run1	Run2	
7.2	276	258	267
14.5	375	363	369
29	1089	948	1018.5
44.0	1503	1236	1369.5

APPENDIX D

COMPUTER CODES

D.1 Procedure of Computations

The pulsed nature of the discharge is simulated in the program by considering two reaction sets to calculate the concentration profiles. During the duration of pulsing, the reaction set which has electron-gas dissociation reactions are used. The time duration of the pulse is assumed to be one microsecond. Since the frequency of pulsing is 60 Hz, the time duration between the pulsing is 16.667 milliseconds. To calculate the concentration profile for the time in between two pulses, the reaction set which does not have the electron-gas reactions are considered.

Initially the program calculates the concentration profile of different species using the initial concentrations given in **conp.inp** file and the set of reactions which has the electron-gas reactions given in **chem.inp** for a period of 1 microsecond. After this time, since the pulsing is no longer there, the reaction set is changed to the set which does not have any electron-gas reactions to calculate the concentration profile for the next 16.667 milliseconds. The reaction set is again interchanged after 16.667 milliseconds to calculate the concentration profile for the next 1 microsecond. This procedure if repeated 120 times corresponding to double the frequency of pulsing would give the concentration of different species after a gas residence time of 1 second. The concentration profile after each second is copied into the file called conc.out. The procedure is repeated till the gas residence time in the reactor

is reached. The program is repeated in this case for 7200 times to calculate the concentrations for a gas residence time of 60 seconds.

The plots shown in the model use the **conc.out** to show the concentrations of different species as a function of residence time.

The program **cycle.sh** is used to repeat the iteration 7200 times. The program **conp.sh** is the shell program which uses the fortran programs (conp.f, vode.f, cklib.f, math.f) and the input files to calculate the concentration.

The program **conp.f** is the actual fortran program which calls the ODE solver **vode.f** and other subroutines in **cklib.f** and **math.f** to solve the ODE. The ODE solver and the other subroutines are a part of the software called CHEMKIN (Kee, et al., 1994).

D.2 cycle.sh

This shell programs runs the cconp.sh program repeatedly till the

final time corresponds to the final time in the reactor.

In this case, the programs runs for 60 seconds.

After that the initial concentrations are added to the conc.out

to get the concentration profile.

```csh
#!/bin/csh -f
set icount = 1
set iend = 7201
while ($icount !=  $iend)
sh conp.sh conp
 @ icount++
end
```

D.3   conp.sh

```
# This shell program uses the conp.f program to calculate the concentration
# profile. It uses a ODE solver called vode.f and list of subroutines
# listed under cklib.f files from the software called CHEMKIN.
# This is shell program calculates the concentration profile till the
# final time, interchanges the reaction set making the computed final
# concentration of the initial concentration for the next set.
# The outputfile are conp.out, conc.out.
# conc.out has the concentration profile of the species after every second.


#!/bin/sh
# to execute:  sh conp.sh logname  &
sh 1> ${1}.log 2>&1 << ENDSH
set -x
#cd /scr/$LOGNAME              #go to user's scratch directory
#mkdir "${1}$$"               #make subdirectory /myrun##
#cd "${1}$$"                  #go to /myrun##
cat << EOF > makefile
include chemmake.h
OBJS = conp.o cklib.o vode.o math.o
INPS = therm.dat chem.inp conp.inp
OUTS = chem.out chem.bin conp.out
EXES = chem.exe conp.exe
chem.exe: ckinterp.o
  $(LINK) chem.exe ckinterp.o
conp.exe: $(OBJS)
  $(LINK) conp.exe $(OBJS)
```

```
EOF
touch makefile; make chem.exe conp.exe
chem.exe; conp.exe < conp.inp > conp.out
cat fort.25 >> conc.out &
rm fort.25
mv Conp.dat conp.inp
mv chem.inp temp.inp
mv tchem.inp chem.inp
mv temp.inp tchem.inp
ENDSH
```

D.4 conp.f

```
C     Modeling of NO Removal From Various Gas Compositions Using A
C     Pulsed Streamer Corona Discharge Reactor.
C
C
C     Input : Pressure, Temperature, Initial Mole Fractions of
C             Different Species, Initial Time, Final Time and
C             Interval in a File Called conp.inp
C           : Set of Chemical Reactions Considered for the NOx Removal
C             in a File Called chem.inp
C     Output: Concentration Profile of Different Species till the
C             Final Time at Requested Intervals in a File Called Chem.out
C
C This Program calls the ODE solver to solve for the given input


C This program is for the mole fractions as its input ..
      PROGRAM CONP
C
C     Integration of adiabatic, constant pressure kinetics problems
C
C     VERSION 1.2:
C     1.  Implement new VODE solver
C
C*****precision > double
      IMPLICIT DOUBLE PRECISION (A-H,O-Z), INTEGER(I-N)
C*****END precision > double
C*****precision > single
```

```fortran
C        IMPLICIT REAL (A-H,O-Z), INTEGER (I-N)
C*****END precision > single
C

       PARAMETER (LENIWK=4000, LENRWK=8000, LENCWK=500, NK=5, NLMAX=55,
      1              LIN=5, LOUT=6, LINKCK=25, KMAX=50, ITOL=1, IOPT=0,
      2              RTOL=1.0E-6, ITASK=1, ATOL=1.0E-20)
C

       DIMENSION IWORK(LENIWK), RWORK(LENRWK), X(KMAX), Z(KMAX)
       CHARACTER CWORK(LENCWK)*16, KSYM(KMAX)*16, LINE*80
       LOGICAL KERR, IERR
       EXTERNAL FUN
C

       COMMON /RCONS/ P, RU
       COMMON /ICONS/ KK, NWT, NH, NWDOT
C

       DATA KERR/.FALSE./, X/KMAX*0.0/, KSYM/KMAX*' '/


C      Initialize CHEMKIN
OPEN(19, FILE="Conp.dat",STATUS="UNKNOWN")
OPEN (22,FILE="CONP.DAT1",STATUS="UNKNOWN")
       OPEN (LINKCK, FORM='UNFORMATTED', STATUS='UNKNOWN',
      1              FILE='chem.bin')
       CALL CKLEN  (LINKCK, LOUT, LENI, LENR, LENC)
       CALL CKINIT (LENIWK, LENRWK, LENCWK, LINKCK, LOUT, IWORK,
      1              RWORK, CWORK)
       CLOSE (LINKCK)
       CALL CKINDX (IWORK, RWORK, MM, KK, II, NFIT)
```

```
      NEQ   = KK + 1
      LRW   = 22 + 9*NEQ + 2*NEQ**2
      NVODE = LENR + 1
      NWT   = NVODE + LRW
      NH    = NWT  + KK
      NWDOT = NH   + KK
      NTOT  = NWDOT+ KK - 1
      LIW   = 30 + NEQ
      IVODE = LENI + 1
      ITOT  = IVODE + LIW - 1
      IF (KK .GT. KMAX) THEN
         WRITE (LOUT, *)
1    ' Error...KMAX too small...must be at least ',KK
         KERR = .TRUE.
      ENDIF
      IF (LENRWK .LT. NTOT) THEN
         KERR = .TRUE.
         WRITE (LOUT, *)
1    ' Error...LENRWK too small...must be at least', NTOT
      ENDIF
      IF (LENIWK .LT. ITOT) THEN
         KERR = .TRUE.
         WRITE (LOUT, *)
1    ' Error...LENIWK too small...must be at least', ITOT
      ENDIF
      IF (KERR) STOP
      CALL CKSYMS (CWORK, LOUT, KSYM, IERR)
```

```
      IF (IERR) KERR = .TRUE.
      CALL CKWT   (IWORK, RWORK, RWORK(NWT))
      CALL CKRP   (IWORK, RWORK, RU, RUC, PATM)
      READ  (LIN,    *) PA, T
      WRITE(19,*) PA, T
      P = PA*PATM
C     Initial non-zero moles
   40 CONTINUE
      LINE = ' '
      READ  (LIN,  '(A)', END=45)   LINE
      ILEN = INDEX (LINE, '!')
      IF (ILEN .EQ. 1) GO TO 40
      ILEN = ILEN - 1
      IF (ILEN .LE. 0) ILEN = LEN(LINE)
      IF (INDEX(LINE(:ILEN), 'END') .EQ. 0) THEN
         IF (LINE(:ILEN) .NE. ' ') THEN
            CALL CKSNUM (LINE(:ILEN), 1, LOUT, KSYM, KK, KNUM,
     1                      NVAL, VAL, IERR)
            IF (IERR) THEN
               WRITE (LOUT,*) ' Error reading moles...'
               KERR = .TRUE.
            ELSE
               X(KNUM) = VAL
            ENDIF
         ENDIF
         GO TO 40
      ENDIF
```

```
   45 CONTINUE
C     Final time and print interval
      READ  (LIN,    *) TT1,T2, DT, III
       WRITE (22,7100) (KSYM(K), K=1,KK)
      IF (KERR) STOP
C     Initial conditions and mass fractions
      Z(1) = T
      CALL CKXTY (X, IWORK, RWORK, Z(2))
C     Integration control parameters for VODE
      TT2   = TT1
      MF = 22
      ISTATE= 1
      NLINES=NLMAX + 1
C     Integration loop
  250 CONTINUE
      T = Z(1)
      CALL CKYTX (Z(2), IWORK, RWORK, X)
      CALL CKMMWY(Z(2), IWORK, RWORK, WW)
      WRITE (LOUT, 7105) TT1, T, (X(K), K=1,KK), WW
      IF (TT2 .GE. T2) THEN
      WRITE(19,7012)(KSYM(K),X(K), K=1,KK)
      WRITE(19,*)'END'
      JJJ=III/2
      QQQ=JJJ*2
        IF(QQQ.EQ.III) THEN
       XINT=1E-6
       T4=TT2
```

```
          TT1=T2

          T2=T2+XINT

          T3=XINT/10

          IF (MOD(III,120).EQ.0) THEN
      WRITE(25,7105) TT2,T,(X(K), K= 1,KK), WW

          ENDIF

          ELSE

          XINT=16.667E-3

          TT1=T2

          T2=T2+XINT

          T3=XINT/10

          ENDIF

          III=III+1

          WRITE(19,*) TT1, T2,T3, III

          STOP

          ELSE

        TT2 = MIN(TT2 + DT, T2)

          ENDIF
C     Call the differential equation solver
  350 CONTINUE
C*****precision > single
C        CALL SVODE
C*****END precision > single
C*****precision > double
        CALL DVODE
C*****END precision > double
        *              (FUN, NEQ, Z, TT1, TT2, ITOL, RTOL, ATOL, ITASK,
```

```
      1               ISTATE, IOPT, RWORK(NVODE), LRW, IWORK(IVODE),
      2               LIW, JAC, MF, RWORK, IWORK)
        IF (ISTATE .LE. -2) THEN
           IF (ISTATE .EQ. -1) THEN
              ISTATE = 2
              GO TO 350
           ELSE
              WRITE (LOUT,*) ' ISTATE=',ISTATE
              STOP
           ENDIF
        ENDIF
        GO TO 250
C          FORMATS
 7003 FORMAT (1H1)
 7100 FORMAT (3X, 'T(SEC)', 9X, 'TMP(K)', 9X, 20(4X,A10))
 7105 FORMAT (50E16.8)
 7110 FORMAT (26X, 5(1X,A10))
 7115 FORMAT (22X, 10E11.3)
 7012 FORMAT ((1X,A10),4X,1E14.8)
      END
      SUBROUTINE FUN (N, TIME, Z, ZP, RPAR, IPAR)
C*****precision > double
      IMPLICIT DOUBLE PRECISION(A-H,O-Z), INTEGER(I-N)
C*****END precision > double
C*****precision > single
C     IMPLICIT REAL (A-H,O-Z), INTEGER(I-N)
C*****END precision > single
```

```
      COMMON /RCONS/ P, RU
      COMMON /ICONS/ KK, NWT, NH, NWDOT
      DIMENSION Z(*), ZP(*), RPAR(*), IPAR(*)
C
C     Variables in Z are:  Z(1)   = T
C                          Z(K+1) = Y(K)
C
C     Call CHEMKIN subroutines
C
      CALL CKRHOY (P, Z(1), Z(2), IPAR, RPAR, RHO)
      CALL CKCPBS (Z(1), Z(2), IPAR, RPAR, CPB)
      CALL CKWYP  (P, Z(1), Z(2), IPAR, RPAR, RPAR(NWDOT))
      CALL CKHMS  (Z(1), IPAR, RPAR, RPAR(NH))
C
C     Form governing equation
C
      SUM = 0.0
      DO 100 K = 1, KK
         H    = RPAR(NH    + K - 1)
         WDOT = RPAR(NWDOT + K - 1)
         WT   = RPAR(NWT   + K - 1)
         ZP(K+1) = WDOT * WT / RHO
C        SUM = SUM + H * WDOT * WT
  100 CONTINUE
      RETURN
      END
```

D.5   conp.inp

```
      1.00000000000000        298.000000000000
O2            0.2099
O             0.
N             0.
N2            0.79
NO            0.0001
O3            0.
NO2           0.
NO3           0.
N2O           0.
END
0 1E-06 1E-07 1
```